Master of Science Thesis

Residual strength of a FML reinforced frame member

A. van der Linden

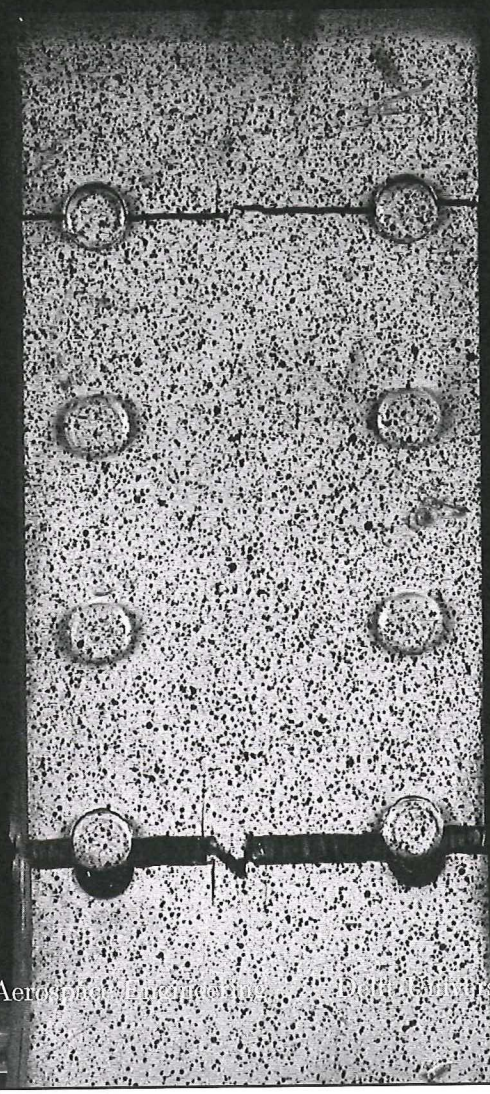

Faculty of Aerospace Engineering — Delft University of Technology

TU Delft Delft University of Technology

Residual strength of a FML reinforced frame member

Master of Science Thesis

For obtaining the degree of Master of Science in Aerospace Engineering
at Delft University of Technology

A. van der Linden

14 July 2015

Faculty of Aerospace Engineering · Delft University of Technology

The work in this thesis was supported by Airbus Germany. Their cooperation is gratefully acknowledged.

Copyright © A. van der Linden
All rights reserved.

14.09

14.30

DELFT UNIVERSITY OF TECHNOLOGY
FACULTY OF AEROSPACE ENGINEERING
DEPARTMENT OF AEROSPACE STRUCTURES AND MATERIALS

diff: de Rijk en fatigue damage

GRADUATION COMMITTEE

dogbone
high stress at rivet
without d.s. in taps?
no, diff failure

Dated: 14 July 2015

Chair holder:

Prof.dr.ir. R. Benedictus

Committee members:

Dr.ir. R.C. Alderliesten

Dr.ir. S. Teixeira de Freitas

Dr.ir. G.N. Saunders

Res steel

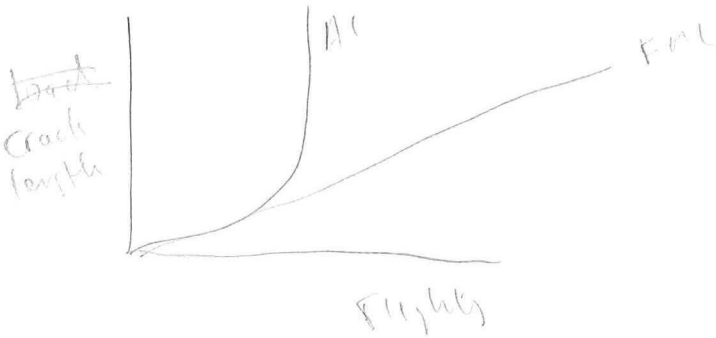

$\sigma_{bu} = 227.4$?

MVF = 3/5

$Al_{bu} = 417$

$St_{bu} = 1600$

Preface

First of all I would like to express my gratitude to my thesis supervisor, Dr. ir. Alderliesten, who always made time, and helped me greatly with his advice, discussions and insights. My thanks go out to Dr. Beumler, who supported this thesis from Airbus and made this thesis possible by providing the coupons to test at the TU Delft DASML lab. My gratitude also goes out to the DASML-lab personnel who assisted me with performing my tests, particularity GJ Mulder, for his assistance and optimism with getting my test setup to work. My thanks go out to Ms. Vollmer, Ms. van der Windt and Ms. de Knegt-Overduin for their assistance.

I would like to thank my parents, who always supported me during my studies. My gratitude goes out to all my friends who provided their input during discussions.

Summary

The current design of the inner flange of the aluminium frame members under the rear wing attachment of the A400M features a Glare strap reinforcement. The advantage of reinforcing the aluminium inner flange of the frame member with a Glare strap is clear: the hybrid design proves to be lighter and more damage tolerant than the conventional monolithic aluminium structure.

The goal of this thesis is to develop a model to predict the residual strength behavior of general Fibre Metal Laminates (FMLs), like the A400M frame flange, containing fatigue damage. This model is based on the concept that the residual strength of general FMLs is a function of the fatigue damage ratio R_D; the fraction of the aluminium area cracked in a cross section of the laminate. To support and validate the model, an experimental investigation is performed in the residual strength of coupons representing the A400M inner frame flange.

There are several requirements for the tool. As it has to be a versatile tool that is able to handle a wide range of lay-up configurations, while still being efficient, an analytical method is preferred. Additionally, it should be integrated with the FML fatigue toolbox developed by Spronk in a previous thesis. Because FMLs are applied in tensile loading, only the residual strength under tensional loading is considered.

A literature study is performed in which existing approaches to predicting the residual strength of Glare with fatigue cracks are presented. Based on the requirements for the tool, a choice is made for a reduced net-section approach developed by de Rijck. This approach then is used to predict the residual strength of the aluminium inner flange reinforced with a Glare strap containing fatigue damage.

The model uses the properties of the constituents, the crack lengths in the aluminium layers and the dimensions of the laminate as input. Using the blunt notch strength properties of the aluminium and the glass fibres layers, the blunt notch strength of the laminate is determined. With the crack lengths known in the aluminium layers of the laminate, the total cracked cross sectional area is calculated. To calculate the residual strength, the strength that would have been provided by the cracked aluminium area is subtracted from the pristine blunt notch strength of the laminate.

When the crack length in every aluminium layer is known, the cracked cross sectional area as a percentage of the total aluminium cross sectional area within the laminate can be calculated. The residual strength is now determined by subtracting the strength that the cracked aluminium would have provided, from the blunt notch strength of the pristine laminate.

10 Coupons have been provided by Airbus to perform residual strength tests to validate the predictions made with the tool. First, these coupons have been loaded by a tensile fatigue loading, to create differing levels of fatigue damage. Afterwards, a dogbone shape is milled in the coupons to prevent the tabs from shearing off. Residual strength testing by quasi statically loading the coupons is performed, while taking DIC measurements from both sides of the coupon to measure the in plane and out of plane deformations.

The results from the residual strength test are compared with the predictions from the De Rijck method. The predictions follow the trend from the residual strength well, but over predict the residual strength by 15%. This over prediction is partially explained from the delamations occurring between the Glare strap and the aluminium flange during the failing of the coupons, which create local stress concentrations.

Table of Contents

List of Figures

List of Tables

Chapter 1

Introduction

There is an ever present drive for lighter and safer aircraft structures. A recent development in this field is the introduction of Fibre Metal Laminates (FMLs) in primary aircraft structures. The FML Glare, which consists of aluminium and glass fibre layers, is used for example in the fuselage crown sections of the Airbus A380. Compared to aluminium, Glare shows a much lower crack propagation rate [13], allowing higher operational stresses. This results in lighter structure without sacrificing safety. Over the years, Airbus and the TU Delft together developed the tools to model the fatigue and damage tolerance of Glare.

A new application of Glare is in the fuselage frame members of the Airbus A400M Military transport aircraft. The fuselage frame members below the rear wing attachment are subjected to high static loads, as well as an intensive, mainly tensional fatigue loading. As these frame members are considered to be a single load path, fatigue and damage tolerance performance was the main driver in the design.
After an extensive study by Plokker [6], a design where the inner flange of the aluminium 7085 frame member is reinforced with a Glare strap, proved to be the lightest, and allowed for easier inspection than a monolithic aluminium design.

For the fatigue and damage tolerance analysis, the Glare strap and the aluminium flange were analysed separately. The thickness of the Glare strap was designed such that it was able to carry limit load if the aluminium flange was completely cracked and a through crack of 11 [mm] was present in the Glare strap. By dividing the flight loads over the strap and the flange based on the individual stiffnesses of these parts, the fatigue analysis of the strap was performed. This analysis showed that flight loads of almost three design lives of the aircraft could be applied before the critical crack length of 11 [mm] in the Glare strap was reached [1].

The models for the prediction of the fatigue crack growth and residual strength of Glare laminates which were used by Airbus are illustrated in the blue top row of figure 1.1. Among these models is the "FML F & DT toolbox" that was developed by Airbus and the TU Delft for the certification of Glare in the Airbus A380. Validation of the fatigue and damage tolerance properties was done by following the testing pyramid, from coupon to full scale aircraft

testing. Currently, this hybrid aluminium Glare design is flying in the A400M.

In a previous research, Spronk [1] developed a tool, which will be called the "general FML Fatigue tool" in this thesis, in order to prevent confusion with the FML FDT Toolbox which is currently in use by Airbus. The general FML Fatigue Tool developed by Spronk [1] can analyse fatigue crack initiation and propagation of general fibre metal laminates to assess the accuracy of the current method and see if there is room for improvement. This tool is based on the work of Alderliesten [2], Wilson [14] and Khan [15]. This is shown in the green box in the bottom row of figure 1.1.

The goal of this thesis is now is to develop a validated tool which can predict the residual strength of general fibre metal laminates, shown in the red box in figure 1.1 and add this capability to the existing tool developed by Spronk [1]. This will result in a complete tool that for the fatigue and residual strength analysis of general fibre metal laminates. It will allow engineers to perform the fatigue and residual strength analysis of general fibre metal laminates in one tool, making it easier to analyse and optimize the performance of these structures.

The requirements of the tool are as follows: it should be an analytical method, making it versatile and computationally efficient. It should be integrated with the general FML Fatigue Tool developed by Spronk [1]. Only the residual strength under tensional loading is considered.

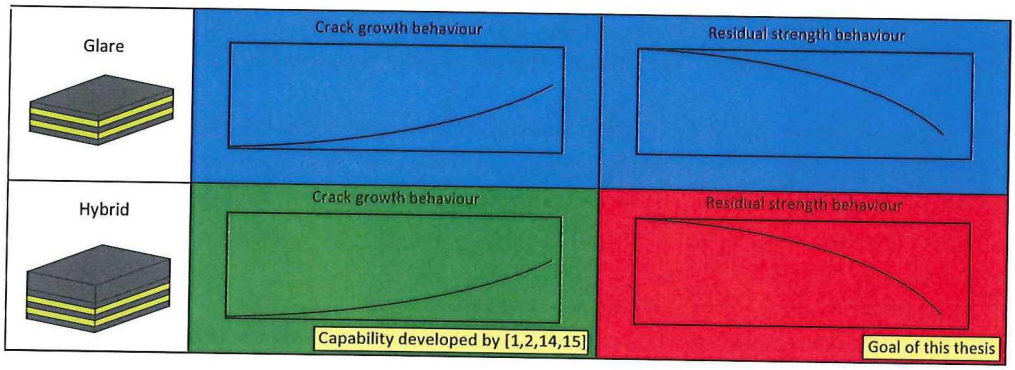

Figure 1.1: Role of this work within the area of existing capabilities

For the validation of the tool, 10 coupons have been provided by Airbus. By applying fatigue loading, differencing levels of fatigue are created. Subsequently, the residual strength of the coupon is tested to validate the predictions made by the residual strength tool. The results and discrepancies are discussed.

This thesis has the following structure. In chapter 2 the damage tolerance philosophy and the regulations applicable to aircraft structures are presented, as they play an important role in the design of the A400M frame member. This is followed by chapter 3 which discusses the material properties and mechanical behaviour of Glare, as well as the fatigue and residual strength behaviour of Glare. The design of the A400M fuselage frame member is presented in chapter 4. In chapter 5 approaches from literature to predict the residual strength of Glare containing fatigue cracks is discussed, and a method to predict the residual strength of an

aluminium flange bonded and riveted to an FML strap is developed. In the following chapter 6 the experiments to validate this residual strength method, as well as predictions made with the general FML Fatigue Tool developed by Spronk [1] are presented. The results from the experiments are presented and discussed in chapter 7. The conclusions from this thesis, and future prospects are made in chapter 8.

Chapter 2

Damage tolerance regulations

2.1 Introduction

Fatigue and Damage Tolerance (F&DT) regulations are important in the design of the fuselage frame member of the A400M. Military aircraft like the A400M are not under the jurisdiction of the Federal Aviation Authority (FAA), but as the A400M is a transport aircraft, it is assumed in this thesis that the FAA design practices are followed.

The FAA mandates regulations which outline how the aircraft structure should be designed to be damage tolerant. For transport category airplanes this design philosophy is called the *Damage tolerance philosophy*, documented in Federal Aviation Regulations (FAR) document FAR 25.571 [16] and is explained in section 2.2. Implementation of the damage tolerance philosophy, as well as acceptable means of compliance are presented in Advisory Circular (AC) AC 25.571-1D [17], and are explained in section 2.3.

2.2 Damage tolerance philosophy

The FAA defines damage tolerance in AC 25.571-1D [17] as follows:

> **Damage tolerance:** *The attribute of the structure that permits it to retain its required residual strength for a period of use after the structure has sustained a given level of fatigue, corrosion, or accidental or discrete source damage.*

The damage tolerance philosophy is based on the concept that the aircraft structure contains initial flaws (accidentally introduced during production, for example), as well as damages which are caused during service, which decrease the strength of the structure. Initial flaws in the structure will grow slowly during the lifetime of the aircraft due to the application of flight loads. The maximum load carrying capability of a structure with the existence of these

damages is named the residual strength [18].

The definition of damage tolerance at the beginning of this section gives three causes for the reduction of the strength of the structure: Fatigue, corrosion or accidental and discrete source damage. However, the reduction of residual strength due to fatigue damage is the only damage considered in this thesis.

Any aluminium parts of the frame member and Glare laminate which are exposed to the environment are protected from corrosion by anodizing and subsequently applying a pimer and a topcoat. [19]. Corrosion is thus unlikely.

Accidental or discrete source damage is expected to occur, as this aircraft will operate in war theatres. Severe discrete source damage (bird strike, engine non-containment or runway debris) cause through cracks in Glare [13]. Glare with through cracks fails different from Glare with fatigue cracks. The failure of Glare with through cracks is outside the scope of this thesis, thus discrete source damage is not considered in this thesis.

To understand how aircraft structures are designed to be damage tolerant, it is necessary to understand the loads for which aircraft structures are designed. The highest load expected during service is defined as limit load. To account for unknown factors in the load spectrum, limit load is multiplied by a safety factor of 1.5. The resulting load is called ultimate load.

The aircraft structure is able to withstand the ultimate load when it enters service. During operation, initial flaws present in the structure will grow, and decrease the residual strength. The aircraft structure is inspected during its life to detect and repair damages. From the regulations, it is mandatory to design the structure such that there two inspections between the moment when a crack becomes detectable, and the moment at which the crack length causes the residual strength to drop below the limit load [20], the critical crack length.

This implies that the structure has to be designed such that it is possible to detect damages during inspections with the prescribed inspection methods. The minimum detectable crack size depends on the inspection method that is used. If special equipment is used, a smaller crack can be detected than with the naked eye, but the inspection becomes more time consuming and expensive. A schematic representation of the crack growth during the operating life of the aircraft is shown in figure 2.1. The required inspection intervals between the moment that a crack is detectable and becomes critical are visualized in figure 2.1.

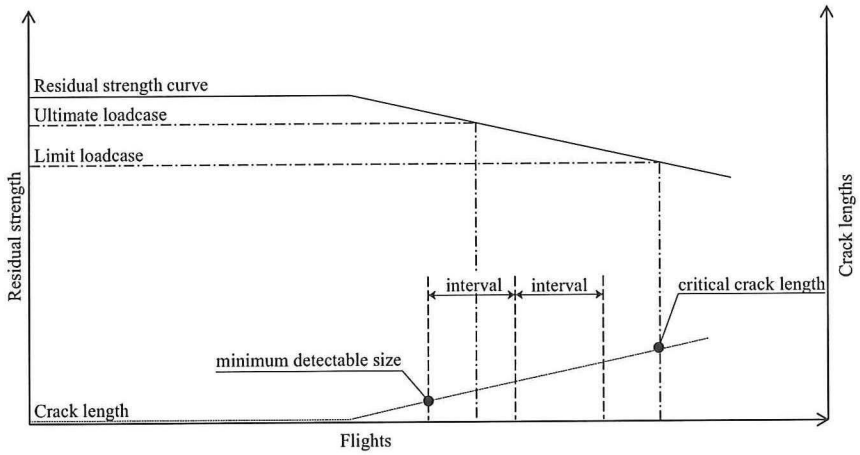

Figure 2.1: The crack length and residual strength are plotted versus the number of flights. The crack length starts at the bottom left of the graph, plotted on the right y-axis. The reduction of the residual strength starts at the top left of the graph, and is reduced by the presence of the crack. The required minimum of the two inspection intervals between the moment that a crack becomes detectable and when it becomes critical cracks are visualized.

2.3 Implementation of the damage tolerance regulations in structural design

The regulations with regards to designing the aircraft structure for damage tolerance are given in FAR 25.571 [16], acceptable means of compliance to these regulations are presented in AC 25.571-1D [21].

As prescribed in FAR 25.571 [16], the Principal Structural Elements (PSE's) have to be identified at the beginning of fatigue and damage tolerance analysis. PSE's are the structures whose integrity are essential for maintaining overall aircraft structural integrity. Failure of a PSE can lead to loss of the airplane, as defined in FAR 25.571 [16]. When a structure is identified as being a PSE, a decision should be made on the philosophy that is to be applied to ensure the structural integrity of this element during the lifetime of the aircraft. The frame members under consideration in this thesis are PSE's by AC 25.571-1D [21].

There are three methodologies within the damage tolerant design philosophy that can be used to design the structure, shown as the end points in figure 2.2. Each of these philosophies are discussed below.

If inspection is not possible, or if repairs prove to be impracticable, the safe-life approach is applied:

> **Safe-life** *The number of events, such as flight cycles, landings, or flight hours, within which the structure strength has a low probability of degrading below its design ultimate value due to fatigue cracking. [17]*

The safe-life approach does not explicitly consider the possibility for crack growth, but treats it as a crack nucleation process. Within this framework, it is assumed that failure takes place

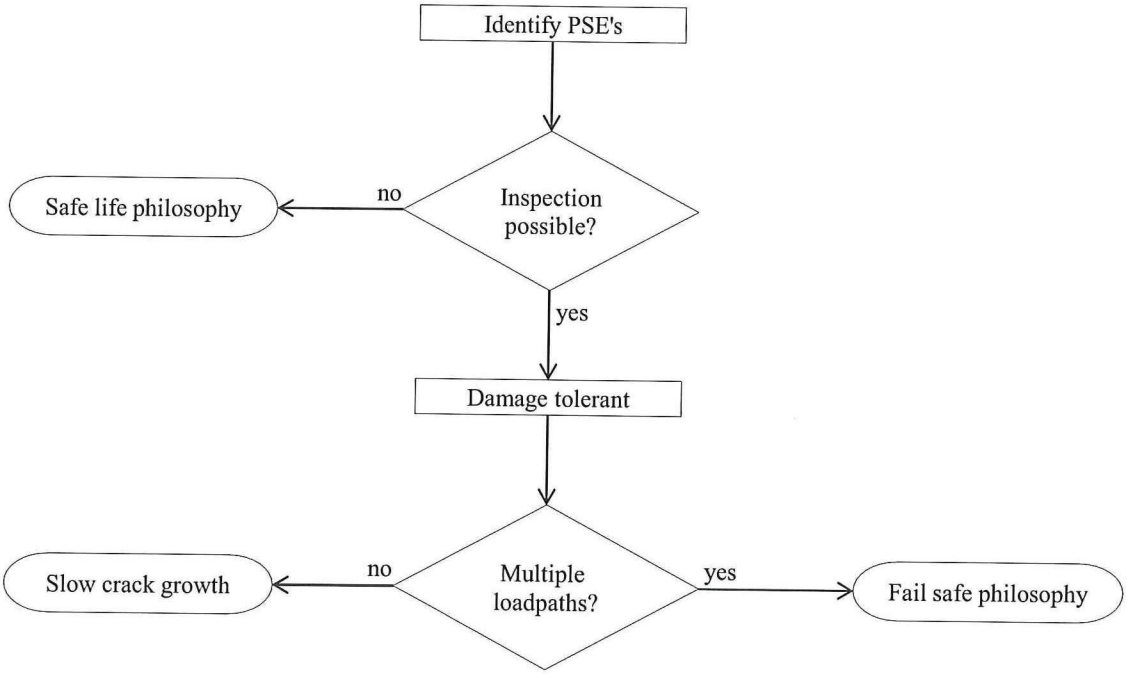

Figure 2.2: Structural design damage tolerance flow chart

when the first crack is formed [22]. The mean fatigue life of the part is established by fatigue tests. The mean fatigue life obtained from these tests is divided by a safety factor, often four, to obtain a fatigue life for which the probability of failure is very low [22]. This process is also described as 'safety-by-retirement' [23]. However, several accidents in the past have shown that unanticipated damage in the structure greatly reduced the fatigue life of components, resulting in inadequate designs. [22]. Nowadays, the safe-life approach is only allowed for the landing gear.

To prevent inadequate designs, the damage tolerance philosophy was developed. The damage tolerance philosophy assumes that in every structure initial flaws are present which grow during the life time of the aircraft. The size of the initial crack which is assumed in the structure is based on capability of the inspection methods [22]. The damage tolerance approach can be implemented in two ways, the fail-safe approach and the slow crack growth approach.

> **Fail-safe:** *The attribute of the structure that permits it to retain its required residual strength for a period of unrepaired use after the failure or partial failure of a principal structural element. [17]*

The basis for this design principle is that the structure would be designed such that damages are obvious to detect, and that there are multiple load paths present:

> **Multiple load path:** *Applies to structure, the applied loads of which are distributed through redundant structural members, so that the failure of a single structural member does not result in the loss of structural capability to carry the applied loads. [17]*

If a failure occurs in one of the primary structural elements, the probability of catastrophic failure is reduced by having multiple elements that are able to carry the flight load (redundancy) in the case of one failed member. However, it is important that as soon as a failed member is detected, it is repaired, as the remaining fatigue life of the structure is significantly reduced by a failed member. This requires for an appropriate inspection interval. [22]. This principle is described as 'safety by design' [23]. A design containing multiple elements that are able to carry flight loads is encouraged by the authorities in achieving a damage tolerant design. However, sometimes it proves unpractical to apply a multiple element structure. The authorities also define a damage tolerant single load path structure:

> **Single load path** *Describes structure, the applied loads of which are eventually distributed through a single structural member, the failure of which would result in the loss of the structural capability to carry the applied loads. [17]*

If this single load path fails however, there is no other structural element to carry the flight load, leading to a possible loss of the aircraft. Thus if a single load path damage tolerant design is chosen, it has to be demonstrated that damage is easily detectable in that element during the required inspections and that this damage would grow slowly and or the element should possess a crack stopping ability in the design [17].

Concluding, it is assumed that in every structure initial flaws are present, and that it accumulates damage over time as well. This damage will detected and repaired through proper inspection at proper inspection intervals. A boundary condition is that the structure can be inspected in a proper way. If this is not the case the structure should be designed using the safe life philosophy. Drawbacks are that the structure becomes heavier, becomes harder to inspect, and more testing is necessary to guarantee safety, as mentioned in the previous paragraph.

In this chapter the damage tolerant design philosophy which is in place for aircraft design has been discussed. The damage tolerant design philosophy is discussed as well as the practical implementation of it. In the next chapter, the material Glare will be discussed and its excellent damage tolerant properties will be elaborated on.

Chapter 3

Fibre metal laminates

3.1 Introduction

Fibre Metal Laminates (FMLs) are a group of composites compromising of metal and fibre layers. Several combinations of a fibre with a metal have been developed: ARALL (Aramid Reinforced ALuminium Laminate), CARE (CArbon fibre REinforced laminate), GLARE (GLAss fibre REinforced laminate) and TIGR (TItanium GRaphite laminate). Glare is the only FML currently in use in aviation, apart from ARALL C17 cargo doors, which are being phased out at the moment.

The three main advantages of Glare over monolithic aluminium are its superb fatigue crack growth resistance, the low density and the possibility to tailor the strength and stiffness to best suit its application, by changing the orientation of the fibres within the laminate [9].

In this chapter an overview of mechanical properties of Glare is given in section 3.2. This is followed by a discussion on the fatigue and damage tolerance properties; the fatigue properties are discussed in section 3.3, while the failure sequence of Glare with fatigue cracks under quasi-static loading is discussed in section 3.4.

3.2 Material definition

A Glare laminate is built up from alternating layers of aluminium 2024-T3 and glass fibre prepregs, where the outer layers of the laminate are aluminium 2024-T3 layers. The aluminium layers generally have a thickness between 0.2 [mm] and 0.5 [mm], while the unidirectional glass fibre prepreg layers have a nominal thickness of 0.133 [mm]. The unidirectional glass fibre prepreg layers are anisotropic: their properties in fibre direction differ from their properties perpendicular to the fibre direction. The aluminium layers however are only slightly anisotropic; the rolling of the aluminium sheets gives it somewhat higher strength in the rolling direction (L-direction) when compared with the perpendicular (LT-direction).

The properties of the constituents of Glare laminates are shown in table 3.1, made by Hagenbeek [10]. The properties of the glass fibres and the epoxy are listed, as well as the properties of a resulting UD laminate which is build up of these two materials. In the last column, the properties of the aluminium 2024-T3 sheets is given. The S in the S2 glass fibres stands for 'Strength' as these fibres possess a high strength and elastic modulus [24].

Table 3.1: Calculation of the glass-fibre epoxy properties from S2 glass-fibre and epoxy data from literature and a fibre volume fraction of 60%. If not stated otherwise the constituents' data is taken from (Matweb 2004). From Hagenbeek [10]

Property	Unit	S2 glass fibre	Epoxy	UD laminate	2024-T3
E_1	GPa	86.9 (88.0[f])	3.9[a] (1.85[f])	53.7 (54.0[f])	73
E_2	GPa	86.9 (88/0[f])	3.9[a] (1.85[f])	9.1 (9.4[f])	73
ν_{12}	-	0.23 (0.33[f])	0.37[b]	0.29 (0.33[f])	0.33
G_{12}	GPa	35.3[c] (33.1[f])	1.4[c]	3.4 (5.5[f])	28
α_1	μ m/m-°C	1.6 (5.2[f])	100 (75.0[f])	4.5 (6.1[f])	23.2
α_2, α_3	μ m/m-°C	1.6 (5.2[f])	100 (75.0[f])	41.0 - 55.2[d] (26.2[f])	23.2
ρ	g/cm^3	2.46	1.2	1.96 (2.0[f])	2.78

[a] Estimated stiffness value based on (Spies 1978) and (Shenoi and Wellicome 1993).
[b] Poisson's ratio is taken from (Shenoi and Wellicome1993).
[c] Calculated value with G12 = E = 2(1 + 12).
[d] Calculation is based on the alternative rule of mixtures given by (Hyer 1998).
[e] Constituents' data is taken from (Graafmans 1995). The calculation for the UD laminate is based on this data and a rule of mixtures given by (Behrens 1968).
[f] (Structural Laminates Industries 1993b) data and calculation (1993a), based on Classical Laminate Theory found for example in (Spies 1978), (Gurdal, Haftka, and Hajela 1998), (Jones 1999) and (Hyer 1998) amongst others.

Before the aluminium sheets are bonded to the glass fibres, the aluminium sheets and the glass fibres are pre-treated to improve adhesion. For the aluminium layers, this pre-treatment consists of degreasing, pickling, anodizing, and priming the aluminium sheets with a corrosion inhibiting primer. The glass fibres are pre-impregnated with the FM94 epoxy resin. After layup, the aluminium layers and the glass fibre prepreg are cured in an autoclave at a temperature of 120°C and a pressure of 6 bar [2], to form a consolidated laminate.

Due to a difference in thermal expansion coefficients of aluminium 2024-T3 and glass fibre prepreg, shown in the 5th and 6th row table 3.1, the aluminium shrinks more during cooling down, but is restricted from doing by the glass fibre layers. This results in a compressive residual stress in the glass fibre prepreg and a tensile residual stress in the aluminium, when the laminate is at room temperature. The tensile residual stresses in the aluminium layers result in a shorter fatigue initiation life as elaborated on in section 3.3.

Within a Glare laminate, the aluminium layers are stacked such that their L-direction (and thus also LT-direction) are aligned. As a convention for the orientation of the unidirectional glass fibre layers, this longitudinal direction is named the 0-degree orientation. Any rotation of a glass fibre layer in the x-y plane shown in figure 3.1 can now be expressed in the variable θ. A unidirectional glass fibre layer with its fibres aligned in the longitudinal direction of the laminate is 'a 0-layer', while a layer with its fibres aligned in the LT direction is rotated 90 degrees with regards to the L-direction, thus named a '90 layer'.

6 standard Glare grades are defined, as shown in table 3.2. The glass fibre layers are positioned in the 0, 45, -45 or 90 degree orientation. An example of a laminate is shown in figure 3.2. This is a Glare 3 laminate, signified by the fibres in the length L, (0) ,direction, as well by fibres in the LT, (90) direction. The layup consists of: [2024-T3/0° glass/90° glass/2024-T3/90° glass/0° glass/2024-T3] and is coded as: Glare 3-3/2-0.3 [2]. Thus, this is a Glare 3 laminate, with 3 aluminium 2024-T3 layers with a thickness of 0.3 mm and two fibre layers, each layer consisting of a 0° and 90° glass fibre prepreg layers.

Table 3.2: Material composition and main beneficial characteristics of Glare laminates. From Roebroeks [11]

Glare grade	sub	Metal sheet thickness [mm] and alloy	Prepreg orientation* in each fibre layer**	Main beneficial characteristics
Glare 1	-	0.3-0.4 7475-T761	0/0	fatigue, strength, yield stress
Glare 2	Glare 2A	0.2-0.5 2024-T3	0/0	fatigue, strength
	Glare 2B	0.2-0.5 2024-T3	90/90	fatigue, strength
Glare 3	-	0.2-0.5 2024-T3	0/90	fatigue, impact
Glare 4	Glare 4A	0.2-0.5 2024-T3	0/90/0	fatigue, strength in 0 direction
	Glare 4B	0.2-0.5 2024-T3	90/0/90	fatigue, strength in 90 direction
Glare 5		0.2-0.5 2024-T3	0/90/90/0	impact
Glare 6	Glare 6A	0.2-0.5 2024-T3	+45/-45	shear, off-axis properties
	Glare 6B	0.2-0.5 2024-T3	-45/+45	shear, off-axis properties

Standard Glare grades from [13].
*All aluminium rolling directions in standard laminates are in the same orientation; the rolling direction is defined as 0°, the transverse rolling direction is defined as 90°.
** The number of orientations in this column is equal to the number of prepregs (each nominally $0.133mm$ mm thick) in each fibre layer.

3.3 Fatigue in Glare

The fatigue damage development in a Glare laminate subjected to a fatigue loading starts with fatigue initiation period. Two new surfaces (a crack) are created in the aluminium layer from an existing flaw or stress concentration. The mechanism of fatigue crack initiation in the aluminium layers of a Glare laminate is identical to that of monolithic aluminium, with the notion that the stress state in the aluminium layers in the Glare laminate is influenced by the presence of the glass fibre layers [2]. The glass fibre layers influence the stress state within the aluminium layers in magnitude and direction in the following manner:

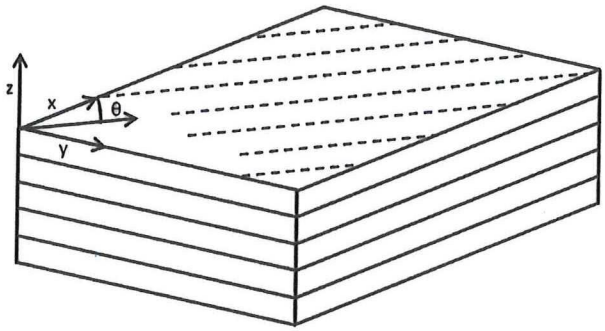

Figure 3.1: Convention of fibre orientation of the laminate

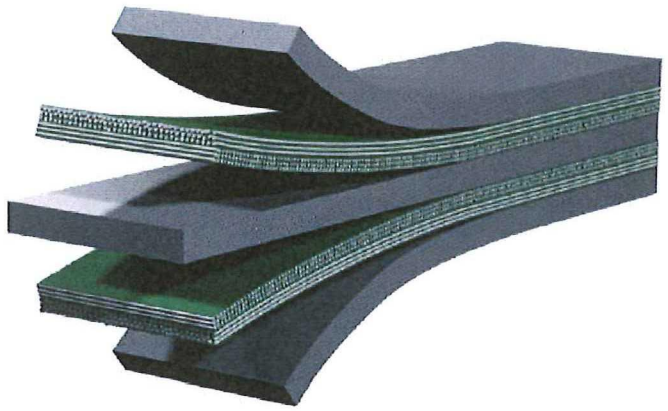

Figure 3.2: Schematic representation of Glare 3 laminate from [2]

- As a result of the higher Young's modulus of aluminium 2024-T3 compared to that of glass fibre prepreg (73 GPa versus 54 GPa), the stresses in the aluminium layers of the laminate are higher than the applied stress on the complete laminate.
- The direction of the glass fibre layers influence the stress state in the aluminium layers of the laminate. In a Glare 6 laminate for instance, the fibre layers are at an angle of $+-45°$. When an external tensile load is applied, the stress state in the aluminium layers within the laminate will differ from that of monolithic aluminium under an identical loading. For instance, the location of fatigue initiation around a circular through hole within the Glare laminate is changed, as the location of the stress concentration is influenced by the presence of the anisotropic fibre layers.
- The aluminium and the glass fibre prepreg possesses different thermal expansion coefficients, as shown in table 3.1, causing a compressive stress in the fibre layers and tensile stresses within the aluminium layers when the laminate is at room temperature, effectively raising the tensile stresses in the aluminium layers when a tensile load is applied.

Two of these factors increase the magnitude of the stress in the aluminium layers when a fatigue load is applied, which in turn causes fatigue cracks in the aluminium layers to initiate earlier than a monolithic aluminium specimen of identical geometry. This is a drawback of Glare compared to monolithic aluminium, but Glare compensates for this in its total fatigue life, with a much slower crack propagation than aluminium, as shown in figure 3.3.

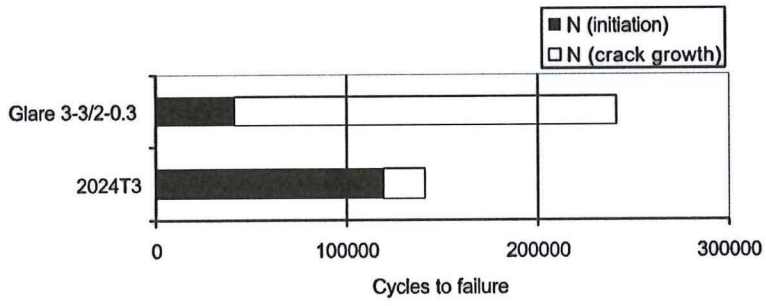

Figure 3.3: Comparison of the initiation life and growth life between Glare and aluminium 2024-T3, from Homan [3]

As an engineering approach, Homan [3] shows that the fatigue initiation life of the aluminium layers in Glare can be equalled to the fatigue life of monolithic aluminium, if the stress state in the aluminium layers is similar to that in the monolithic aluminium. This is a very valuable notion, as it enables the use of extensive existing data on fatigue life in monolithic aluminium to predict the fatigue initiation life in Glare. A comparison by Homan [3] of the fatigue initiation life of a Glare laminate using the fatigue life of aluminium 2024-T3, is presented in figure 3.4. It shows that this method yields good results. In [25], Alderliesten demonstrated that choosing a transition length of 1 [mm] yields the best results for this method.

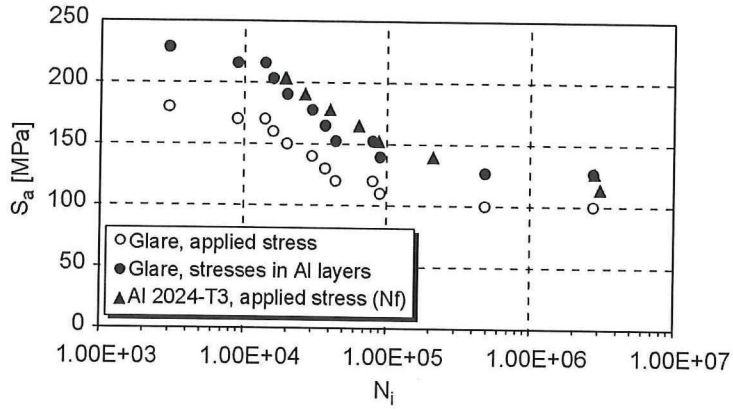

Figure 3.4: Comparison of fatigue initiation lives between Glare 3-3/2-0.3 and 2024-T3 unnotched specimens at RT. Stresses in Glare are related to the overall applied stresses as well as to the stresses in the aluminium layers. from Homan [3]

When the crack length in the aluminium becomes larger than the size of 0.1 mm to a few millimetres, the crack growth mechanism changes. The crack growth is no longer governed by surface defects in the aluminium layers which raise the stress locally, but it is dependent on the crack resistance as a bulk material property of the aluminium [26].

At this point the fibre layers start to play an active role in the crack growth rate [27]. The fatigue insensitive fibres start to bridge the crack; part of the load that was carried by the now cracked aluminium is transferred by the fibres over the crack. In this way, the fibres restrain the crack opening in the aluminium layers, reducing the stress intensity at the crack tip. This is shown in figure 3.5 from Alderliesten [2]. Two mechanisms controlling the crack growth are identified: the crack growth in the aluminium layers and the fibre layers delaminating at the fibre-metal interface, bridging the gap. These two mechanism influence each other.

The fibre layers transfer part of the load over the cracked aluminium, shown in figure 3.5. The stress transfer from the intact aluminium layers to the glass fibre layers causes a cyclic shear stress at the interface between the aluminium and the fibre layers [2]. These cyclic shear stresses cause a delamination between the fibre and aluminium layers. A delamination caused by the application of a fatigue load is called a fatigue delamination.

In an overview of de Vries [7] the potential locations within the laminate where the glass fibre delaminate from the aluminium layers are indicated. Rodi [4] writes that it is general practice to design the FML such that cohesive failure of the resin rich layer is the critical failure mode. This is done by modifying the energy required for adhesive failure by proper pre-treatment of the glass fibres and aluminium layers. As the glass fibres delaminate from the aluminium, the length over which the fibres can be stretched increases locally, reducing the stress in the fibres that bridge the crack.

The stress intensity at the crack tip in the aluminium layers are influenced by the bridging fibres and the plasticity in the wake of the crack tip. When a fatigue crack in the metal

layer of Glare propagates, it creates a plastic zone in front of the crack tip. As the fatigue crack grows through the plastic zone, this plastic created in previous cycles is now located at the wake of the fatigue crack tip. This plasticity reduces the crack tip opening displacement, reducing the stress intensity at the crack tip.

The glass fibre prepreg, which is relatively insensitive to fatigue, bridges the crack, also reducing the stress intensity at the crack tip. During the crack growth phase the stress intensity factor at the crack tip in the aluminium layers remains almost constant, instead of an increase in stress intensity factor which is observed in monolithic aluminium.

There is balance between crack growth in the aluminium which causes larger crack opening, which increase the stresses in the delaminated fibres, and the size of the delamination, which enables the fibres to stretch over a longer length, decreasing the stresses in the fibres. If the stress in the fibres reaches a critical value, the delamination will grow. The magnitude of the stresses in the fibres as a result of the crack opening depends on material and loading parameters. This critical value depends on the delamination resistance of the metal-fibre interface [2].

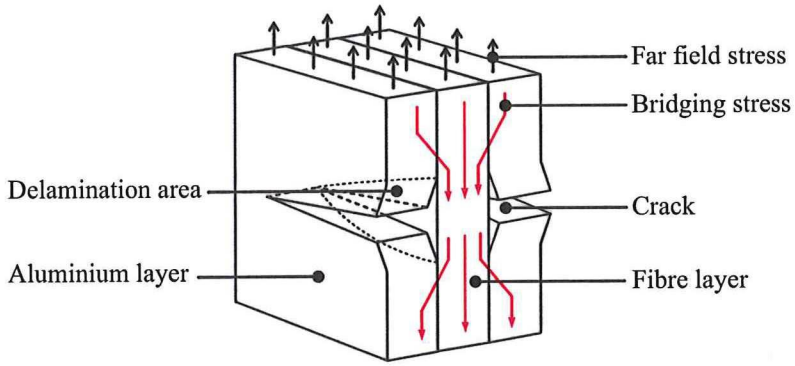

Figure 3.5: Illustration of the effect of fibre bridging, from Alderliesten [2]

3.4 Failure sequence of FMLs with fatigue cracks under quasi-static loading

This section describes the failure sequence of Glare laminates under quasi-static loading, containing with fatigue cracks which are bridged by fibres. Two mechanisms can be distinguished during failing of the Glare laminate under quasi-static loading: plasticity in the aluminium layers and a growth of the delamination. These two mechanism occur at the same time, and influence each other.

When the load on a Glare laminate with fatigue cracks is quasi-statically increased, the existing fatigue delamination will grow into the loading direction. Due to the increased load, the bridging fibres transfer more load over the cracks in the aluminium layers. This increases the shear stress at the boundary of the fatigue delamination. When the shear stresses becomes higher than the delamination resistance of metal-fibre interface, the fatigue delamination ex-

tends further in the direction of the load. This delamination is called the static delamination. This extension of the delamination allows the delaminated fibres to elongate more, reducing the stress in the fibres. This will postpone final failure. The visual difference between the fatigue delamination and the static delamination is shown by Rodi [4] in figure 3.6. The darker coloured part of the delamination is the fatigue delamination, and the lighter coloured part the static delamination.

When the load on a Glare laminate with fatigue cracks is quasi-statically increased, plastic zones develop in front of the crack tip, and at the boundary of the delamination. Due to the increased loading, the stress intensity at the crack tip is increased. This causes an increase in the plastic zone size in front of the crack tip. However, this plastic zone is significantly smaller compared to that in monolithic aluminium with identical crack geometry and loading, as part of the load is now transferred over the crack by the glass fibres. The increase in stress transferred by the fibres over the crack in the aluminium, when the load is quasi -statically increased causes plasticity in the aluminium at the delamination boundary.

The plasticity in the aluminium layers and the static delamination influence each other [4]. As the plastically deformed area in front of the crack tip loses stiffness, the fibres bridging the crack are loaded more. Additionally, due to the high plastic deformation of area in front of the crack tip, fibres also delaminate in this area [28]. In this case, the plasticity in the metal layers causes larger static delaminations.

However, plasticity in metal layers also reduces the growth of the static delamination. As the metal is plastically deformed, part of applied energy is absorbed, reducing the elastic strain energy in the laminate, which may delay occurrence of delamination.

Concluding, complex redistribution of the load take place between the metal and fibre layers, in which main drivers are the plasticity of the metal layers and the delamination resistance of the fibre-metal interface.

Final failure of the laminate with fatigue cracks is caused by an overloading of the glass fibres. The glass fibres fail at a strain of around 4.7% , while aluminium 2024-T3 at a strain of 19% [8]. From this perspective it can be explained that a large static delamination is beneficial for the residual strength of the material; it allows the fibres to strain over a longer length, decreasing the fibre stress and thus postpone failure. When the fibres fail they a release their stored elastic energy into the remaining material.

Whether the remaining material is able to take up this energy without failing depends on the crack length. For longer crack lengths, more load is stored in the fibres that bridge the crack. As these fibres store a large part of the load, the material that is left is not strong enough to take this load, resulting in brittle failure of the whole, without stable crack extension. Shorter fatigue cracks lengths show some stable crack propagation before unstable failure occurs while for longer fatigue cracks no stable crack extensions takes place. The location of the first fibre failure fail now depends on the fibre bridging stress on the one hand, which has a peak at the crack tip, and the far field stress, which generates a peak at the origin of the crack [4].

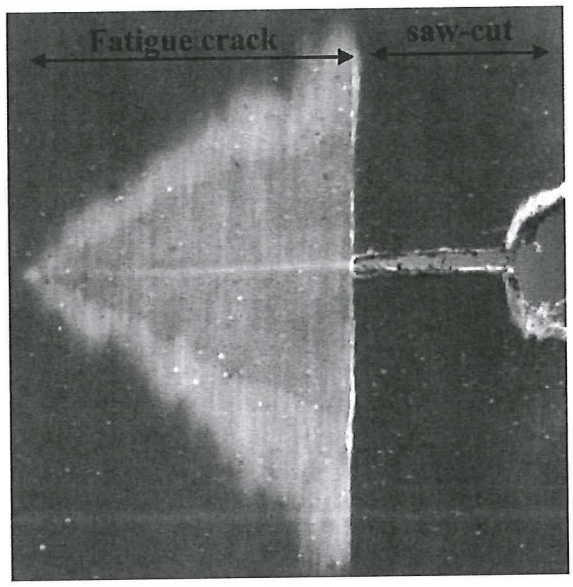

Figure 3.6: Darker coloured fatigue delamination, lighter coloured the static delamination from Rodi [4]

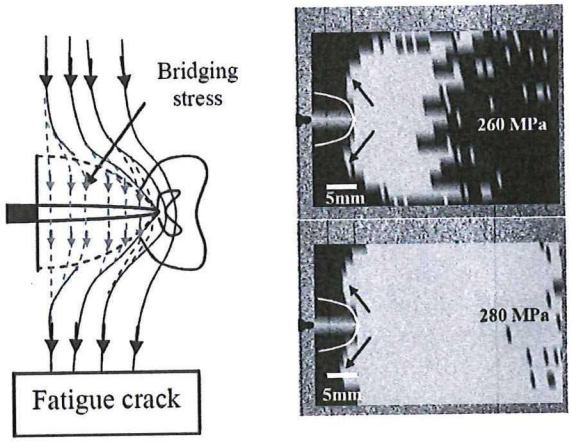

Figure 3.7: Illustration of the plastic zone in quasi-statically loaded Glare with a fatigue crack, from Rodi [4]

Chapter 4

Design of FML reinforced fuselage member

4.1 The A400M aircraft

The A400M is a military transport aircraft developed by Airbus, able to perform both tactical (short- to medium range) and strategic (long range) missions. An image of it is shown in figure 4.1. It is designed to operate in challenging conditions: short take off and landing distances, soft and rough airfields and to withstand enemy action [29].

To perform under these conditions, the aircraft features a robust design, including a high wing with a span of 42.2 meters, T tail and four counter rotating turboprop engines. The Airbus A400M features a payload of 37 tonnes, a maximum take off weight of 130 tonnes and a range of 6500km.

The design life is 10.000 flight cycles, or 30.000 flight hours or 30 years, whichever occurs first. Furthermore, the inspection threshold is 5000 flight cycles or 15.000 flight hours and the inspection interval is 2500 flight cycles or 7500 flight hours, whichever comes first, as stated by Plokker [6].

4.2 A400M frame member design

In the A400M, wing loads are introduced into the fuselage through aluminium frames member that connect the wing with the fuselage, as shown in figure 4.2a. Investigation showed that the frame member under the rear wing attachment is a single load path [6]. Failure of this frame member would lead to a loss of structural capability to carry the applied loads, which can lead to catastrophic failure of the aircraft. This leads to stricter inspection requirements, as this frame member needs to be inspected on small cracks instead of a failed member. The

Figure 4.1: The A400M, from Aviationweek [5]

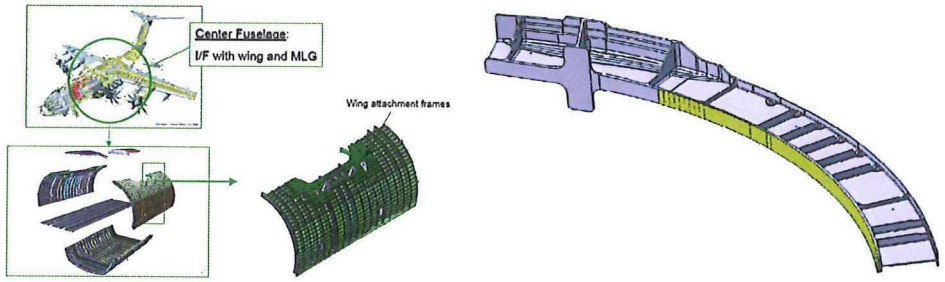

(a) Position of the frame member in the aircraft structure

(b) Aluminium frame with Glare reinforced inner flange

Figure 4.2: Design of the A400M fuselage frame member, presented by [6]

design had to be improved, as the concept of an integral frame member would lead to a severe weight impact [6].

Plokker [6] investigated the options for reinforcing the critical part of the frame. The wing spectrum causes high static loads and high fatigue stresses in the inner flange of the fuselage frame member under the rear wing attachment. Three concepts were studied for reinforcing the inner flange:

1. Thickening the inner flange of the frame to reduce the stress levels
2. Attaching a titanium strap to the inner flange
3. Attaching a Glare strap to the inner flange

The original design was a monolithic aluminium frame. As this was considered to be a single load path structure which was inspectable, slow crack growth had to be ensured. In order to obtain this slow crack growth, the stress in the frame member had to be decreased by increasing the thickness. The disadvantage of thickening the flange is that the fracture toughness decreases with an increasing material thickness. This results in smaller cracks being critical

for the structure. This makes the time between the crack becoming detectable and becoming critical smaller. As there need to be at least two inspections in which the crack can be found [20] and presented in chapter 2, more inspection intervals are necessary, or special equipment has to be used to enable the detection of smaller cracks.

In the case of concept 2 and 3, the function of the strap is to contain the damage in the case that fatigue damage is present in the flange, providing a second load path, redistributing the load and retarding crack growth. Plokker [6] showed that the FML strap proved to be the lightest solution, while showing a constant and slow crack growth, as well as a long critical crack length. The slow crack growth and long critical crack length makes it acceptable for longer cracks to be present, simplifying crack detection. For the designs including the strap, the product of the area and stiffness was kept the same as the initial design of the flange, to prevent a redistribution of loads or a change in the load path.

As the tools to assess the fatigue and damage tolerance performance of this hybrid design as a whole did not exist at Airbus, the strap and the aluminium flange were analysed separately in a conservative approach. To determine the critical crack length in the Glare strap, it was assumed that the aluminium flange was completely cracked, while the Glare strap should be able to carry the highest load expected during the lifetime, the limit load. To analyse when this critical crack length was reached, crack growth in the Glare strap was analysed. The FML strap was analysed separately, under a fatigue load spectrum that was determined by dividing the loads on the flange and the strap based on the individual stiffnesses of these parts. To justify the fatigue and damage tolerance approach of the design and analysis of the inner flange reinforced by the FML strap, a test pyramid of coupon, component and full scale tests were designed and executed. [1]

4.2.1 Fatigue damage growth approach used for the A400M frame member design

To predict the fatigue damage growth in the FML strap, an empirical model from the FML F&DT toolbox was used. As it is not possible to model a GLARE 2 laminate with the FML F&DT toolbox, the layup of a GLARE 3 laminate was used. This is a conservative choice, as 50% of the fibres in a GLARE 3 laminate are perpendicular to the loading direction, while all the fibres in a GLARE 2 laminate are in line with the loading.

4.2.2 Residual strength analysis

Müller [8] developed an approach to determine the residual strength of a Glare 3 panel with blunt notches present, and extended this approach to include the influence of fatigue cracks emanating from these blunt notches on the residual strength. Müller [8] stated that the strength of a sheet containing blunt notches (round holes) can be calculated from the ultimate strength of the material multiplied by a blunt notch factor, K_{bn}, that is approximately constant for hole type notches. For Glare 3 it was shown that a value of $K_{bn} = 0.64$ was a good approximation (For aluminium 2024-T3 0.9 seemed to be appropriate).

To calculate the strength reduction of the Glare strap due to fatigue cracks in the aluminium

layers, a net-section reduction approach was used. From the crack lengths in the aluminium layers, the cracked cross sectional area can be determined. The residual strength is then calculated by subtracting the strength that the cracked aluminium area would have provided, from the pristine strength of the strap. A more in depth discussion of this method is presented in section 5.4

Using this method, it was determined that a crack (all the aluminium layers cracked for an equal length) of 11 mm is the maximum crack length allowed in the reinforcement. [1].

4.2.3 Test program

To verify the fatigue calculations, a test program was performed at Airbus. 10 Coupons of a 5.2 mm thick 7085 aluminium flange attached to a Glare2A-16/15-0.4 laminate were tested on different fatigue amplitudes until a crack was detected. Crack detection was performed using comparative vacuum monitoring sensors. These circular sensors were placed around the rivet heads so that cracks protruding from under the rivet could be detected. The drawback was that the minimal crack length to be detected was 4.4 mm. This length was defined as initiation. After initiation was detected, the fatigue test was halted. Additionally, one identical specimen was used in pristine condition and tested for failure strength, and one coupon fatigue crack propagation was tested until the crack reached the end of the specimen. These coupons were provided to the TU Delft and used in this research to determine the residual strength curve.

Chapter 5

Residual strength methods for FML's with fatigue cracks

5.1 Introduction

This chapter presents the approaches from literature that describe the residual strength of Glare structures with fatigue cracks. For this thesis, it is assumed that the aluminium flange can be regarded as a standard Glare laminate, only with one thick aluminium layer, the aluminium flange. Since the development of Glare, several authors have published their work on predicting the residual strength of Glare structures [30], [8], [7] , [12], [4]. Directly applying the models developed for monolithic metal structures on FMLs is not possible, because the fibres play an important role in the failure of the laminate. However, many authors [30], [8], [7] , [12], [4] studied how existing residual strength approaches for metal can be modified to accurately predict the failure of Glare.

The R-curve approach, widely used and accepted in aircraft industry for metals, was studied by Vermeeren [30] and later De Vries [7] for application to Glare structures. This approach is explained in section 5.2. To better take plasticity in the material around the crack tip into account, Vermeeren [30] proposed the J-integral, explained in section 5.3.
Müller [8] and De Rijck [12] developed a reduced net section approach for Glare, based on the net section yield criterion in metals, explained in section 5.4.
Rodi [4] investigated the use of the Crack Tip Opening Angle (CTOA) approach to predict residual strength of Glare with through cracks and fatigue cracks. By taking into account the effect of fibre bridging and plasticity, a more accurate modelling of the mechanism is obtained. This approach is explained in section 5.5

5.2 The R-curve approach

A lot of research has been performed into applying existing residual strength approaches which were developed for metals to predict the residual strength of FMLs. Most of this research focused on the residual strength of FMLs with a through crack. This is because the residual strength of Glare with through-thickness-cracks is always lower than Glare with fatigue cracks, as shown by Vermeeren [30].

For this type of damage, the R-curve has proved to be a powerful approach to determine the residual strength of FMLs with through cracks, and is currently used in industry to assess the residual strength of aluminium aircraft structure [7].

The R-curve approach proposed by Irwin [7] is an energy balance between the energy available for crack growth or energy release rate (G) and the crack resistance of the material (R) to oppose crack growth. The power of this approach is that it can deal with stable crack extension and limited plasticity [7], opposed to the stress intensity factor approach which is only applicable for elastic fracture.

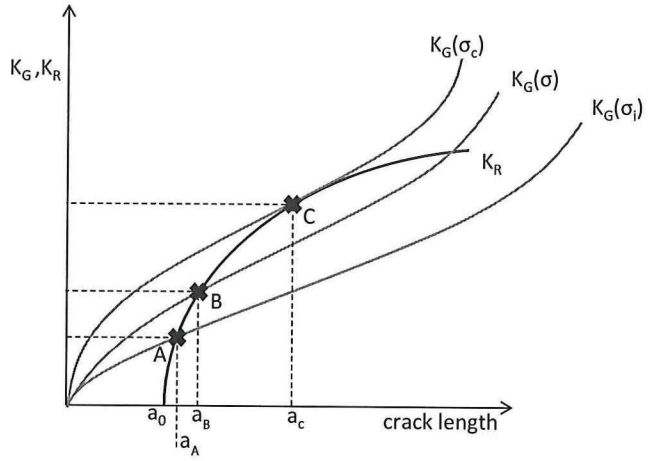

Figure 5.1: Schematic illustration of the R-curve from De Vries [7]

In the illustration from De Vries [7], shown in figure 5.1. The energy release rate G and crack growth resistance curve R are both functions of the crack length a, which is on the x-axis. Additionally, for every stress level, a different G curve exists, of which three are plotted in figure 5.1. Intersection points are indicated with crosses and named A and B, while the third line has only a tangency at C. Thus, for a centrally cracked plate, containing a crack with length $2a_0$ under an applied stress of σ_i the crack will grow to crack length a_A. No further crack growth is possible as the crack resistance R is higher for this stress level at this crack length. When the stress is increased to $G(\sigma)$ the crack grows in a stable manner to a length of a_B When the stress is further increased to σ_c, G remains higher than R for any crack length a, and thus instability is reached at point C, with a crack length of a_c.

From a fracture mechanics point of view the R-curve approach cannot be applied for FMLs

containing fatigue cracks, because there is often no stable crack extension. An effective crack length is hard to define as it seems smaller due to crack bridging, while the effective crack would later on appear to be longer than the width of the specimen due to net section yield [30].

Still, as a conservative approach, the R-curve could be used, by assuming a through crack with the average length of the cracks in the metal layers. However, Vermeeren [30] showed that for Glare 3 the strength of samples with identical crack length with the fibres intact is 5% to 40% higher depending on the sample width, crack length, and size of the delamination, while for Glare 2 this ranges from 40% to 100% higher, depending on the sample width, crack length and size of delamination. It could thus be said that, especially for Glare 2, this approach is overly conservative for Glare with fatigue cracks.

5.3 J-integral

Instead of using elastic fracture mechanics, elastic-plastic fracture mechanics could be used to describe the failure of a Glare laminate with fatigue cracks, bridges by fibres. An example of this is the J-integral approach, which is able to take into account moderate crack tip plasticity. However, it is a very complex method. Vermeeren [30] presented results obtained by Caprice [31] and concluded that the J-integral showed interesting results, but more experiments were necessary. However, to date there seems to be no new research into this approach. Additionally, a FEM is necessary to perform predictions, making it less versatile. The subject of the J-integral will thus not be discussed further in this chapter, as it is quite complex and not regarded as a suitable option to predict the residual strength.

5.4 Net section approach

5.4.1 Müller (1995)

As a part of the PhD thesis of Müller [8], the residual strength reduction of Glare 3 due to fatigue cracks was investigated and analysed. Müller [8] developed an approach to determine the residual strength of a Glare 3 panel with blunt notches present, and extended this approach to include the influence of fatigue cracks emanating from these blunt notches on the residual strength.

Müller [8] stated that the strength of a sheet containing blunt notches (round holes) can be calculated from the ultimate strength of the material multiplied by a blunt notch factor, K_{bn}, that is approximately constant for hole type notches. For Glare 3 it was shown that a value of $K_{bn} = 0.64$ was a good approximation. The formula for the blunt notch strength from [8] is shown in equation 5.1.

$$\sigma_{bn} = K_{bn} \cdot \frac{\sigma_U \cdot A_{net}}{W \cdot t} \tag{5.1}$$

where:

σ_{bn}	is the blunt notch strength based on the gross section
K_{bn}	is the blunt notch factor
σ_U	is the tensile strength of the sheet material
A_{net}	is the net section area
W	is the specimen width
t	is the sheet thickness

The value of σ_U, the tensile strength of the Glare 3 sheet, can be determined using the rule of mixtures of the constituents, called the Metal Volume Fraction (MVF) in the case of FMLs.

$$MVF = \frac{\sum_1^n t_{al}}{t_{tot}} \tag{5.2}$$

where:

n	is the number of aluminium layers
t_{al}	thickness of aluminium layer
t_{tot}	is the total thickness of the laminate

Furthermore it is known that the glass fibre prepreg has a failure strain of 4.5% while the aluminium 2024-T3 constituent has a failure strain of 19% [8]. However, a small correction factor is necessary due to the residual stresses introduced in the laminate after curing. At room temperature, the fibres are under a small compressive strain of 0.15 %, while the aluminium experiences a small tensile strain, of 0.05%. It can be imagined that these strain values depend on the layup of the Glare as well, as a change in volume of the constituents will also change the residual strain distribution. Thus, a failure strain of 4.7% will be used for the glass fibre prepreg.

When the glass fibre prepreg fails, the stress is redistributed to the aluminium. This sudden increase of stress in the aluminium layers will cause failure of the entire sheet. Thus the laminate will fail at failure of the glass fibre prepreg layers. Now using the rule of mixtures, the strength of a Glare 3 sheet can be calculated:

$$\sigma_U = (MVF) \cdot \sigma_{al(\epsilon=4.7\%)} + (1 - MVF) \cdot \sigma_{U,pL} \tag{5.3}$$

where:

σ_{al}	is the ultimate strength of the aluminium
Σt_{pL}	is the sum of the thicknesses of all the glass fibre prepreg layers in the laminate
$\sigma_{U,pL}$	is the ultimate strength of the glass fiber prepreg in the loading direction

This approach gives a prediction for the blunt notch strength of a Glare 3 laminate. Due to repetitive loading of the strap with loads smaller than the limit load case, fatigue cracks

start to grow in the aluminium layers at the edge of blunt notch. While these cracks propagate in the aluminium layers, the glass fibre prepreg layers delaminate locally from the aluminium but remain able to carry the load. As an engineering approach, it may be assumed that at the locations where the aluminium is cracked, only the glass fibres will carry load. The reduction of strength due to the presence of fatigue cracks can thus be approximated by:

$$\sigma_{reduction} = A_{cracked} \cdot \sigma_{al(\epsilon=4.7\%)} \tag{5.4}$$

Combining this equation with the equation in (5.3), leads to:

$$\sigma_{residual,cracked} = \sigma_{residual,uncracked} - \frac{2 \cdot a}{A_{net}} \cdot \Sigma t_{al} t_{lam} \cdot \sigma_{al(\epsilon=4.7\%)} \tag{5.5}$$

where:

$\sigma_{residual,cracked}$	is the strength of the laminate with fatigue cracks present
$\sigma_{residual,uncracked}$	is the strength of the laminate without fatigue cracks present
$2 \cdot a$	is the total crack length
A_{net}	is the net-section area
Σt_{al}	is the sum of the thicknesses of the aluminium layers in the laminate
t_{lam}	is the thickness of the total laminate
$\sigma_{al(\epsilon=4.7\%)}$	is the stress in the aluminium at a strain of 4.7%

5.4.2 De Rijck (2005)

The approach developed by de Rijck follows the same steps as the approach by Müller, but replaces the blunt notch reduction factor with a blunt notch factor based on the blunt notches of the constituents. Müller used an empirically determined blunt notch factor ($K_{bn} = 0.64$ for Glare 3). The drawback of such an empirical blunt notch factor based on the laminate is that for every new laminate configuration a new blunt notch factor has to be determined experimentally. De Rijck replaced this empirical blunt notch factor of a laminate with blunt notch factors for the materials of which the laminate consists of, in this case glass fibre prepreg and aluminium 2024-T3. Using the MVF the blunt notch strength of any laminate consisting of aluminium 2024-T3 and glass fibres can be determined. The values for the blunt notch strength of aluminium 2024-T3 and glass fibre in different standard glare laminates is presented in table 5.1

The advantage of this modification is that only the values of the glass fibre and aluminium layers have to be determined, which are then applicable for every laminate. The values of this table can be explained as follows: Glare 2A has all the fibres in the loading direction, thus they have a high strength in this application. In Glare 2B they are under a 90 degree angle, having a negligible contribution. For Glare 3 and 4, the laminate exists of fibres in the 0 and the 90 direction, resulting in a mixed strength.

In formula form, to determine the residual strength of a laminate, first the Metal Volume Fraction (MVF) has to be determined, which is identical to the MVF in the method of Müller, shown in as shown in equation 5.2.

Table 5.1: Contribution of each layer to the blunt notch strength for standard Glare laminates, from De Rijck [12]

Glare	Layer contribution	Blunt notch strength (MPa)
Glare 2A	Metal	417
	Fiber	1193
Glare 2B	Metal	417
	Fiber	0
Glare 3	Metal	417
	Fiber	597
Glare 4A	Metal	417
	Fiber	795
Glare 4B	Metal	417
	Fiber	398

With the MVF determined, the blunt notch strength of the laminate σ_{bn} can be determined, as shown in equation 5.6, in which $\sigma_{bn_{al}}$ is the blunt notch strength of the aluminium from table 5.1, and $\sigma_{bn_{fiber}}$ the blunt notch strength of the fibre from the same table.

$$\sigma_{bnGlare} = MVF \cdot \sigma_{bn_{al}} + (1 - MVF) \cdot \sigma_{bn_{fiber}} \tag{5.6}$$

Now with the blunt notch strength of the Glare determined, the reduction of the blunt notch strength, and thus the residual strength, can be determined by subtracting the blunt notch strength that the area of the aluminium that is cracked would have contributed to the total residual strength, as shown in equation 5.7

$$\sigma_{res_{cracked}} = \sigma_{bn_{Glare}} - MVF \cdot \frac{A_{al_{cracked}}}{A_{al_{pristine}}} \sigma_{bn_{al}} \tag{5.7}$$

Where $A_{al_{pristine}}$ is defined as shown in equation 5.8

$$A_{al_{pristine}} = b \cdot t_{al} \cdot n_{al} \tag{5.8}$$

where:

$\sigma_{res,cracked}$	Residual strength of the Glare laminate
$\sigma_{BN_{Glare}}$	Blunt notch strength from equation 5.6
$\sigma_{BN_{al}}$	Blunt notch strength from table 5.1
$A_{al_{cracked}}$	Total area of the aluminium removed due to fatigue crack
$A_{al_{pristine}}$	Pristine area of aluminium in Glare
b	Width of specimen
t_{al}	Thickness of single aluminium layer
n_{al}	Number of aluminium layers

An example of the results obtained by De Rijck with this method is shown in figure 5.2, where the square markers are the results from residual strength tests, and the black line the

predicted residual strength as a function of a percentage of the aluminium in the FML laminate that was cracked. As can be seen in figure 5.2 this method gives good results, especially considering the simplicity of this approach. De Rijck applied an extra reduction factor of 10% on the blunt notch strength to account for the influence of secondary bending which was present in the lap joints that were tested in his thesis.

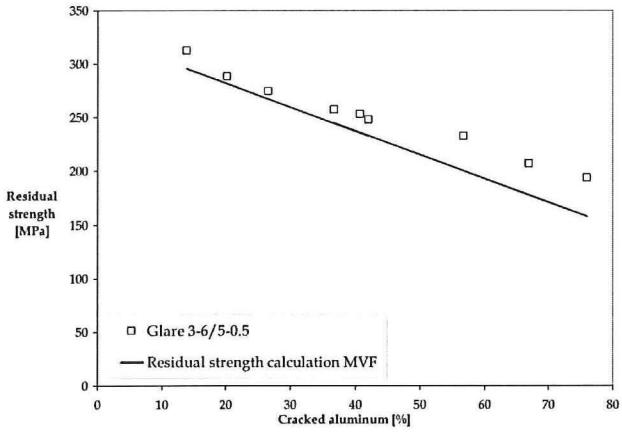

Figure 5.2: Example of the data points obtained by experiments by De Rijck, shown as the squares, and the residual strength calculation as the black line

5.5 Crack tip opening angle

De Vries [7] investigated the applicability of the Crack Tip Opening Angle (CTOA) approach, illustrated in figure 5.3, for the prediction of failure of Glare laminates containing a sharp through crack. The CTOA approach assumes that there exists a relationship between the critical crack tip opening angle ($CTOA_c$) and the propagation of a crack. When the $CTOA_c$ is reached when a load is applied, the crack will grow, until the CTOA is again lower than the $CTOA_c$. Furthermore, it is assumed that this $CTOA_c$ should remain constant during stable crack propagation. However, measurements show that for the first part of the crack growth, this is not the case, this is shown in figure 5.4, from measurements by Rodi [4]. Because the CTOA is a very local parameter, it can be easily implemented in a FEA model to predict the crack growth [7]. Rodi [4] Made a numerical implementation of the CTOA in a model to predict crack growth in Glare laminates with through cracks, and with part through fatigue cracks. This is elaborated on in the next section.

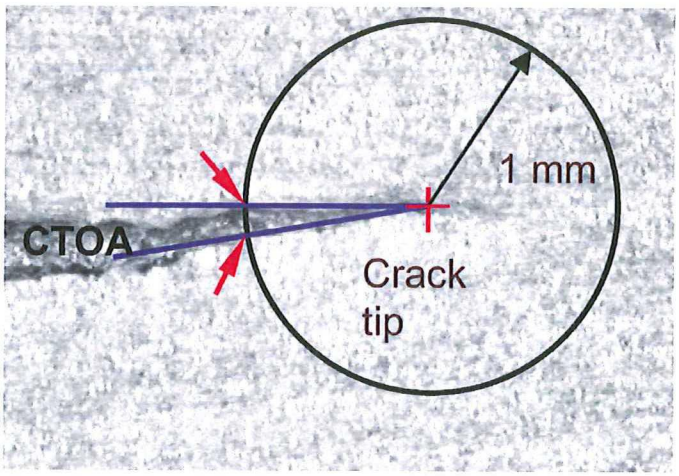

Figure 5.3: Definition of the CTOA, from De Vries [7]

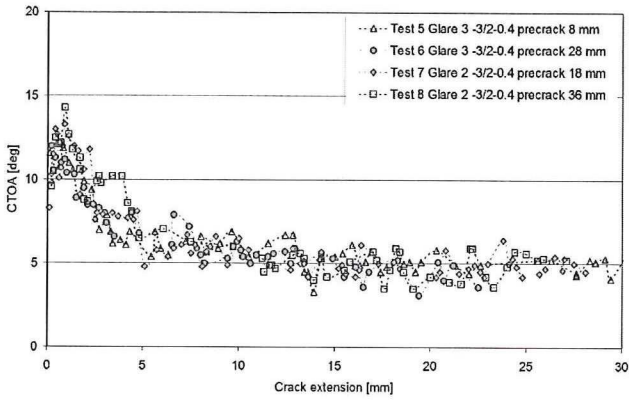

Figure 5.4: Example of the CTOA measured obtained in the research by Rodi [4].

5.5.1 Numerical implementation of the CTOA criterion for fatigue cracks

The following input parameters are needed for the numerical calculation of fracture using the CTOA approach:

- Material properties of the aluminium and glass fibre layers (Young's modulus, shear modulus, yield strength, Poisson's ratio etc)
- Geometry and loading parameters (coupon dimensions, force on crack)
- Failure criteria: CTOA for aluminium 2024-T3, and Strain-to-failure of S2 glass embedded in FM94
- The critical strain energy release rate, Gc.
- The initial fatigue delamination shape
- The saw-cut length and the initial fatigue crack length

The model developed by Rodi [4] uses superposition principle to obtain the CTOA from the several failure events (like delamination extension, fibre failure and plastic zone extension) that occur which influence the CTOA. Crack growth takes place when the CTOA of the FML reaches the $CTOA_c$ of the metal, taking into account the delamination extension, fibre failure and plastic zone extension.

Using the following assumptions from Rodi [4]:

- *Linear elastic-plastic fracture mechanics can be applied.*
- *The metal crack growth occurs in mode I only and is governed by the CTOA parameter.*
- *Metal and composite constituents are equally strained if no delamination is present.*
- *The CTOA curve for the metal constituent alone is also valid for the metal constituent of the FML being considered.*
- *When fibre failure occurs all the energy stored inside the broken fibres transfers to the intact part of the laminate. Fibre failure occurs when the strain-to-failure of the fibre is reached locally.*

The CTOA in the metal depends on the following contributors:

- Opening of the crack due to the far field load, as well as plastic deformation
- A crack closure due to fibre bridging stress
- The opening of the crack due to breaking of the fibres

Opening of the crack due to the far field load, as well as plastic zone in front of the crack tip
The opening of the crack due to far field load can be determined using the Westergaard stress function Z, using an equation which takes into account the plastic zone. Irwin's correction factor is used to account for plasticity.

$$\nu_m(x) = \frac{1}{2G}\left(\frac{\kappa+1}{2} Im\bar{Z} - yReZ - \frac{\kappa-3}{2}\frac{\sigma_m}{2}y\right) \tag{5.9}$$

More information on the implementation of this equation can be found in the report of Rodi [4].

Plasticity in the wake of the crack tip When the cracks extends through the plastic zone in the aluminium, the plasticity which is now behind the crack tip, will also influence the crack tip opening angle. This plasticity in the wake of the crack tip causes the crack to close, resulting in a smaller COD than without plasticity. To take this plasticity in the wake of the crack into account, Rodi [4] modelled the residual plastic strain by means of yielded bar elements.

Displacement compatibility equation
The vertical displacement of the metal layers at the boundary of the delamination has to be equal to the elongation of the fibres over the delaminated length. Also, the deformation of the prepreg must be added to this equation, as elaborated on in the thesis by Alderliesten [2]. The vertical displacement in the crack in the aluminium thus depends on the opening contribution of fibres failed, (energy stored in fibres released into metal) and the closing contribution due to bridging fibres.

A crack closure due to fibre bridging stress
To calculate the bridging stress within the bridging fibres, the opening of the metal layers is equalled to a part deformation of the fibres and a part elongation of the prepreg over the delaminated length.

$$v_m(x,y) - v_{br}(x,y) + v_f(x,y) = \delta_f(x) + \delta_{pp}(x) \tag{5.10}$$

As there exists no closed solution for this equation for $\sigma_{br}(x)$ which is present on both sides of this equation, (in δ_f and in v_{br}), the solution is approached numerically by dividing the crack length is N bars with variable width w_i.

The opening of the crack due to breaking of the fibres
Energy stored by fibres that break is released into the material. The load released into the metal layers, $\sigma_{metal,f}$ is equal to the load per unit of width stored in the broken fibres at the moment of failure:

$$\sigma_{metal,f} = \sigma_{f,failure}\frac{t_{fibre}n_{fibre}}{t_{metal}n_{metal}} \tag{5.11}$$

To determine when failure of fibres occurs, it is assumed that there is already a crack like damage in the fibre layer present, in the case of Rodi [4] a saw cut, with a length of $a_{fibre} = a_s + \Sigma w_k$, where a_s is the initial saw cut and Σw_k the cumulative extension of broken fibres.

$$K_{If} = \beta \sigma_{f,farfield} \sqrt{\pi a} \tag{5.12}$$

where $\sigma_{f,farfield}$ is the far field stress in the composite layer from CLT. Then:

$$\sigma_f(x) = \frac{K_{If}}{\sqrt{2\pi x}} \tag{5.13}$$

Now the total fibre stress in the wake of the crack can be determined by adding the bridging stress to far field stress.

Delamination growth

Static delamination growth is determined by using a Strain Energy Release Rate (SERR) concept similar to that of fatigue delamination growth. However in the fatigue case it is based on Paris type relation, while static delamination growth is based on critical value of SERR, Gc. A Complex relationship between plastic zone in metal layers and static delamination is modelled in simplified manner. Using the following equation for each bar element:

$$G(x) = \frac{n_j t_f}{2jE_f} \left(\frac{n_m t_m E_m}{n_m t_m E_m + n_f t_f E_f} \right) (\sigma_{f,tot}(x))^2 \tag{5.14}$$

This is then solved for each bar element until $G < G_c$. When the delamination progresses, the local stress is reduced and thus the SERR reduces. When all locations along the delamination satisfy $G < G_c$, the load is increased and the loop starts over.

5.6 Conclusions

In this chapter, the approaches to predict the residual strength of Glare are discussed.
The R-curve is a good approach to predict the residual strength of Glare with through cracks, as it is widely accepted in aircraft industry. However, this approach has several drawbacks. New experimental data is required for each configuration. The predictions made with the R-curve for Glare with fatigue cracks it is overly conservative.

The CTOA approach shows promising results for Glare with cracks. For through cracks, the method has been shown to be accurate and effective in predicting failure. The CTOA approach for fatigue cracks however has been validated by a relatively small number of experimental data. Because failure of fatigue cracks is more complicated, simplifications had to be made, resulting in a model with less predictive capability than the through the thickness crack model. The CTOA depends on the thickness of the metal layers. New experimental data has been acquired if the metal layers differs. Additionally, it was observed that the value for G_c has a strong dependency on the MVF, stiffness of constituents, surface treatment and yielding strength of the metal. This dependency on many variables that have to be obtained experimentally makes it not ideal in an optimization tool.

The net section approaches of Müller [8] and De Rijck [12] do not model the mechanics of fracture. However, they do give reasonable residual strength results. They do not require a finite element model or lay-up dependent experimental results as input. This makes these approaches versatile and easy to implement in an analytical approach.

The De Rijck method has the preference, as it does not require an experimentally determined blunt notch factor which depends on the lay up, but can use the already determined blunt notch values presented in table 5.1. This method will thus be used in this thesis to predict the residual strength of the A400M frame flange reinforced with a Glare strap.

Chapter 6

Experiments

6.1 Introduction

To obtain the experimental data to validate the predictions using the De Rijck [12] approach to predict the residual strength, residual strength tests have been performed on coupons representing the A400M flange reinforced with a Glare strap. Creating differing levels of fatigue damage in the coupons was necessary and this opportunity is used to validate the general FML Fatigue Tool developed by Spronk [1]

This chapter presents the experiments in the following order: In section 6.2, the creation of different levels of fatigue damage in the available coupons is presented. Additionally, the method of predicting the crack lengths as a result of the applied load, using the general FML Fatigue Tool developed by Spronk [1] is elaborated on. This is followed by section 6.3 in which the approach to the residual strength test is presented.

6.2 Fatigue Tests

6.2.1 Programme objective

The primary programme objective is to create fatigue damage in the coupons. Secondary is the measurement of the relationship between the number of fatigue cycles that were applied and the crack length, to validate the predictions made with general FML Fatigue Tool developed by Spronk [1]

6.2.2 Coupon geometry

Ten coupons representing the A400M frame member flange reinforced with an FML strap are provided by Airbus. These coupons are approximately 500 mm x 90 mm x 16 mm (length

x width x height) and consist of a 5.2 mm thick aluminium 7085 layer, which is bonded and riveted with 8 interference rivets to a Glare2A-16/15-0.4 laminate. The interface between the aluminium 7085 and Glare2A consist of a FM94 adhesive layer and 2 glass fibre prepreg layers [32]. A sketch of the coupon is shown in figure 6.1.

These coupons have previously been used in a testing program by Klein [32] to investigate the crack initiation and propagation in the rivet area. In this investigation by Klein [32], eight of the ten coupons were subjected to constant fatigue loading (R=0.1) at different stress amplitude levels, until a crack was detected using vacuum sensors around the rivet heads. This to obtain a 'fatigue initiation curve' for these coupons. When the first crack was detected, the test was stopped. As these sensors were mounted around the rivet heads, which were larger than the shaft of the rivet, as shown in a schematic representation in figure 6.2, the smallest crack that could be measured was (a = 6.8 mm). A list of these coupons and the stress amplitude they were tested for is shown in table 6.1.

Table 6.1: Overview of the provided coupons

#	S_a
FS01416a1	100
FS01416a2	75
FS01416a4	125
FS01416a5	87.5
FS01416a6	62.5
FS01416a7	50
FS01416a8	39
FS01416a9	*
FS01416a10	45.3

* Pristine, not subject to fatigue loading

In the investigation by Klein [32], in one coupon (Coupon FS01416a2) the initiated crack(s) were propagated until the edge of the coupon has been reached, to obtain a crack growth curve. Another coupon (coupon FS01416a9) was not subjected to fatigue loading, but was only to be strength tested. However, the tabs sheared off before the failure strength was reached. This coupon was re-used in the residual strength testing programme performed here, which is elaborated on in section 6.3.

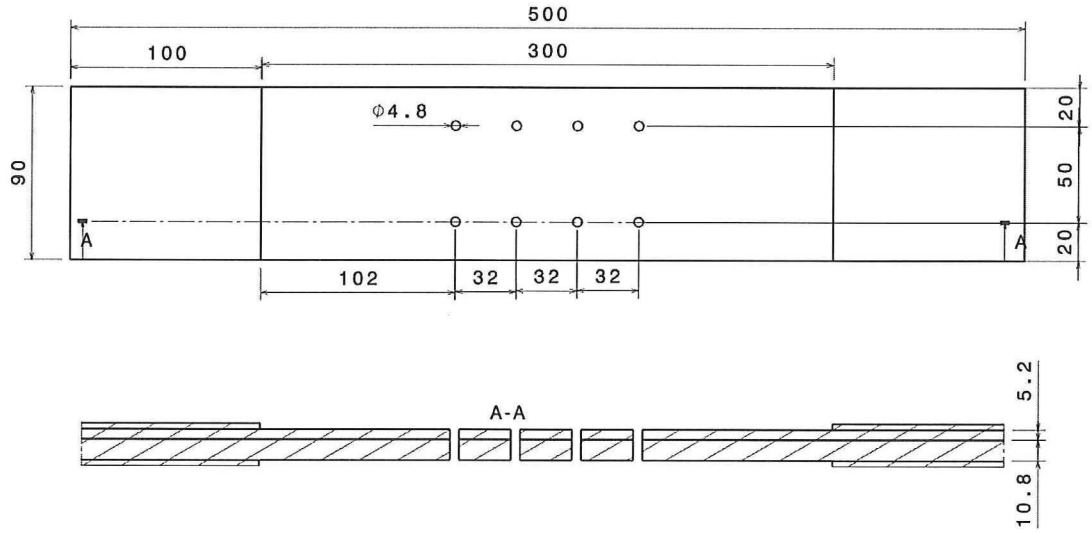

Figure 6.1: Schematic drawing; front view shown at the top, side view at the bottom

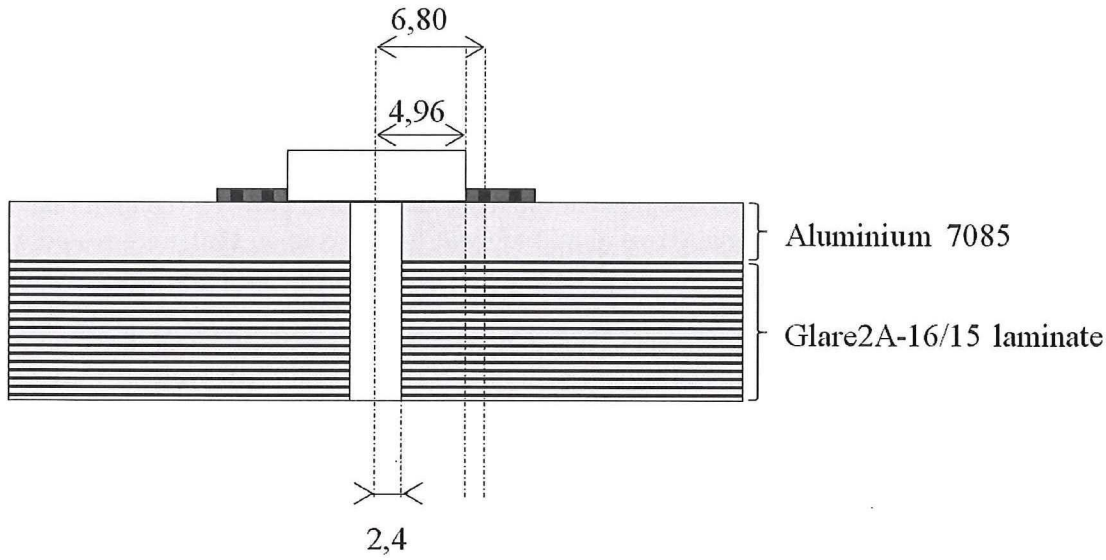

Figure 6.2: Illustration of the vacuum sensor around the rivet head. Dimensions are in mm. The smallest crack to be measured is a = 6.8 [mm]

6.2.3 Test Matrix and test set-up

Of the ten coupons provided, shown in table 6.1, seven are used for residual strength testing as part of this thesis. This included the coupons that had been used to perform fatigue crack propagation testing on (Coupon FS01416a2), as well as the pristine coupon (Coupon FS01416a9) by Klein [32]. The other five coupons all contain approximately the same amount of fatigue initiation damage, as the tests by Klein [32] were stopped when a fatigue crack was detected at a rivet as was mentioned in subsection 6.2.2.

For the investigation into the relationship between the amount of fatigue damage and the residual strength, it is preferred to create data points over the full range between pristine and fully cracked, and thus additional fatigue cycles were applied at the TU Delft Structures and Materials Lab. As boundary condition, it is decided that the aluminium 7085 flange should not be fully cracked, as this would result in the coupon not being representative for the structure to be studied. A completely cracked flange would results in large secondary bending loads, which would not occur in reality as the flange is attached to a web. The fatigue damage ratio, called R_D, which is the percentage of aluminium cracked of all the aluminium in the laminate, is distributed in intervals of 10%. This results in the test matrix shown in table 7.7. There is no specimen tested with a fatigue damage ratio of 10%, because with the fatigue damage present after testing by Klein [32], all the coupons contain a fatigue damage ratio of more than 10%.

Coupons FS01416a2, FS01416a8 and FS01416a9 already contain the fatigue damage ratio needed for the residual strength test programme. For the other four coupons, the initiated cracks are propagated further to obtain the fatigue damage ratio required. So coupons FS01416a5, FS01416a6, FS01416a7 and FS01416a10 are subjected to additional fatigue load cycles.

In the test campaign by Klein [32] each coupon was loaded by a constant fatigue stress amplitude, but each with a different amplitude. To create the fatigue damage in these coupons, each of these coupons were loaded at the TU Delft Structures and Materials Lab with the same fatigue stress amplitude as was done in the research by Klein [32]. The coupon that was subjected to the smallest fatigue stress amplitude will be the coupon that were tested with the least amount of fatigue damage (in this case, 20%), the coupon with the second smallest fatigue stress amplitude to 30% and so on. This is done to keep the number of fatigue cycles that have to be applied to a minimum. The coupons that will be tested, with the number of cycles that will be applied, determined with the use of the general FML Fatigue Tool developed by Spronk [1], are shown in table 7.7.

6.2.4 Prediction of the number of fatigue cycles with the general FML Fatigue Tool developed by Spronk [1]

Spronk [1] developed the FML Fatigue Tool as part of his thesis to predict the fatigue crack initiation and damage growth of the frame flange reinforced with the Glare strap. This tool is used here to predict the number of cycles required to obtain the required Fatigue Damage

Table 6.2: Overview of the coupons that were tested, and the required number of cycles to create the fatigue damage

	S_a	Fatigue Damage Ratio, R_D [%]	Fatigue cycles to be applied
FS01416a9	-	0	0
*	-	10	-
FS01416a8	39	20	**
FS01416a10	45.3	30	9524
FS01416a7	50	40	7205
FS01416a6	62.5	50	14316
FS01416a5	87.5	60	5531
FS01416a2	75	70	**

* Fatigue damage in all provided coupon is already past this point. With fatigue crack of 8mm as starting point, the coupons contain already more than 10% damage, assuming dog bone shape is made.
** No additional fatigue cycles need to be applied

Ratio as shown in the third column of table 7.7. The coupon is simulated as a 5.2 mm thick aluminium flange attached to a Glare2A-16/15-0.4 laminate, with 2 additional layers of glass fibres in the 0-direction between the flange and the Glare 2A laminate.

The model was simplified by only simulating one rivet hole, and assuming that the crack would grow with the same propagation rate at both sides of the hole. So, the total coupon was simulated as only a 40 mm wide coupon, indicated with the dashed line shown in figure 6.3. Using symmetry, only the dotted box in figure 6.3 was simulated. The simulation runs until the crack reached the total length of the coupon.

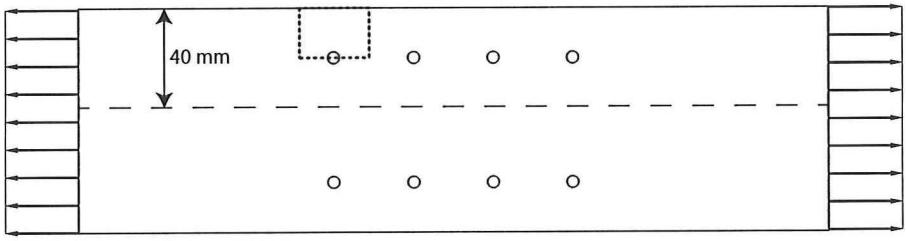

Figure 6.3: Simplification made for the crack growth simulation

To determine the number of fatigue cycles required to reach the necessary fatigue damage ratio, the damage ratio was extracted from the simulations. As one of the outputs of the general FML Fatigue Tool developed by Spronk [1], the crack length in each layer at each iteration is saved, visualized in figure 6.4a. Each curve represents a layer in the laminate, lighter curves indicate layers located deeper in the laminate. In this case the crack in the aluminium flange, which is defined as the bottom layer of the laminate, is seen to increase sharply at around 22 500 cycles.

Now from the results of the simulation, which was ended at half crack length, $a = 20[mm]$, it is possible to determine the fatigue damage ratio, by summing all the crack lengths, multi-

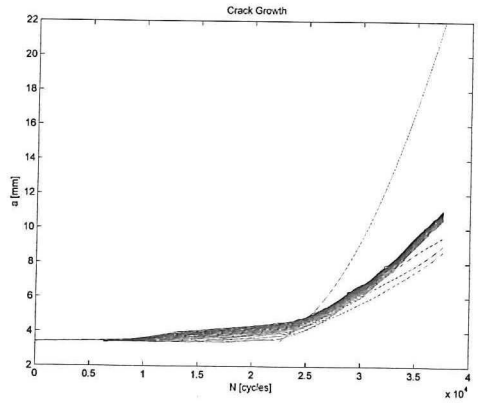

(a) Result of fatigue crack simulation with the FML tool of coupon FS01416a5

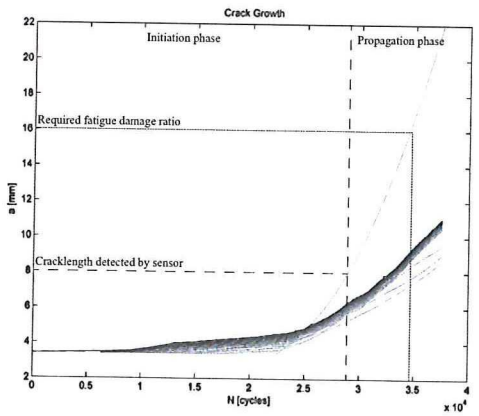

(b) Crack Initiation and Propagation using the general FML Fatigue Tool developed by Spronk [1]

Figure 6.4: Crack growth results made with the general FML Fatigue Tool developed by Spronk [1]

plied by the respective aluminium layer thickness, at a given number of cycles. For instance, for coupon FS01416a5 the required fatigue damage ratio is reached at a half crack length in the flange of a = 16 [mm], (and the half cracks in the aluminium layers in the Glare about a = 8.3 [mm]. To determine the number of cycles required for fatigue testing, the fatigue life is separated into an initiation phase, here defined as the phase up till a crack length of 8 [mm], which was the crack length detected in the flange by Klein [32] and at which the test was stopped. This is shown in figure 6.4b. On the other hand, the propagation phase is here defined to start at 8 mm. As the coupon already contained a crack of 8 mm, only the additional cycles necessary to obtain a crack of 16 mm in the flange are applied, which were 5531 cycles from the simulation, as was shown in table 7.7. Keep in mind that this crack length is only half of the total crack in the rivet, and it was assumed that the other rivet in the rivet row showed the same crack growth.

6.2.5 Measurement and analysis approach

The coupons were tested in the 1000kN fatigue machine in the TU Delft Aerospace Laboratory. They were clamped on their tabs within the hydraulic grips. The coupons were aligned using a digital spirit level. An image of the coupons clamped in the machine is shown in figure 6.5. Each coupon was subjected to the same fatigue load amplitude and R-ratio of 0.1, as they were tested by Klein [32] listed in table 6.1. The fatigue load cycles were applied with a frequency of 10 Hz.

Depending on the expected crack growth speed, (differing for each coupon due to different stress amplitude), the machine was stopped a number of times during the testing, and measurements were be taken of the crack length in the aluminium flange, and the top layer of the Glare 2A, at the other side. The measurements of the crack were done by pausing the machine at the max fatigue load S_{max}, and measured by eye using a loupe. A strap of graph paper was applied below the crack to increase accuracy. The crack length was measured with

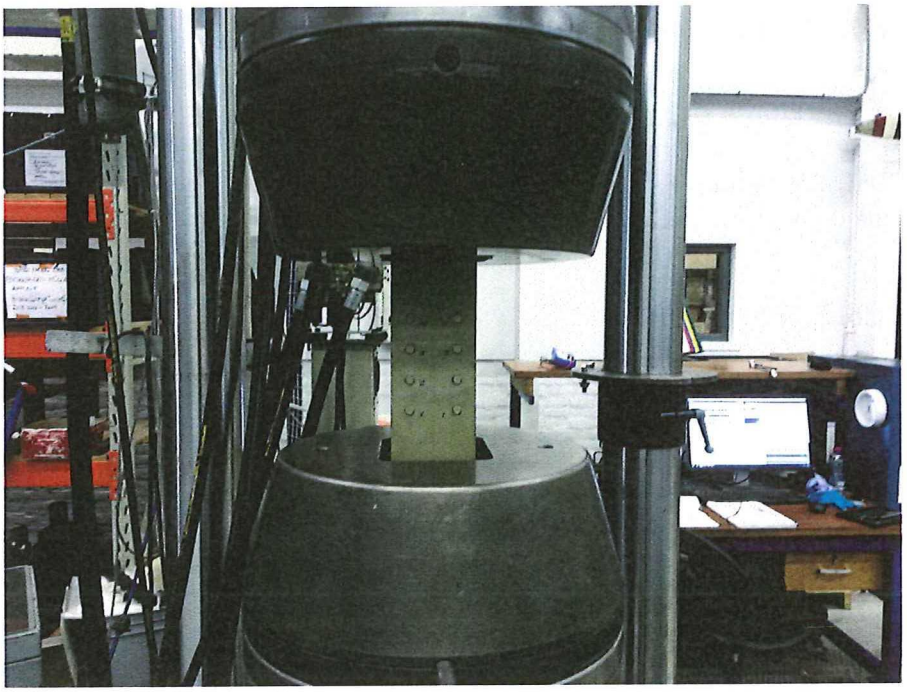

Figure 6.5: Coupon in the 1000 kN fatigue machine

an accuracy of $+-0.1$ [mm] this way.

Depending on the crack length required for the residual strength testing, determined by the general FML Fatigue Tool developed by Spronk [1], the test was stopped earlier, or continued longer to reach the desired crack length.

6.3 Residual strength tests

6.3.1 Programme objective

The objective of the residual strength test programme is to obtain the relationship between the fatigue damage ratio and the residual strength.

6.3.2 Coupon geometry

The 7 coupons that were presented in subsection 6.2.2 were used to generate residual strength data points. To get experience with test setup, the coupon that had a crack propagated in the flange to the end of the coupon (Coupon FS01416a2) was tested as it was. After this preliminary testing, the test setup was modified before the other coupons were tested.

In the research of Klein [32] it was observed that during destructive tensile testing of a pristine coupon, the tabs sheared of the coupon at high loads (600kN) instead of the coupon failing, which is expected to occur at 650kN. It was decided to modify the other coupons to a dog bone shape before residual strength testing, to make sure that the failure load of the coupon was reached before the tabs would shear off. This reduction is chosen such that even the pristine coupon will fail below 650kN. To prevent this modification to influence the test results unequally, this modification was applied to all the remaining coupons (excluding coupon FS01416a2 which was already tested). This is shown in figure 6.6.

From blunt notch strength calculations using the values from table 5.1, it was calculated that the laminate would have a failure stress of 625 MPa. Reducing the cross section by 20% made sure that coupon would fail before the tabs were sheared off. Furthermore, a large radius was applied to the coupon to prevent stress concentrations influencing the residual strength test results.

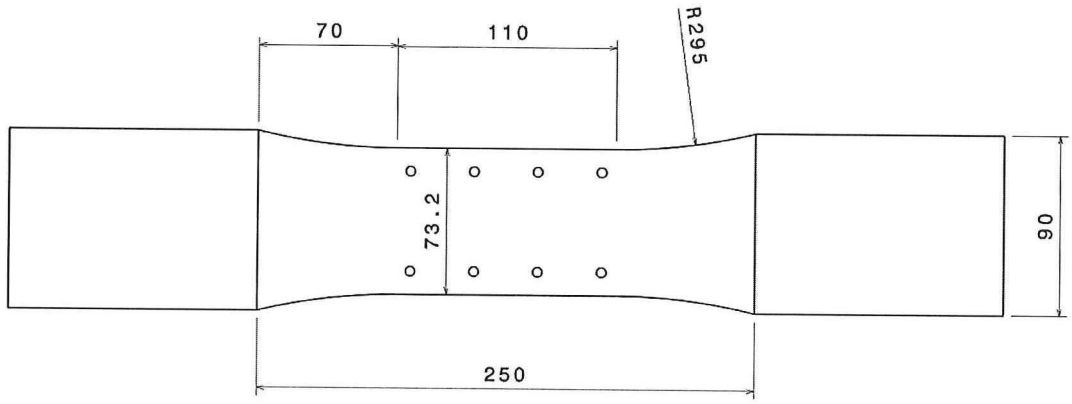

Figure 6.6: Radius milled in the coupon to create a dog bone shape and raise the stress in the middle of the coupon

6.3.3 Test Matrix and test set-up

The crack configuration of the coupons is graphically shown in figure 6.7. The top left image defines the numbering of the rivets. Each coupon is shown in the shape it was subjected to fatigue loads (the rectangular shape) as well as the modified dog bone shape, indicated with the dotted lines. Coupon FS01416a2 shows no dotted dog bone shapes, as it was tested without being modified beforehand. Coupon FS01416a9 shows no cracks, as it was tested in pristine condition.

6.3.4 Measurement and analysis approach

As shown in the test matrix, 7 coupons have been tested to investigate the relation of the residual strength to the fatigue damage rate, R_D. A speckle pattern was be applied on both sides of the coupon in order to perform Digital Image Correlation (DIC) measurements during testing simultaneous from both sides of the coupon.
The test bench measured the force and displacement of the head, although the displacement of the head could not be taken as measurement for the deformation of the coupon due to the influence of the stiffness of the machine. This was calculated from measurements with the DIC system. The coupon was loaded quasi-statically at a rate of 2 $[mm/min]$. The test was stopped when the load drops to more than 70% of the maximum load. The force and displacement measurements of the machine were logged simultaneously with the DIC system so that displacement and force could be linked to the images. A schematic drawing with a top and side view is shown in figure 6.8.

After the coupon has completed residual strength testing, the crack surfaces was inspected with an optic microscope with a magnification range of 2 times to 8 times, to measure the fatigue crack length that was present in the laminate before the residual strength testing. This is possible to do after the residual strength test because a clear difference between the fracture surface of the fatigue crack and the failure crack can be seen, as reported by Rodi [4].

6.3.5 Digital Image Correlation

Digital Image Correlation (DIC) is used to measure the deformation of the FML and aluminium surfaces of the samples during testing. By correlating an image of an undeformed state, and compare this with an image deformed state, the deformations at the surface of the coupon can be measured. Using two cameras placed side by side, 30 centimeters apart, also out of plane deformation can be measured.

The out of plane deformations at both sides of the coupons were of interest, as de Rijck [12] included a reduction factor in his equation for the prediction of the residual strength. By measuring the bending at the surface of both sides of the coupon, this factor can be quantified. Additionally, it was expected during the failing of the coupon, the aluminium flange would delaminate from the FML strap, resulting in independent out of plane deformation for the strap and the flange. Two DIC systems with each 2 cameras were used, one DIC system at each side, to measure the out of plane displacements. Additionally, it was assumed that the bending at the surface of the coupon is constant throughout the non-delaminated part.

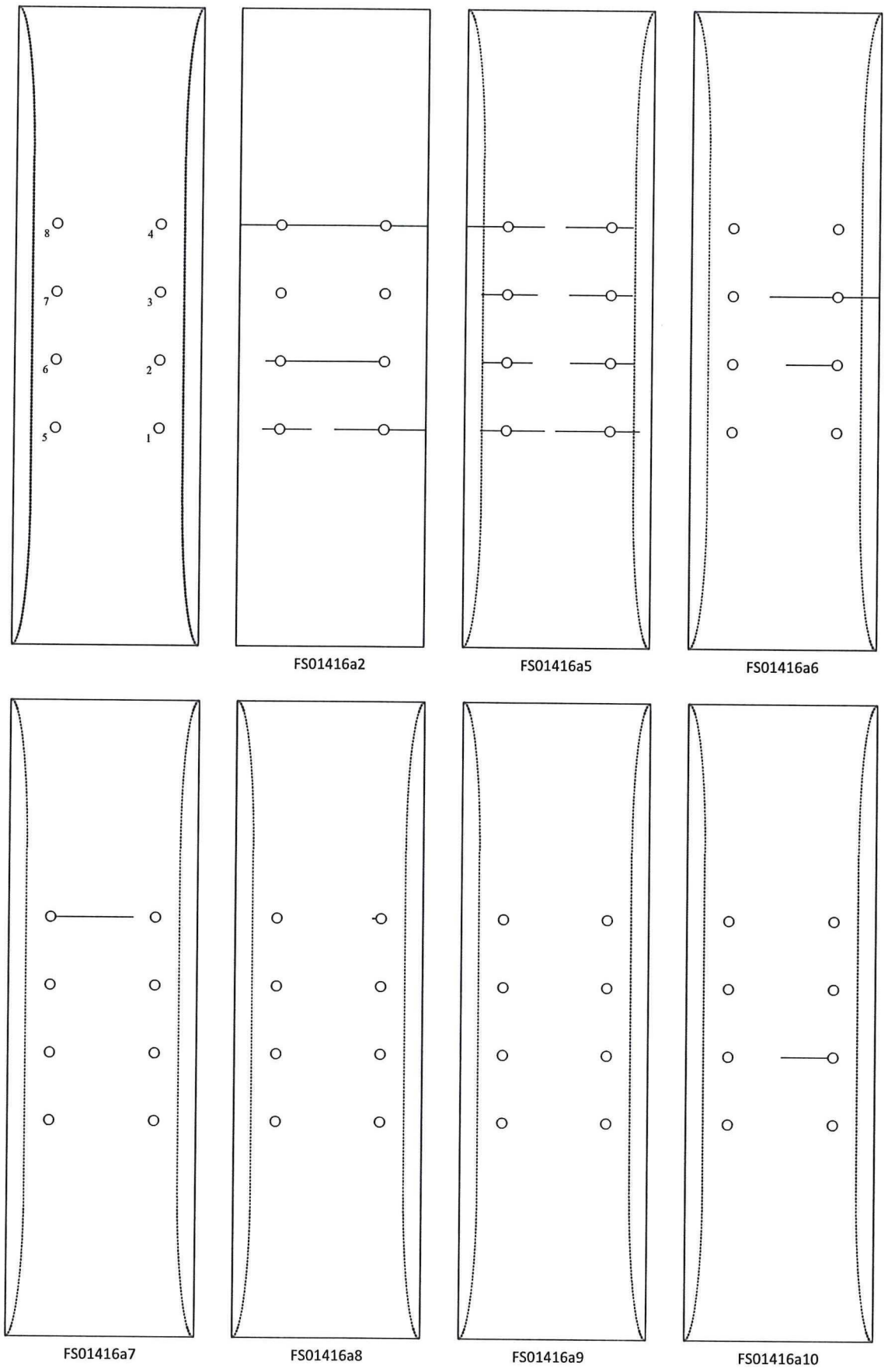

Figure 6.7: Fatigue crack configuration in coupons at the metal flange side

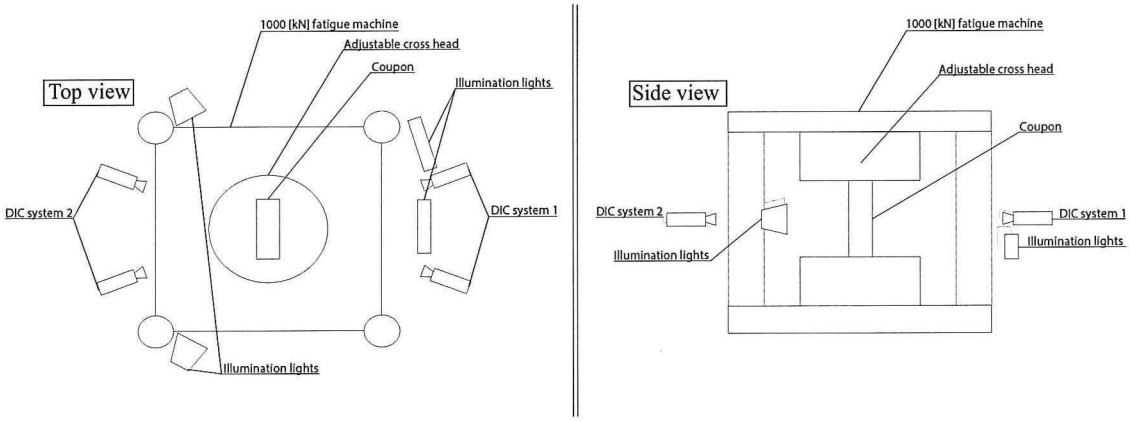

Figure 6.8: Schematic representation of the test setup, left the top view, right the side view

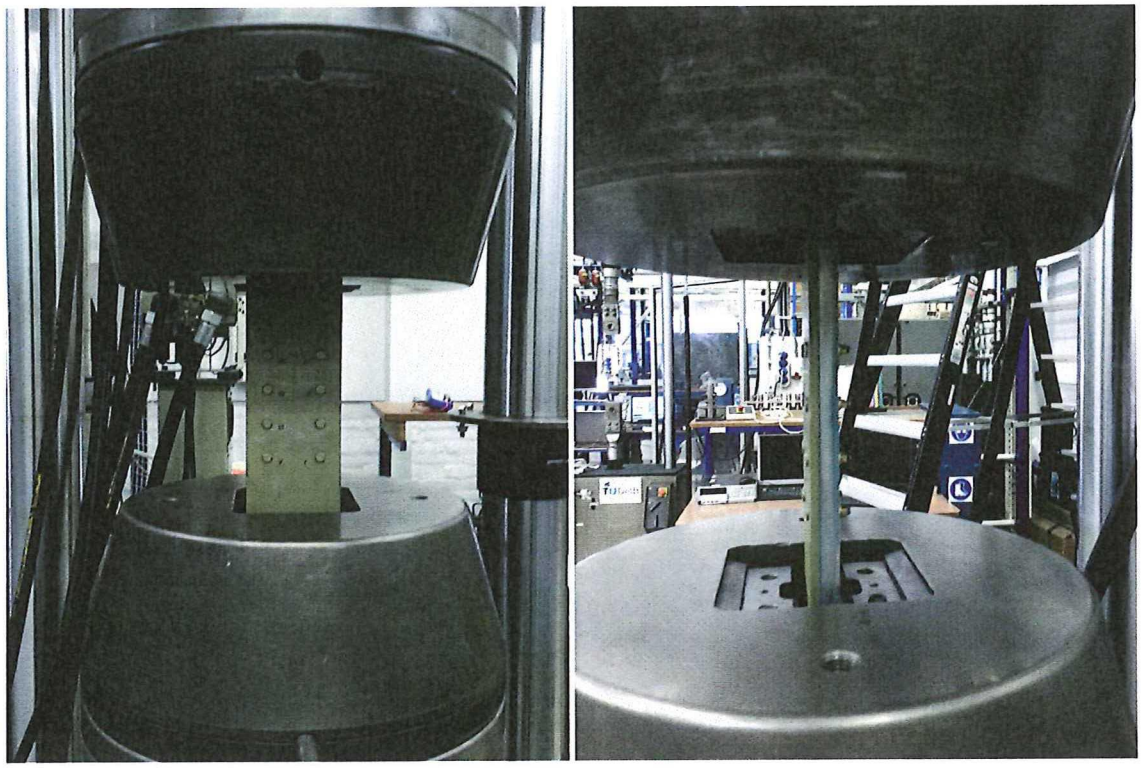

(a) Front view **(b)** Side view

Figure 6.9: Photos of the testing, left front view of the coupon, right the side view

The area containing rivets was measured using the DIC system, which is 73.2 [mm] x 250 [mm]. To increase contrast, first a spray painted speckle pattern was applied on the coupons, which consisted of black speckles on a white background. To get proper bonding of the paint to sample, it was first degreased. After spray painting a white layer on the coupon, the black speckle pattern was created by only marginally pressing the button of the spray paint can, making it 'sputter'. The result is effective, shown in figure 6.10. Two different DIC systems were used, with different resolutions. At the FML side, the VIC 3D DIC system was able to measure data points in a grid with a measurement point 0.8mm spaced apart. At the aluminium flange side, a Match ID system was used, which generated a grid with a data point each 1.3mm.

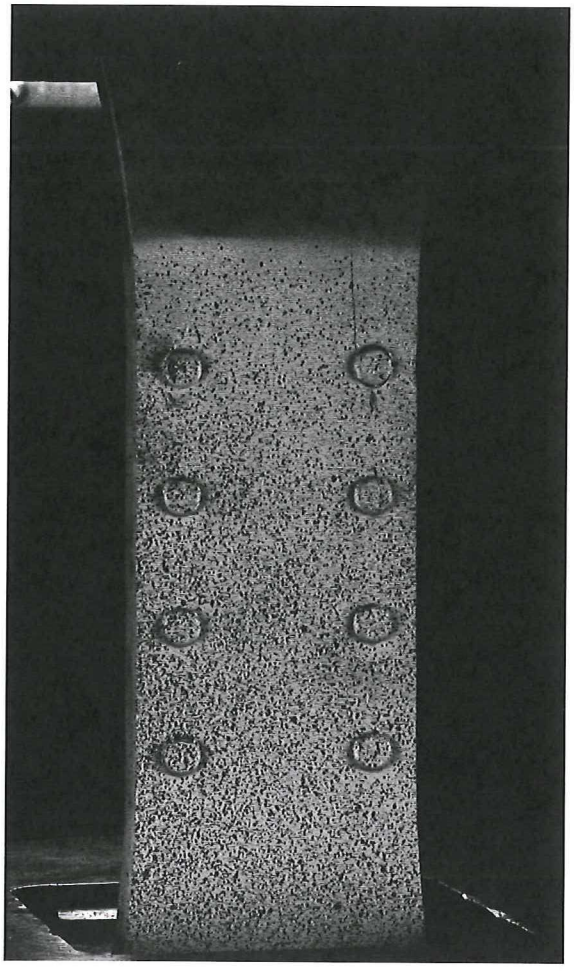

Figure 6.10: Example of the speckle pattern, on the aluminium flange side of coupon FS01416a8

Chapter 7

Results and Discussion

7.1 Introduction

In this chapter, the results obtained from the experiments which were outlined in chapter 6 are presented and then discussed with the prediction made from the models. The results and discussion of the residual strength tests are presented in section 7.2. In section 7.3 the results of the fatigue testing are discussed. Although this is in reverse chronological order of the testing, the residual strength is the main part of this thesis and thus is presented first.

7.2 Residual strength tests

7.2.1 Results

Seven coupons have been destructively tested. For each coupon, the strength and displacement were measured. After the destructive test the fatigue damage ratio was measured with the use of an optical microscope. A distinction can be made between fatigue cracks and final failure cracks in the aluminium layers in the Glare [4]. During the application of the quasi-static loading, DIC measurements have been made to capture the deformation field. These measurements are used in the discussion to interpret the residual strength results.

Force measurements

During the residual strength tests, the force and the displacement were measured with the 1000kN fatigue machine. An example of such a results is shown in figure 7.1.

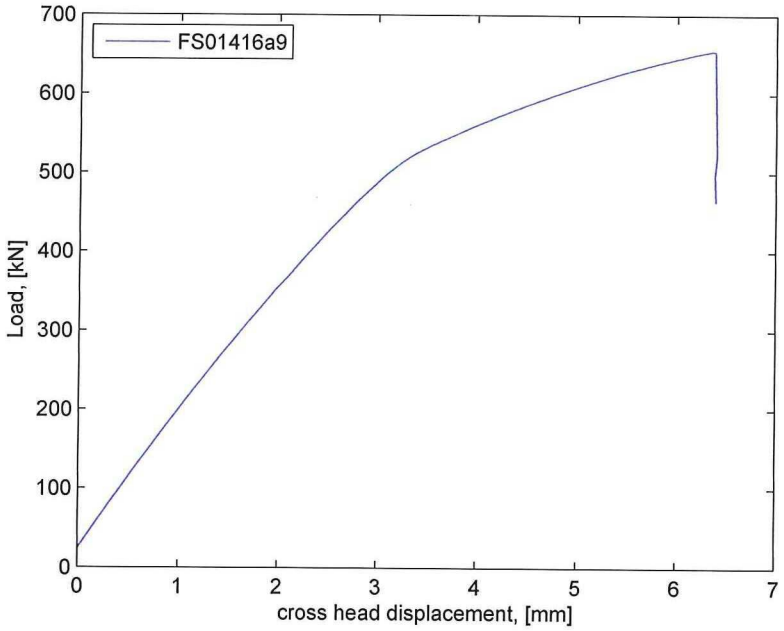

Figure 7.1: Load displacement curve for coupon FS01416a9

The test was stopped when the load dropped below 75% of maximum measured load. From the maximum load obtained during the test the residual strength was calculated. The force was converted to a residual strength by dividing it through cross sectional area of the coupon. The residual strength of all the tested coupons is presented in table 7.1. The load displacement diagrams of the other coupons are documented in appendix A

Table 7.1: Results of residual strength test

Coupon	Residual strength [MPa]
FS01416a2	398.9
FS01416a5	385.2
FS01416a6	435.6
FS01416a7	478.2
FS01416a8	522.8
FS01416a9	660.3
FS01416a10	520.6

In figure 6.7 the crack configuration of each coupon is presented. For each coupon, the cracks in the aluminium flange are presented left and the cracks in the FML flange right. Fatigue

cracks, which were present before residual strength testing, are indicated with a solid line, while cracks from final failure are indicated with a dotted line.

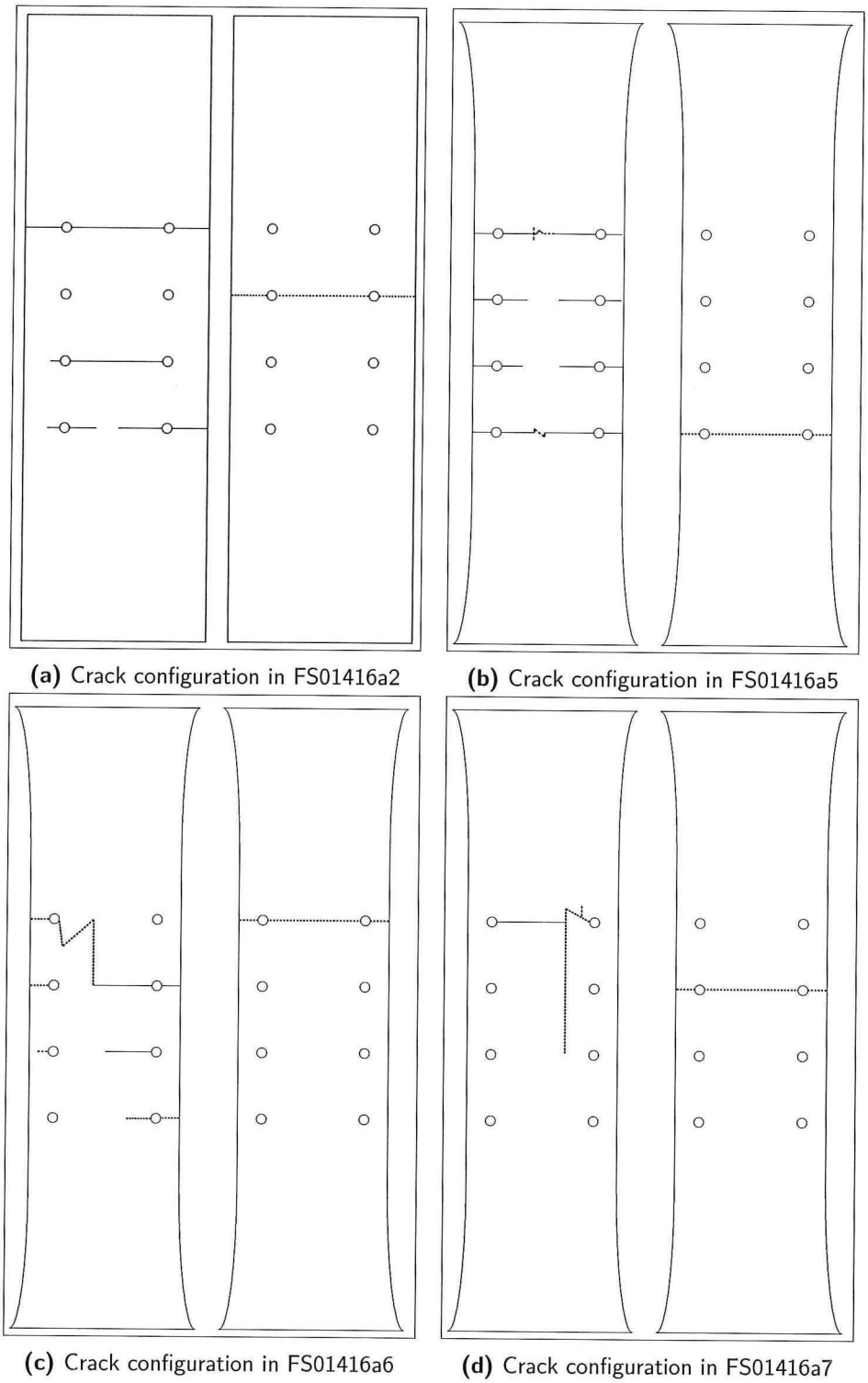

(a) Crack configuration in FS01416a2

(b) Crack configuration in FS01416a5

(c) Crack configuration in FS01416a6

(d) Crack configuration in FS01416a7

Figure 7.2: Crack configuration in the coupons after failure. For each coupon, the left image shows the crack configuration in the aluminium flange, the right image shows the crack configuration at the Glare side. Fatigue cracks are represented by a solid line, final failure crack are represented by a dotted line

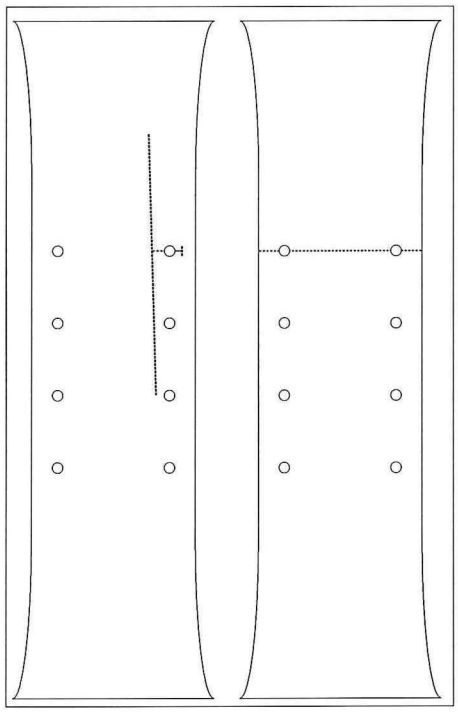

(e) Crack configuration in FS01416a8

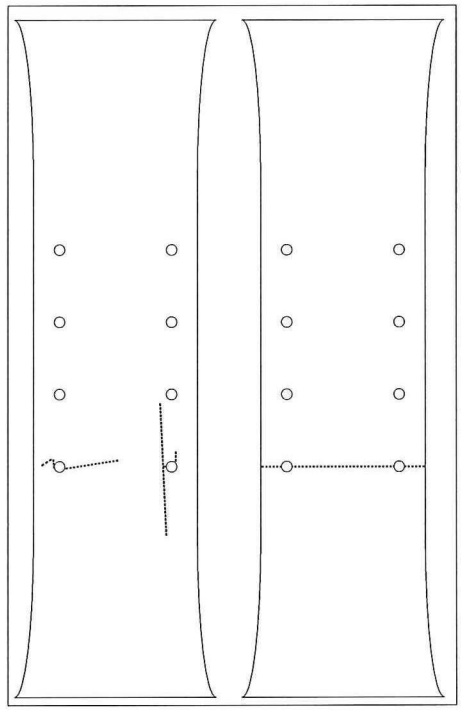

(f) Crack configuration in FS01416a9

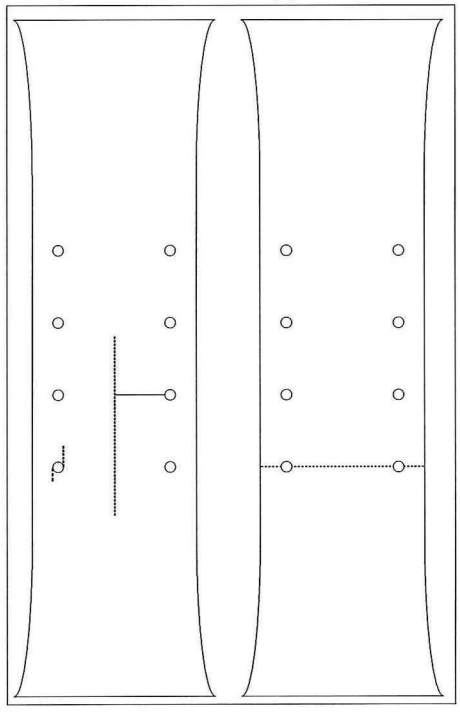

(g) Crack configuration in FS01416a10

Measurement of the fatigue damage ratio, R_D [%]

The fatigue damage ratio in each coupon was determined by adding the cracked aluminium in the cross section of the aluminium 7085 flange to the cracked aluminium in the cross section of the Glare strap, and dividing it by the total pristine aluminium in the cross section. This yields the fatigue damage ratio R_D[%] of the complete coupon. The cracked area in the aluminium flange was determined after the fatigue testing, but before the residual strength testing, as the crack in the flange could be measured easily. The cracked area in the cross section in the Glare strap could not be determined beforehand, because only the crack length in the surface aluminium layer was visible and could be measured. Thus, the fatigue damage ratio for the Glare laminate was determined after the residual strength test. Due to a difference in crack surface, a distinction can be made under the a visual microscope with an magnification up to 8x, between a fatigue crack and a final failure crack [4]. An example from measurements taken with an optical microscope with a magnification of 8x is shown in figure 7.4. Measurement of all the crack lengths of each coupon can be found in appendix A. Using these measurements the fatigue damage ratio of each of the coupon was determined.

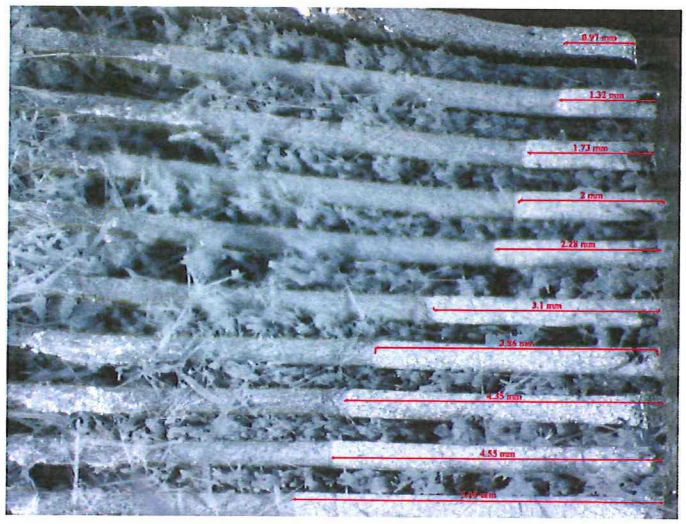

Figure 7.4: Fatigue crack length measurement with microscope

As can be seen in figure 7.2, only half of the coupons failed at the same rivet row in the aluminium flange as the Glare strap. The other half of the coupons, the aluminium flange failed at a different rivet row than the aluminium flange. An illustration of this effect is shown in figure 7.5, of coupon FS01416a-2.

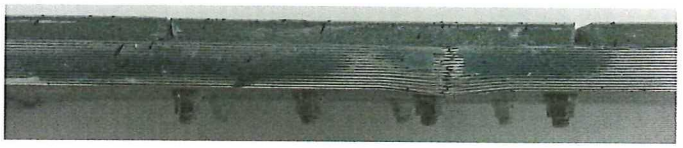

Figure 7.5: Final failure of FS01416a2. It can be seen that aluminium flange (top) failed at the right most rivet row, while the Glare strap (bottom) failed at the second rivet row from the right.

This begs the question: At which rivet row should the fatigue damage ratio for the whole laminate be determined? Three theories can be proposed:

1. The fatigue damage ratio for the complete laminate should be determined in the cross section at the rivet row where the crack in the aluminium layer is the longest, shown in figure 7.6a
2. The fatigue damage ratio for the complete laminate should be determined in the cross section at the rivet row where the Glare laminate fails, shown in figure 7.6b
3. The fatigue damage ratio for the complete laminate should be determined by adding the largest fatigue damage ratio at the cross section at a rivet row in the aluminium flange, to the fatigue damage ratio at the rivet row where the Glare laminate fails, shown in figure 7.6c

Now to determine which method is best there are a few requirements: First, the method should closely resemble the reality, in the sense that it can be shown that the fatigue damage ratio actually is the dominant variable that determines the residual strength. This is a prerequisite to be able to use the De Rijck method. Secondly, it should be conservative in predicting the residual strength, and it should be useful in combination with the general FML Fatigue Tool developed by Spronk [1].

Based on what is observed during residual strength testing, it would be unrealistic to use the fatigue damage ratio in another rivet row in the Glare laminate than the rivet row where the Glare laminate fails. Theory 1 is discarded. However, both the theories 2 and 3 are feasible.

For all these requirements presented above, theory 3 gives better results. This is also a realistic approach, because the fatigue crack in the aluminium plays an important role. It is thus decided to determine the fatigue damage ratio at the cross section of the rivet row with the longest fatigue crack in the flange and the fatigue damage ratio in the Glare laminate on the line of failure. Theory 3 is used to predict the residual strength.

The combined results from the residual strength of the coupons and the fatigue damage ratio are shown in table 7.2. These results are plotted in figure 7.7

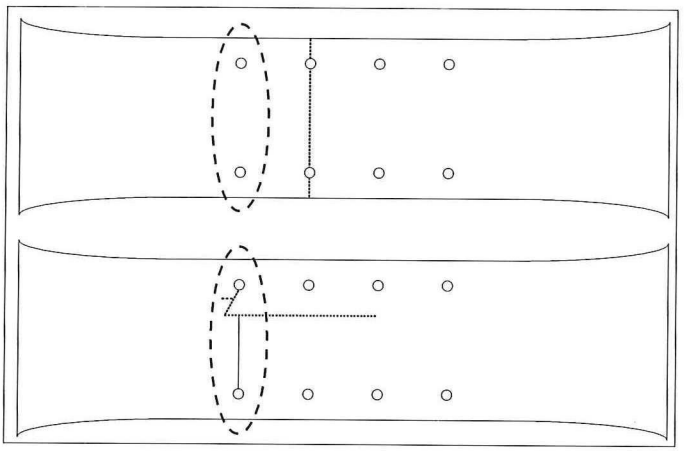

(a) The fatigue damage ratio determined at the rivet row where the crack in the aluminium flange is the longest

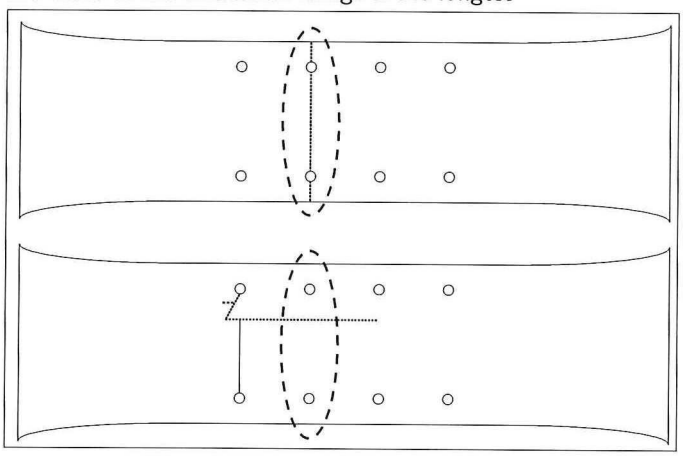

(b) The fatigue damage ratio is determined at the cross section of the rivet row where the Glare laminate fails

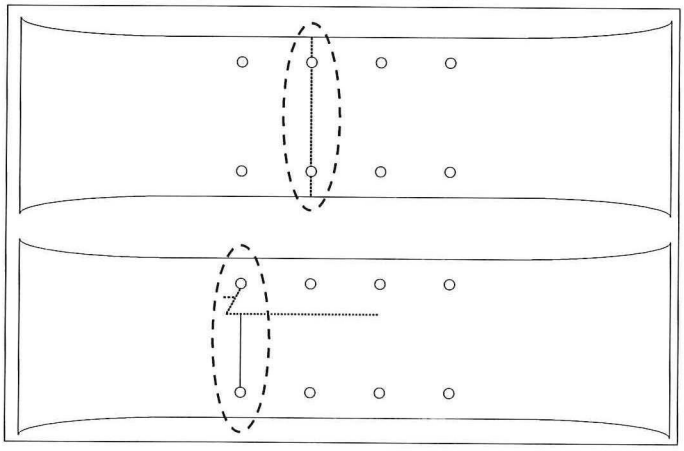

(c) The fatigue damage ratio of the Glare laminate is determined at the cross section of the rivet row where the Glare laminate fails, and the fatigue damage ratio of the aluminium flange is added where the fatigue crack is the longest.

Figure 7.6: The different approaches to determining the fatigue damage ratio

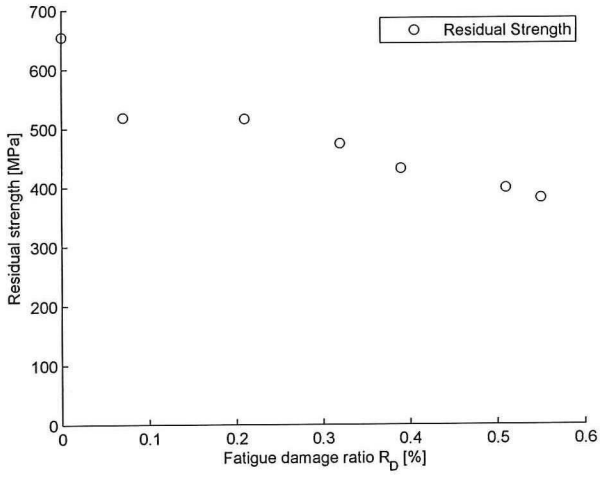

Figure 7.7: Results of the residual strength test

Table 7.2: Results of residual strength test

Coupon	Fatigue damage ratio, R_D [%]	Residual strength [MPa]
FS01416a2	52	398.9
FS01416a5	55	385.2
FS01416a6	39	435.6
FS01416a7	32	478.2
FS01416a8	7.2	522.8
FS01416a9	0	660.3
FS01416a10	22	520.6

Residual strength trend line

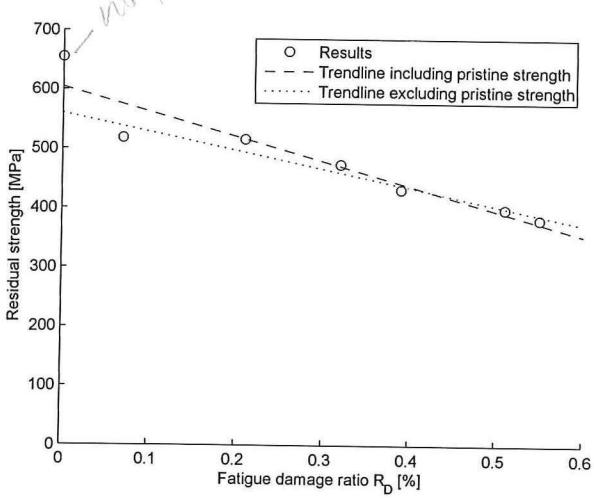

Figure 7.8: Comparison of the linear trend lines

To analyse the performance of the residual strength tool, it is important to know if the trend of the predictions follow the trend of the results. For that matter, a linear regression line is fitted to the data. However, it can be discussed whether or not the pristine strength of the coupon should be taken into account in determining the residual strength regression line.

It seems that for the first 10% to 20% of the fatigue damage ratio the strength decreases at a different rate than the rest of the graph. Similar results are shown in figure 7.9, from test results by Müller [8] and figure 7.10 from [9]. It can be seen in figure 7.9 that the data points for Glare tested under lab conditions, the open circles, show little decrease of strength, while after the first 20% of the fatigue damage ratio, the strength decreases linearly. In figure 7.10 Beumler shows a different trend than Müller; the strength is reduced more strongly the first 20% of the fatigue damage ratio, and flattens out later.

It seems thus that the residual strength is not solely a linear phenomenon, but slightly non-linear, as shown in the plot on the right in figure 7.10 by Beumler [9]. However, this does not remove the value of a linear approach as engineering approach; it is a simple and reasonable accurate approach, which, using the appropriate knock down factors can be useful. The first 45% of the fatigue damage ratio, the approach excluding the pristine strength is more conservative, as can be seen in figure 7.8. As almost all fatigue damage ratios should be detected before this level, this is the approach used in this thesis for the trend through the residual strength data points.

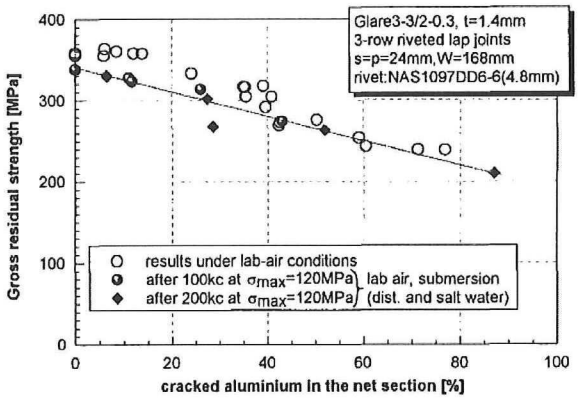

Figure 12.30 Residual strength of Glare3-3/2-0.3 riveted lap joints under different environmental conditions.

Figure 7.9: Test results from Müller [8]

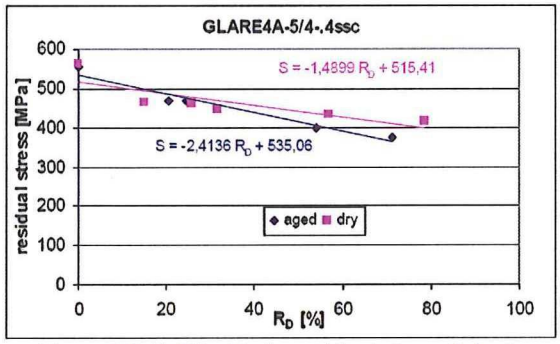

Figure 6.9.7. Filled hole residual strength test results and linear regression GLARE4A

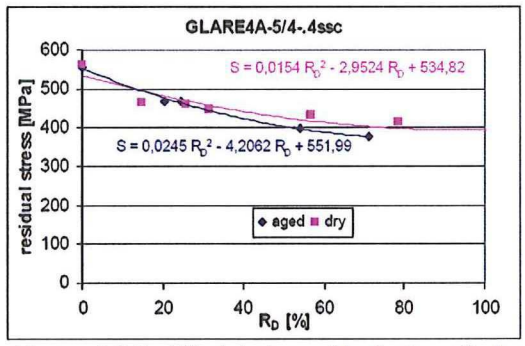

Figure 6.9.8. Filled hole residual strength test results and polynomic regression, GLARE4A

Figure 7.10: Residual strength interpolation by Beumler [9]

DIC measurements

During the residual strength test, DIC measurements were taken of both sides of the coupon. From these measurements, the in plane and out of plane deformations are determined. The goal of these measurements is to support the discussion of the residual strength results with the predictions. De Rijck [12] initially over predicted the residual strength. This was explained from the bending that occurs in the coupon, as he was testing lap splice and butt joint specimens. He reduced the blunt notch strength value of the Glare laminate with 10% and this yielded an acceptable conservative approach for his results. Bending in the coupons that were tested here was also expected, due to the difference in stiffnesses of the aluminium flange and the Glare strap. Additionally, it was expected that the strap would delaminate from the flange, enabling it to deform separately. Thus, DIC measurements were taken from both the Glare as the flange side of the coupon.

From the DIC measurements, the in plane strain, out of plane displacement and out of plane curvature were determined at both sides, the moment before failure. An example of these results for coupon FS01416a5 are shown in figure 7.11. The other results are presented in the appendix A

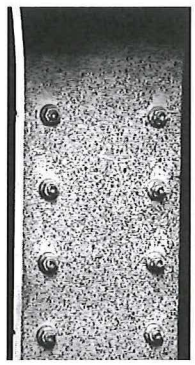

Image of the Glare side of the coupon

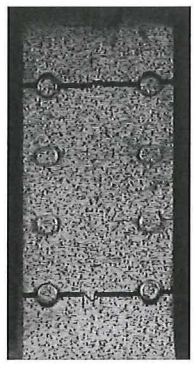

Image of the Aluminium side of the coupon

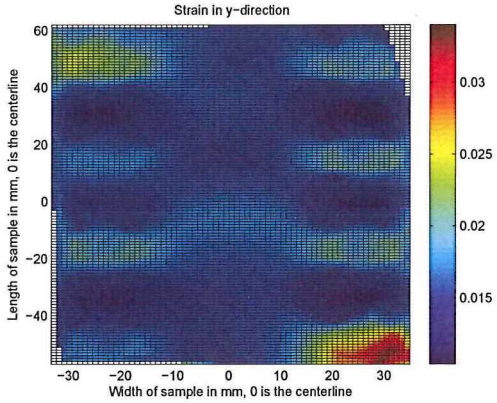

In plane strain in at the Glare side of the coupon

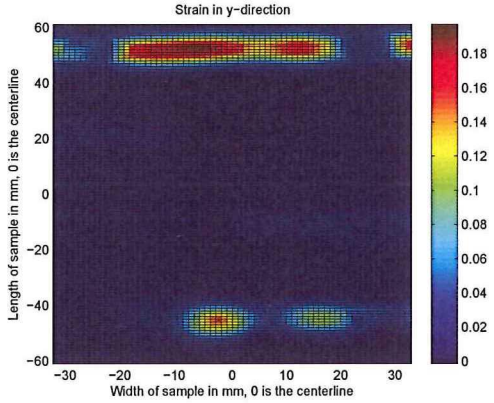

In plane strain in at the Aluminium side of the coupon

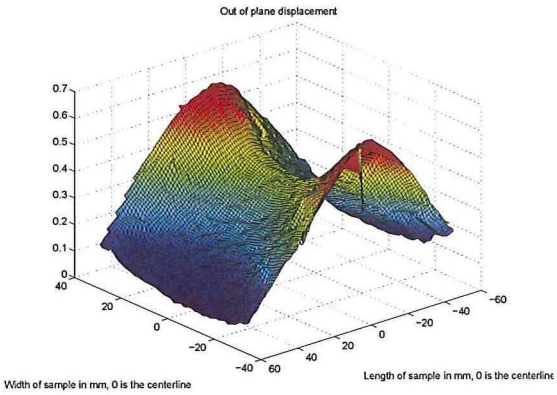

Out of plane deformation at the Glare side of the coupon

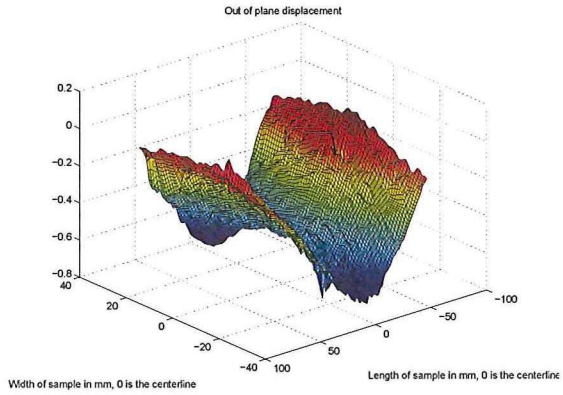

Out of plane deformation at the aluminium side of the coupon

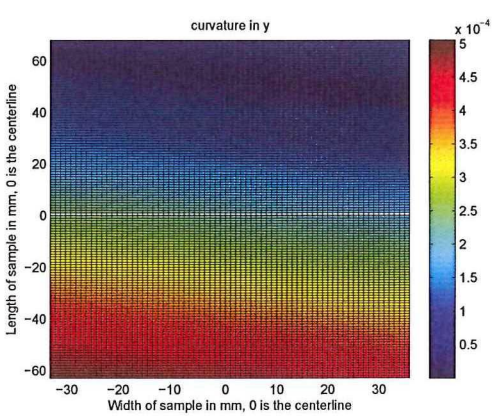

Curvature at the Glare side of the coupon

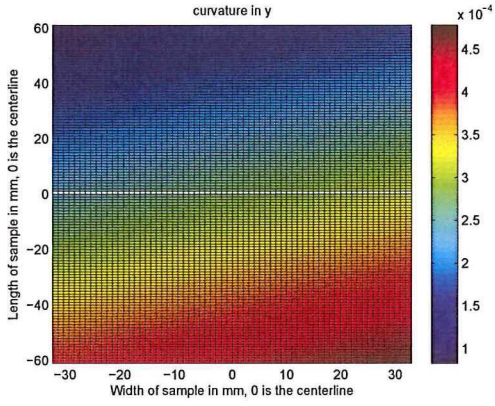

Curvature at the Aluminium side of the coupon

7.2.2 Discussion

In this section, the results of the residual strength test are compared with predictions made with the De Rijck method. The discrepancies between the predictions and the results are discussed.

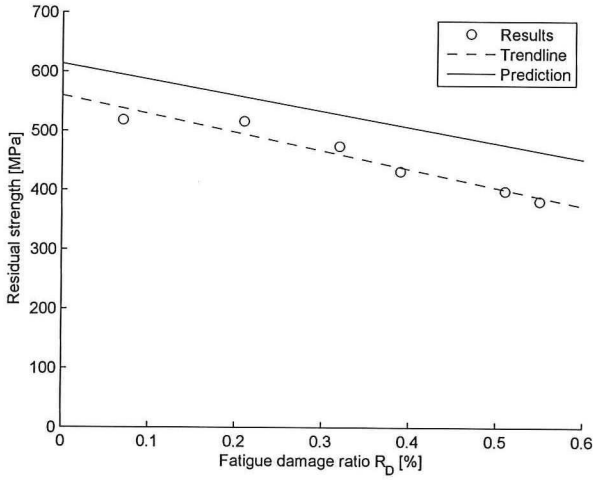

Figure 7.12: Residual strength prediction and test results of the tested coupons

In figure 7.12 the results and the residual strength prediction are shown. The prediction is made with the De Rijck method, presented in section 5.4.2. The prediction is made by assuming that all aluminium is 2024-T3. First, the MVF is determined:

$$MVF = \frac{\sum_1^n t_{al}}{t_{tot}} = \frac{11.6}{16} = 0.73 \tag{7.1}$$

With the use of the MVF, the blunt notch strength of the laminate can be calculated using table 5.1:

$$\sigma_{BNGlare} = MVF{\cdot}\sigma_{BN_{al}} + (1-MVF){\cdot}\sigma_{BN_{fiber}} = 0.73{\cdot}417[MPa] + (1-0.73){\cdot}1193[MPa] = 625.3MPa \tag{7.2}$$

And the residual strength is calculated with

$$\sigma_{res_{cracked}} = \sigma_{BN_{Glare}} - MVF \cdot \frac{A_{al_{cracked}}}{A_{al_{pristine}}}\sigma_{BN_{al}} \tag{7.3}$$

Where $\sigma_{BN_{Glare}}$ the blunt notch strength of the total laminate, determined in equation 7.2, $\sigma_{BN_{al}}$ the blunt notch strength of the aluminium and $\frac{A_{al_{cracked}}}{A_{al_{pristine}}}$ is the fatigue damage ratio on the x-axis of in the residual strength graphs.

Overprediction of the residual strength by the model

Although the trend line through the results matches the prediction made with the De Rijck method, shown in figure 7.12, the residual strengths are about 15% lower than predicted from De Rijck method. De Rijck [12] also observed a lower residual strength in his tests than predicted by his model. This was explained from the bending that occurs in the coupon, as he was testing lap splice and butt joint specimens. He reduced the blunt notch strength value of the Glare laminate with 10% and this yielded an acceptable conservative approach for his results.

However, reduction due to bending does not seem present here. DIC measurements have been made during the residual strength testing of the coupons. The results of these at the last image before failure are shown in appendix A. From these results it is observed that the curvature of the coupons when at failure is very small, in the range of $0.0005m^{-1}$. This can be seen in the images of curvature shown in appendix C. This does not explain the reduction in residual strength, as this only raises the stresses on the surface of the laminate with a couple of MPa's.

There seems to be an alternative explanation which suits the results better. From the discussion presented in chapter 3 it has been shown that the fibres delaminating from the aluminium layers during quasi static loading play a significant role in the residual strength. By delaminating, the fibres can strain more, thus a higher residual strength can be obtained. Before final failure, cracks in the loading direction, emanating for the fatigue crack in the flange, start appearing in all coupons.

The delaminating of the aluminium flange from the Glare laminate can be seen in the out of plane deformation from the DIC measurements. The out of plane deformations of coupon FS01416a7 and coupon FS01416a10 just before failure are shown in figure 7.13.

The theory is now that the flange delaminates from the fibre metal laminate strap, (static delamination), (this difference in out of plane displacement is not visible in the strap). This delamination is stopped by the rivet rows above and below the fatigue crack. At these location stress concentrations occur, as at these locations the load that was originally taken up by the flange is now introduced into the strap.

This stress concentration now determines the residual strength of the coupon. As was mentioned in chapter 3, the glass fibres in the laminate that determine the residual strength; when they start failing (at about 4.5%), the load that they carried has to be absorbed by the still intact part of the laminate. Rodi [4] mentions that the capability of the laminate to do this depends on the length of the crack; at a certain crack length the laminate is no longer able to take up the load of broken fibres, and the laminate shows brittle failure.

It is however difficult to determine the stress concentration, as both the aluminium in the flange and the strap is yielding, resulting in load redistribution between the still intact part of the flange, flange at the end of the delamination, the strap, and the fibres in the strap.

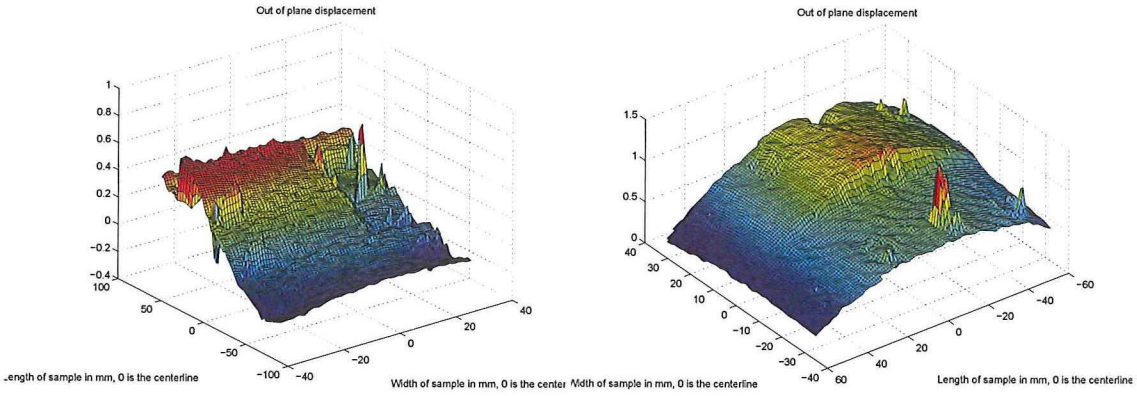

(a) Out of plane displacement of aluminium flange coupon FS01416A7 just before final failure

(b) Out of plane displacement of aluminium flange coupon FS01416A10 just before final failure

Figure 7.13: Illustration of the out of plane deformations of the aluminium flange, measured with DIC

7.3 Fatigue test results

7.3.1 Results

During the application of the fatigue loads at specified fatigue stress amplitude, listed in table 7.7, the crack length of the longest crack in the flange has been measured. Only cracks in the aluminium flange were visible and measured. The resulting fatigue crack lengths at intervals is shown in table 7.3 to table 7.6. In figure 7.14 the measured crack lengths are compared with the results from the general FML Fatigue Tool developed by Spronk [1].

# Cycles	Measured crack length 2a [mm]	Predicted crack length 2a [mm]
1	7	7
5000	7	7
10000	11	16
20000	27	30
25000	36	-

Table 7.3: Crack length results for coupon FS01416a5

# Cycles	Measured crack length 2a [mm]	Predicted crack length 2a [mm]
1	0	8
5000	8,4	10
15000	18	16
25000	26,8	20
35000	48	32

Table 7.4: Crack length results for coupon FS01416a6

# Cycles	Measured crack length 2a [mm]	Predicted crack length 2a [mm]
1	7	8
5000	10	9
10000	12	10
15000	13	12
20000	14	12
25000	17	15
30000	19	16
35000	21	18
40000	22	20
45000	23	22
50000	25	24
65000	37	31

Table 7.5: Crack length results for coupon FS01416a7

# Cycles	Measured crack length 2a [mm]	Predicted crack length 2a [mm]
1	8	8
5000	8	9
10000	9	10
15000	12	11
20000	14	12
25000	16	13
30000	18	14
35000	22	15

Table 7.6: Crack length results for coupon FS01416a10

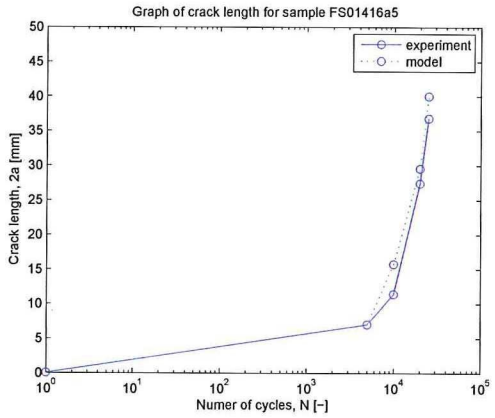

(a) Crack lengths vs number of cycles for coupon FS01416a5

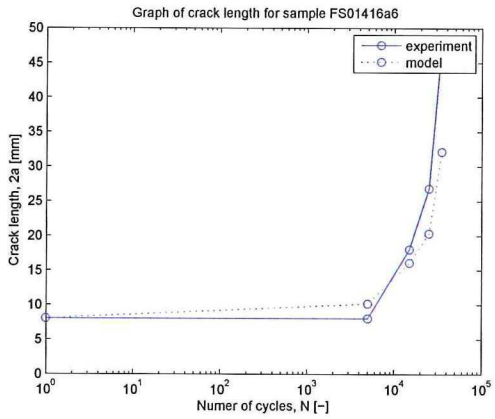

(b) Crack lengths vs number of cycles for coupon FS01416a6

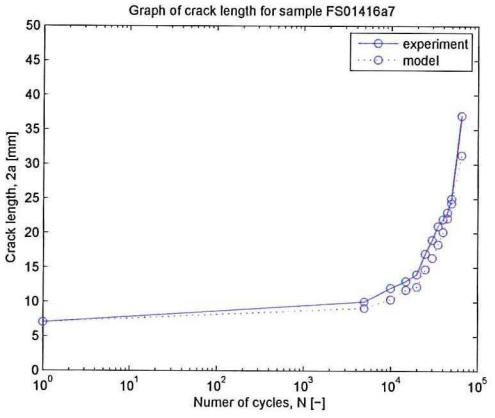

(c) Crack lengths vs number of cycles for coupon FS01416a7

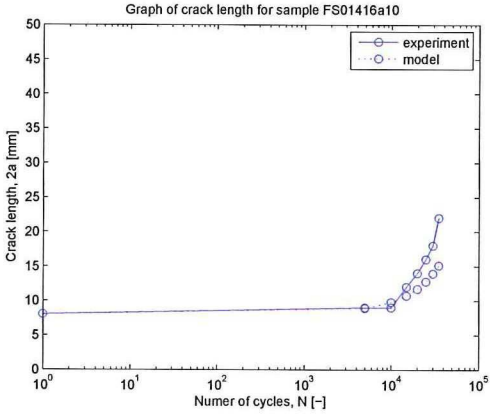

(d) Crack lengths vs number of cycles for coupon FS01416a5

Figure 7.14: Measured crack lengths compared to predicted crack lengths

7.3.2 Discussion

Comparison of crack length from experiment and model

In figure 7.14a to figure 7.14d the crack lengths versus the number of cycles is plotted. There is a close match between the experiment and the model, although the model slightly under predicts the crack growth. As an assumption, only the crack growth was modelled; the coupons were already initiated. Spronk [1] compared the initiation lives from the model with initiation measured by Klein [32]. Spronk [1] found a close match between the crack initiation predictions he made his developed tool, and the measurements from Klein [32].

Under prediction of cycles required for specified damage

In chapter 6, table 7.7 a prediction was made on the number of fatigue cycles necessary to create the required damage in the coupons. However, the assumption here was that fatigue cracks would propagate from every rivet hole at the same time with the same crack growth rate. At low fatigue amplitudes, there is a large spread in the fatigue initiation life, causing only one crack to grow. Based on these observations, new observations are made with regards to the number of fatigue cycles required to reach the damages, assuming that only crack would grow. The results are shown in table 7.7. The results are now much closer. To make predictions with the tool, it is important to take the effect of the initiation scatter into account. For higher stress amplitude this becomes smaller, while for lower stress amplitudes, there is a high probability that only a single crack will grow.

Table 7.7: Overview of the coupons that were tested, and the required number of cycles to create the fatigue damage

Coupon	S_a	Initial number of cycles predicted	Corrected prediction	Cycles required
FS01416a10	45.3	9524	35000	59962
FS01416a7	50	7205	65000	73990
FS01416a6	62.5	14316	35000	40011
FS01416a5	87.5	5531	25000	16184

∗ Fatigue damage in all provided coupon is already past this point. With fatigue crack of 8mm as starting point, the coupons contain already more than 10% damage, assuming dogbone shape is made.
∗∗ No additional fatigue cycles need to be applied

7.4 Complete FML tool

In this section, the performance of the complete tool to predict the fatigue crack growth and residual strength is evaluated. In table 7.8 the fatigue crack initiation, fatigue crack growth and residual strength from experiments and predictions from the general FML Fatigue Tool developed by Spronk [1] are presented. For the crack growth, the number of cycles necessary to reach the required crack length for the residual strength are compared. The ratio's between the values from experiment and model, which were presented in table 7.8 are compared in table 7.9.

Table 7.8: Fatigue crack initiation, (from Spronk [1]), fatigue crack growth and residual strength from experiments and FML the general FML tool. The subscript $_m$ indicates values from the model, while the subscript $_e$ indicates values from the experiments.

Coupon	$FCI_m[N]$	$FCI_e[N]$	$FCG_m[N]$	$FCG_e[N]$	$Strength_m[MPa]$	$Strength_e[MPa]$
FS01416a2	56832	38873	*	*	461.9	395.5
FS01416a5	26906	22445	16184	25000	452.6	385.2
FS01416a6	108773	52505	40011	35000	502.2	435.6
FS01416a7	237855	109797	73990	65000	522.7	478.2
FS01416a8	568193	3000000	*	*	597.5	522.8
FS01416a9	**	**	*	*	618.9	660.3
FS01416a10	335867	626900	59962	35000	554.8	520.6

* No values as no fatigue crack propagation was performed on this coupon.
** No values as no fatigue initiation was performed on this coupon

Table 7.9: Results of Complete tool, FCI, FCG, Res strength

Coupon	FCI [1]	FCG	Residual strength
FS01416a2	1.46	*	1.17
FS01416a5	1.20	0.65	1.17
FS01416a6	2.07	1.14	1.15
FS01416a7	2.17	1.14	1.09
FS01416a8	0.19	*	1.14
FS01416a9	**	**	0.94
FS01416a10	0.54	1.71	1.07

* No values as no fatigue crack propagation was performed on this coupon.
** No values as no fatigue initiation was performed on this coupon

In table 7.9 it can be seen that the crack growth shows a good match with the results from the experiment. There seems to be a tendency of under predicting the number of cycles for high stress amplitudes, while an over prediction of the cycles for lower stress amplitudes occurs. The tool shows an over prediction of the residual strength, except for the pristine strength. However, this is not relevant, as was discussed in subsection 7.2.1, this tool is not to be used for the pristine strength.

As now the crack growth capability and the residual strength capability have been devel-

oped, the residual strength curves as function of the applied cycles can be plotted. These are shown in figure 7.15 to figure 7.18 for the four coupons. The predictions made with the fatigue crack growth and residual strength modules of FML toolbox are presented for each coupon, and compared with the results from the tests. The crack growth and the residual strength are plotted against the number of cycles applied on the x-axis. The fatigue crack initiation is not taken into account, as there is a large scatter in this data, and is not of interest in this thesis.

During the experiments, only crack growth in the flange occurred. In the strap, no visible cracks appeared. As both the strap and the flange contribute to the residual strength of the coupon, the crack growth in both parts is required to make accurate residual strength predictions. For the calculation of the residual strength from the experiment, the measured crack length in the flange and the modelled crack length in the strap is used. For the residual strength from the model, the modelled crack lengths in the flange and the strap are used.

In the left image of the four coupons, the crack growth rate is shown. A good agreement with the test and the tool is shown. This effect is seen again in the residual strength graphs, as these are directly a function of the crack lengths. The consistent over prediction of the residual strength by about 15% is also seen in these figures. For coupon FS01416a5, shown in figure 7.15, it has to be noted that cracks started to grow from both rivet in the rivet row, resulting in a significantly lower residual strength. However, in the crack growth figure for this coupon, only the crack growth of one crack is plotted.

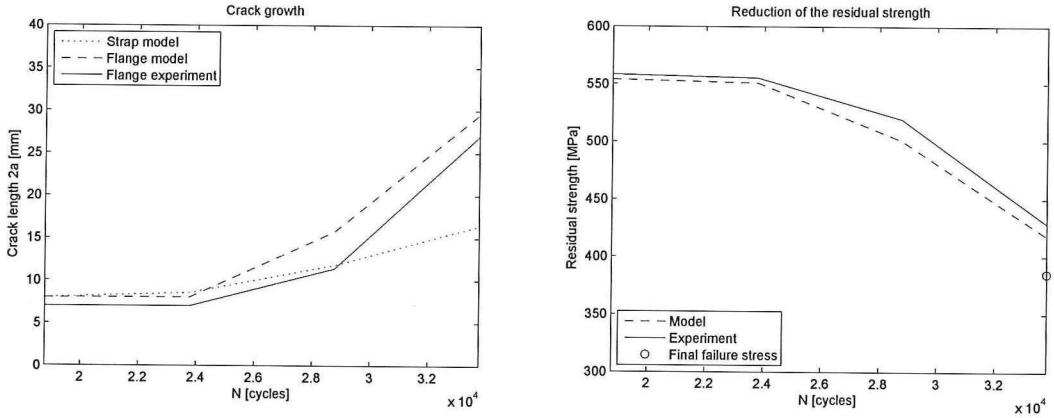

Figure 7.15: The crack growth from the FML model and the test is shown in figure 7.15a. The residual strength from FML model and the test is shown in figure 7.15b. Final failure from the experiment is indicated in figure 7.15b with a circular marker

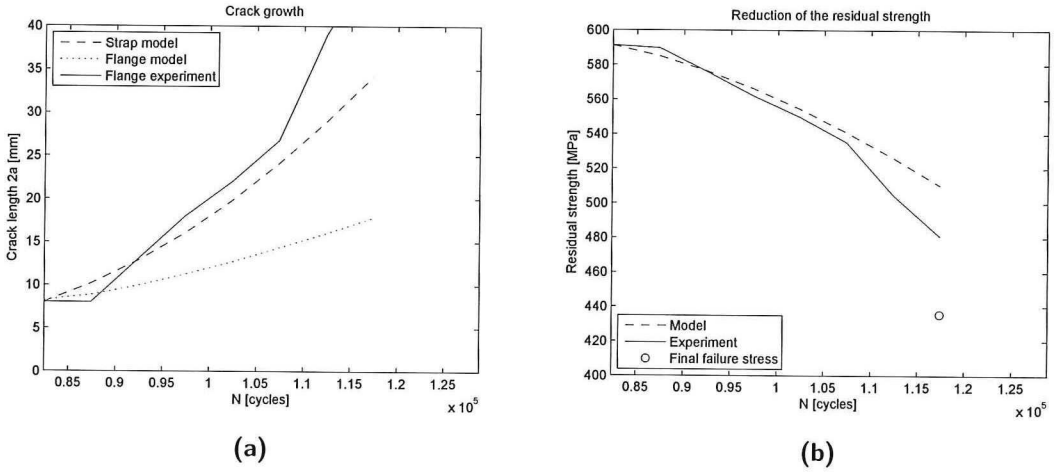

Figure 7.16: The crack growth from the FML model and the test of coupon FS01416a6 is shown in figure 7.16a. The residual strength from FML model and the test of coupon FS01416a6 is shown in figure 7.16b, Final failure from the experiment is indicated in figure 7.16b with a circular marker

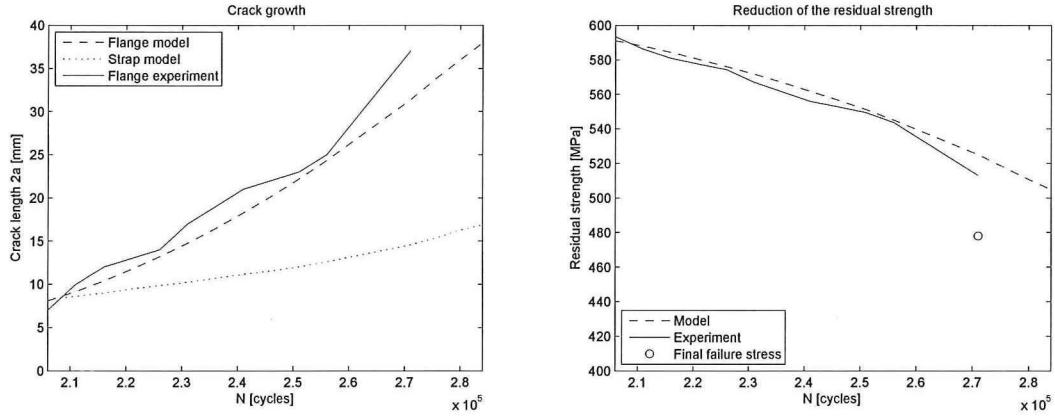

(a) (b)

Figure 7.17: The crack growth from the FML model and the test of coupon FS01416a7 is shown in figure 7.17a. The residual strength from FML model and the test of coupon FS01416a7 is shown in figure 7.17b. Final failure from the experiment is indicated in figure 7.17b with a circular marker

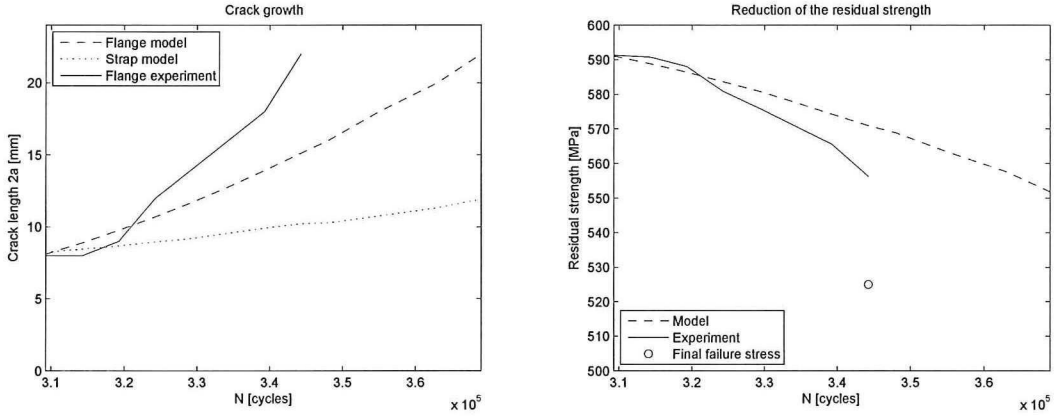

(a) (b)

Figure 7.18: The crack growth from the FML model and the test of coupon FS01416a10 is shown in figure 7.18a. The residual strength from FML model and the test of coupon FS01416a10 is shown in figure 7.18b, Final failure from the experiment is indicated in figure 7.18b with a circular marker

Chapter 8

Conclusion and future prospects

In this thesis an approach is presented to predict the residual strength of an aluminium flange reinforced with a FML strap, which was subjected to fatigue loading. This should be an analytical tool which is easy to use and being integrated with the FML fatigue toolbox. The relevance of such a tool within the fatigue and damage tolerance regulations is discussed. The existing approaches with regards to the residual strength of FMLs containing fatigue cracks was discussed. A net section loss approach, similar to the approach presented by de Rijck [12], which subtracts the strength provided by the aluminium layers that are crack, from the strength of the laminate, was determined to be best applicable to the requirements.

To validate the applicability of this method on a flange reinforced with a FML strap, testing was performed on coupons consisting of such a structure. Different levels of fatigue damage was created in coupons, which were subsequently tested up to failure.

The results are discussed and compared with the predictions made with the net section loss model. Additionally, the results were compared with findings from literature. The overall trend of the reduction in residual strength due to the fatigue damage ratio showed good agreement. However, an over prediction of the residual strength 15% was found. During residual strength testing, it was observed that the aluminium flange delaminated from the FML strap, causing stress concentrations in the FML strap at the edge of the delamination, at a rivet row. The author thinks that this stress concentration is the cause for the lower residual strength than predicted. To improve the model, research into quantification of this stress concentration is required.

References

[1] S.W.F. Spronk. Predicting fatigue crack initiation and propagation in glare reinforced frames. 2013.

[2] RC Alderliesten. *Fatigue crack propagation and delamination growth in Glare.* Dissertation Delft 2005, 2005. 9040725888 (NL-LeOCL) 277327938.

[3] J.J. Homan. Fatigue initiation in fibre metal laminates. *International Journal of Fatigue*, 28, 2005.

[4] R. Rodi. *The Residual Strength Failure Sequence in Fibre Metal Laminates.* Dissertation Delft 2005.

[5] aviationweek. A400m.

[6] M. Plokker and D. Daverschot. Hybrid structure solution for the a400m wing attachment frames. In *ICAF*, 2009.

[7] Tjerk Johan de Vries. *Blunt and sharp notch behaviour of Glare laminates.* Diss delft 2001, 2001.

[8] R.P.G. Müller. *An Experimental and Analytical Investigation on the Fatigue Behaviour of Fuselage Riveted Lap Joints: The Significance of the Rivet Squeeze Force, and a Comparison of 2024-T3 and Glare 3.* Delft University of Technology, 1995.

[9] Thomas Beumler. Flying glare. *A contribution to aircraft certification issues on strength properties in non-damaged and fatigue damaged GLAREÂő structures., Technical University Delft, Faculty of Aerospace Engineering, Diss*, 2004.

[10] M. Hagenbeek, C. Van Hengel, O. J. Bosker, and C. A. J. R. Vermeeren. Static properties of fibre metal laminates. *Applied Composite Materials*, 10(4-5):207–222, 2003. 718CR Times Cited:22 Cited References Count:11.

[11] GHJJ Roebroeks, Peter A Hooijmeijer, Erik J Kroon, and Markus B Heinimann. The development of central. In *Proceedings of the 1st international conference on damage tolerance of aircraft structures, Delft, The Netherlands.*

[12] Johannes Jacobus Maria de Rijck. *Stress analysis of fatigue cracks in mechanically fastened joints: an analytical and experimental investigation.* DUP Science, 2005.

[13] Ad Vlot and Jan Willem Gunnink. *Fibre metal laminates: an introduction.* Springer, 2001.

[14] Gregory S Wilson. *Fatigue Crack Growth Prediction for generalized fiber metal laminates and hybrid materials.* PhD thesis, TU Delft, Delft University of Technology, 2013.

[15] S Khan. *Fatigue Crack and Delamination Growth in Fibre Metal Laminates under Variable Amplitude Loading.* PhD thesis, TU Delft, Delft University of Technology, 2013.

[16] Federal Aviation Administration. Part 25: Airworthiness standards: Transport category. 2014.

[17] Federal Aviation Administration. Ac 25.571-1d damage tolerance and fatigue evaluation of structure. 2011.

[18] Scott C Forth, Dy Le, and Jay Turnberg. An evaluation of the applicability of damage tolerance to dynamic systems. 2005.

[19] RL Twite and GP Bierwagen. Review of alternatives to chromate for corrosion protection of aluminum aerospace alloys. *Progress in organic coatings*, 33(2):91–100, 1998.

[20] Federal Aviation Administration. Ac 91-82a fatigue management programs for in-service issues. 2011.

[21] FAA. Advisory circular 91-82a fatigue management programs for in-service issues, 2011.

[22] Alten F Grandt Jr. *Fundamentals of structural integrity: damage tolerant design and nondestructive evaluation.* John Wiley & Sons, 2003.

[23] Graham Clark. 26th icaf symposium–montreal, 1-3 june 2011. In *ICAF 2011 Structural Integrity: Influence of Efficiency and Green Imperatives: Proceedings of the 26th Symposium of the International Committee on Aeronautical Fatigue, Montreal, Canada, 1-3 June 2011*, page 1. Springer Science & Business Media, 2011.

[24] D. Hartman, M. E. Greenwood, and D.M. Miller. High strength glass fibres. 2006.

[25] RC Alderliesten. *Fatigue and Damage Tolerance of Hybrid Materials and StructuresâĂŞ-Some Myths, Facts and Fairytales*, pages 1245–1260. Springer, 2009.

[26] Jaap Schijve. *Fatigue of structures and materials.* Springer, 2001.

[27] RC Alderliesten. Understanding the fatigue behavior of fml structures and materials under complex variable amplitude loading. In *Aircraft Structural Integrity Program Conference.*

[28] Riccardo Rodi, Rinze Benedictus, et al. Experimental characterization of the crack-tip-opening angle in fibre metal laminates. *Engineering Fracture Mechanics*, 77(6):1012–1024, 2010.

[29] Airbus Military. Airbus military | A400M.

[30] Cornelis Adrianus Johannes Robertus Vermeeren. *The residual strength of fibre metal laminates.* Delft University of Technology, Faculty of Aerospace Engineering, 1995.

[31] Manfredo D'Alessandro Caprice, Marco Oriunno, and Coen Vermeeren. Evaluation of residual strength of glareÂľ by experimental measurement of the j-integral. *Engineering fracture mechanics*, 49(5):727–740, 1994.

[32] S. Klein. Fatigue coupon testing of bonded and riveted glare-aluminium specimens). fs01416. 2011.

Appendix A

Appendix: Residual strength results

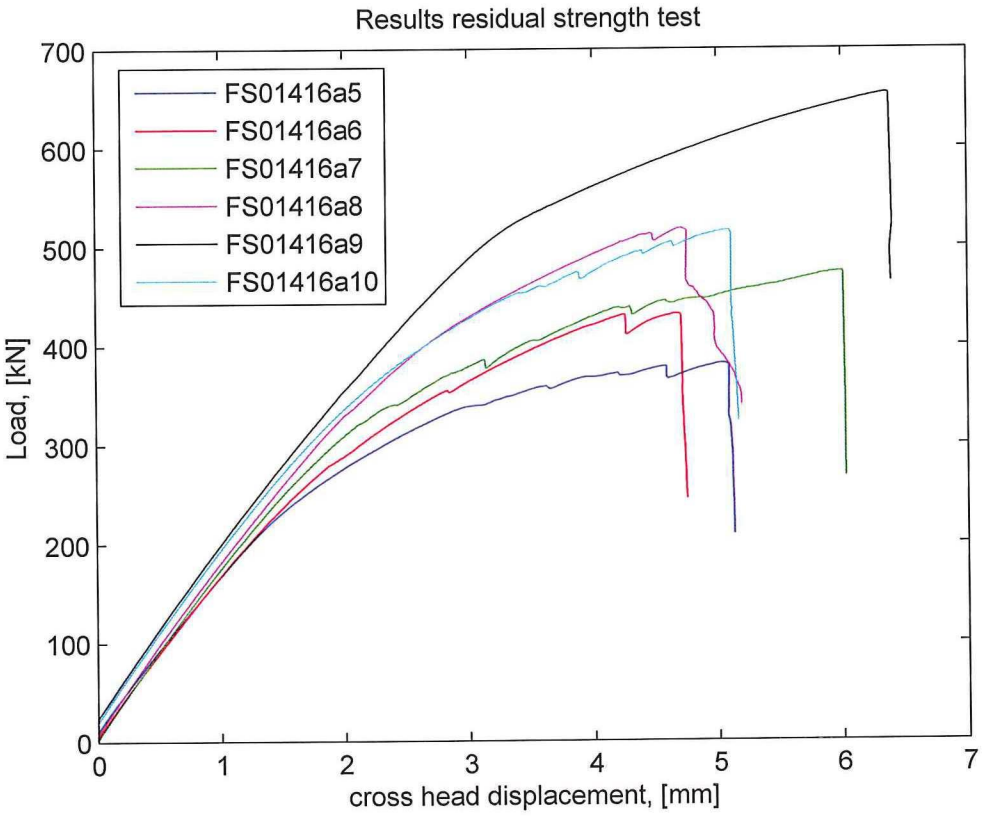

Figure A.1: Resulting graphs from residual strength testing

FS01416a5

Table A.1: Fatigue crack lengths in sample FS01416a5

	Left Rivet		Right Rivet	
Layer	Left crack [mm]	Right crack [mm]	Left crack [mm]	Right crack [mm]
1	8,8	8,1	6,5	9,1
2	5,7	5,9	7,5	6,4
3	5,4	6,9	7,1	6,2
4	5,4	6,2	6,4	5,4
5	4,7	4,6	5,7	5,0
6	4,3	4,8	4,8	3,9
7	4,1	5,0	4,5	4,1
8	4,4	4,5	4,7	3,1
9	3,9	4,1	4,2	3,7
10	3,7	3,9	3,7	3,6
11	2,3	3,1	2,9	3,1
12	0,0	2,3	2,3	2,6
13	1,0	2,0	1,3	2,3
14	1,2	1,7	1,5	2,1
15	0,9	1,3	1,5	1,5
16	0,8	1,0	1,1	1,4

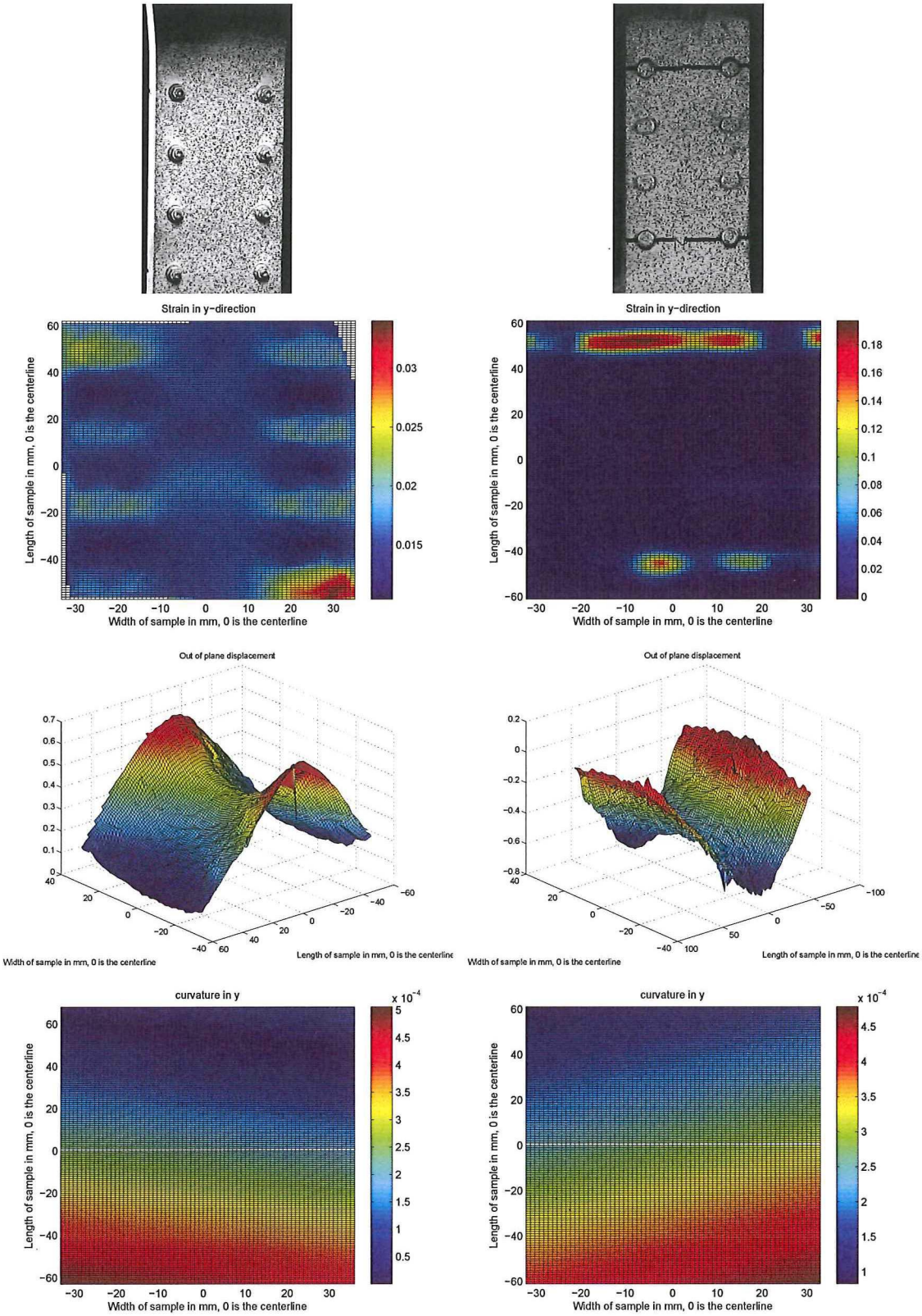

Figure A.2: FS01416A6

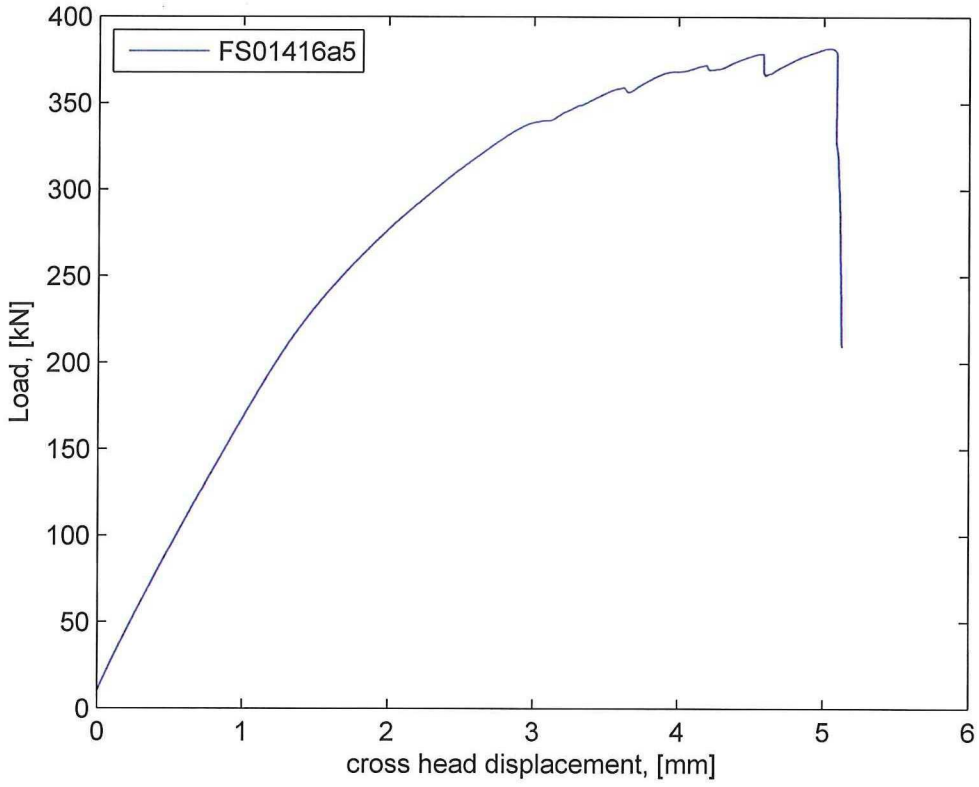

Figure A.3: FS01416a5

FS01416a6

Table A.2: Fatigue crack lengths in sample FS01416a6

	Left Rivet		Right Rivet	
Layer	Left crack [mm]	Right crack [mm]	Left crack [mm]	Right crack [mm]
1	3,6	1,1	1,9	1,3
2	2,8	2,1	1,7	0,7
3	2,5	1,4	1,5	0,9
4	2,2	1,7	1,8	0,6
5	2,2	1,1	1,9	0,4
6	1,9	0,8	1,7	0,7
7	1,9	1,1	1,4	0,7
8	1,2	1,4	1,8	0,9
9	1,2	1,1	1,7	0,5
10	1,5	1,6	1,8	0,8
11	1,4	1,6	1,8	1,5
12	0,8	0,8	1,8	1,3
13	0,5	1,0	1,4	1,6
14	0,2	0,9	1,5	0,9
15	0,0	0,0	1,3	0,6
16	0,2	0,0	1,2	0,0

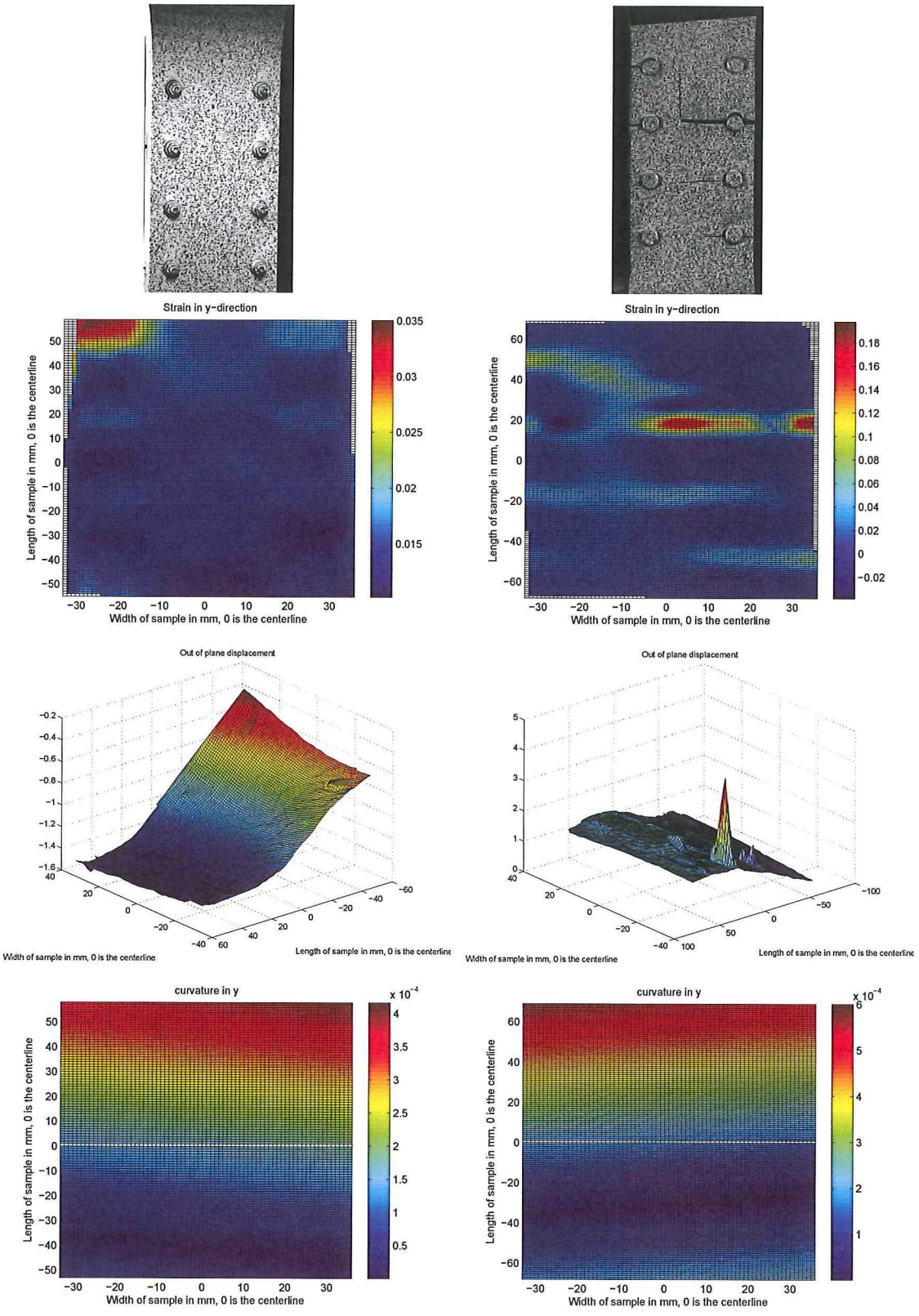

Figure A.4: FS01416A6

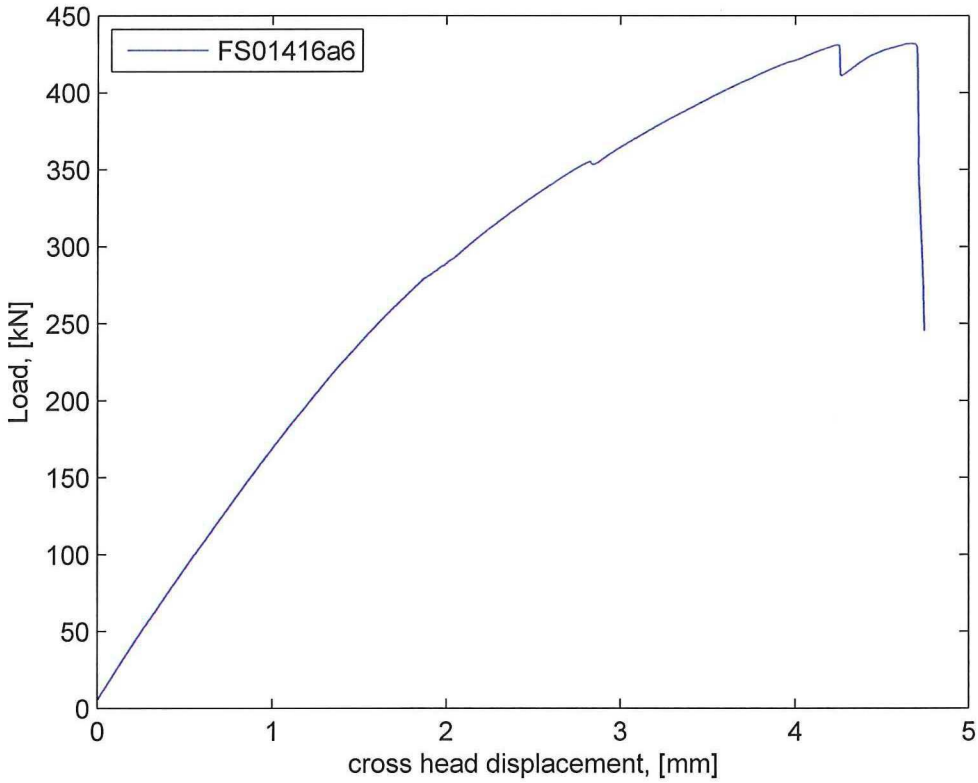

Figure A.5: FS01416a6

FS01416a7

Table A.3: Fatigue crack lengths in sample FS01416a7

	Left Rivet		Right Rivet	
Layer	Left crack [mm]	Right crack [mm]	Left crack [mm]	Right crack [mm]
1	1,4	1,4	0,0	0,0
2	0,0	0,0	0,0	0,0
3	0,0	1,3	0,0	0,0
4	1,1	0,0	0,0	0,0
5	0,0	0,8	0,0	0,0
6	0,5	1,0	0,0	0,0
7	1,6	0,4	0,0	0,0
8	0,0	0,3	0,0	0,0
9	0,0	1,1	0,0	0,0
10	1,2	0,7	0,0	0,0
11	0,0	0,0	0,0	0,0
12	0,0	0,9	0,0	0,0
13	0,0	0,0	0,0	0,0
14	0,0	0,0	0,0	0,0
15	0,0	0,0	0,0	0,0
16	0,0	0,0	0,0	0,0

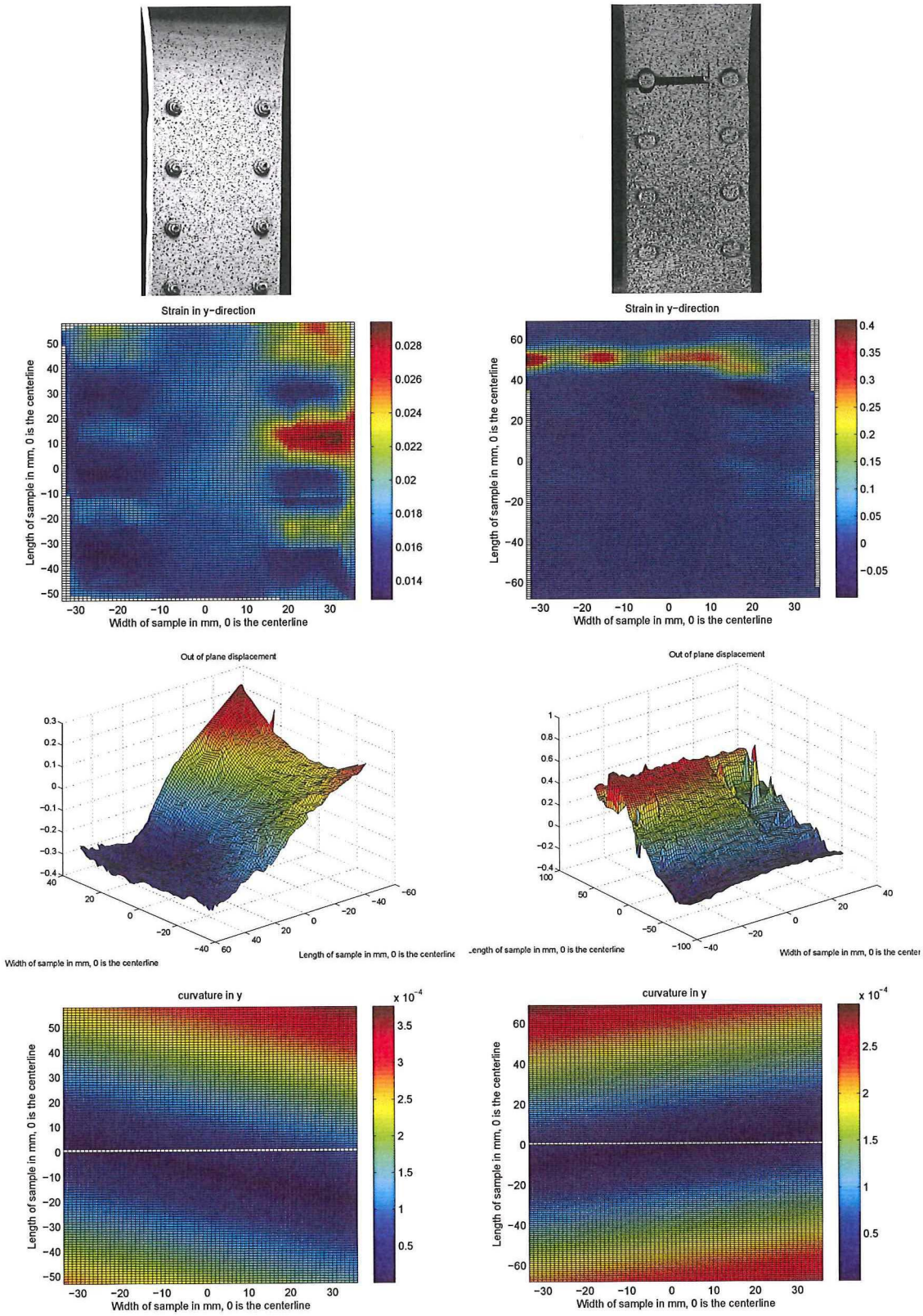

Figure A.6: FS01416A7

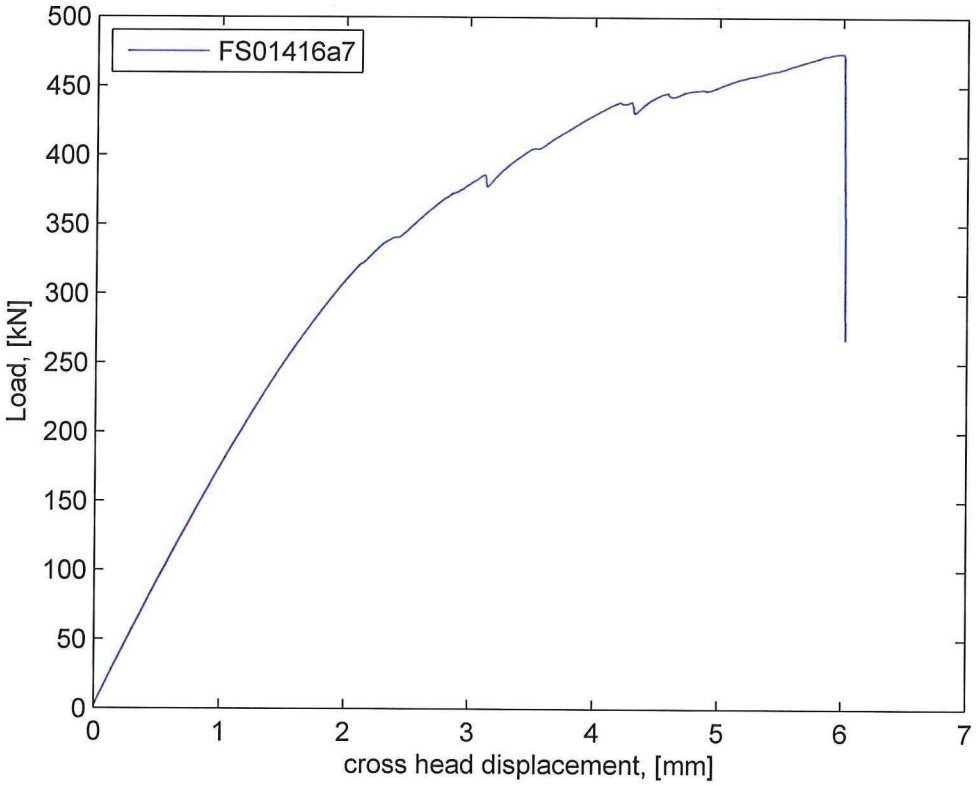

Figure A.7: FS01416a7

FS01416a8

Table A.4: Fatigue crack lengths in sample FS01416a8

	Left Rivet		Right Rivet	
Layer	Left crack [mm]	Right crack [mm]	Left crack [mm]	Right crack [mm]
1	0,0	1,2	3,6	6,1
2	0,0	0,9	2,6	6,1
3	0,5	5,2	2,3	3,4
4	0,8	0,9	2,1	2,1
5	0,5	1,1	1,9	1,9
6	1,3	1,4	1,5	2,1
7	0,7	0,8	1,5	6,7
8	0,0	0,5	1,0	4,6
9	1,0	0,7	1,1	1,6
10	1,0	0,7	1,2	1,1
11	0,5	0,9	1,6	1,1
12	0,5	0,5	1,6	1,6
13	0,4	0,7	1,1	1,0
14	0,3	0,6	1,2	1,4
15	0,2	0,7	1,1	0,9
16	0,2	0,2	0,5	0,9

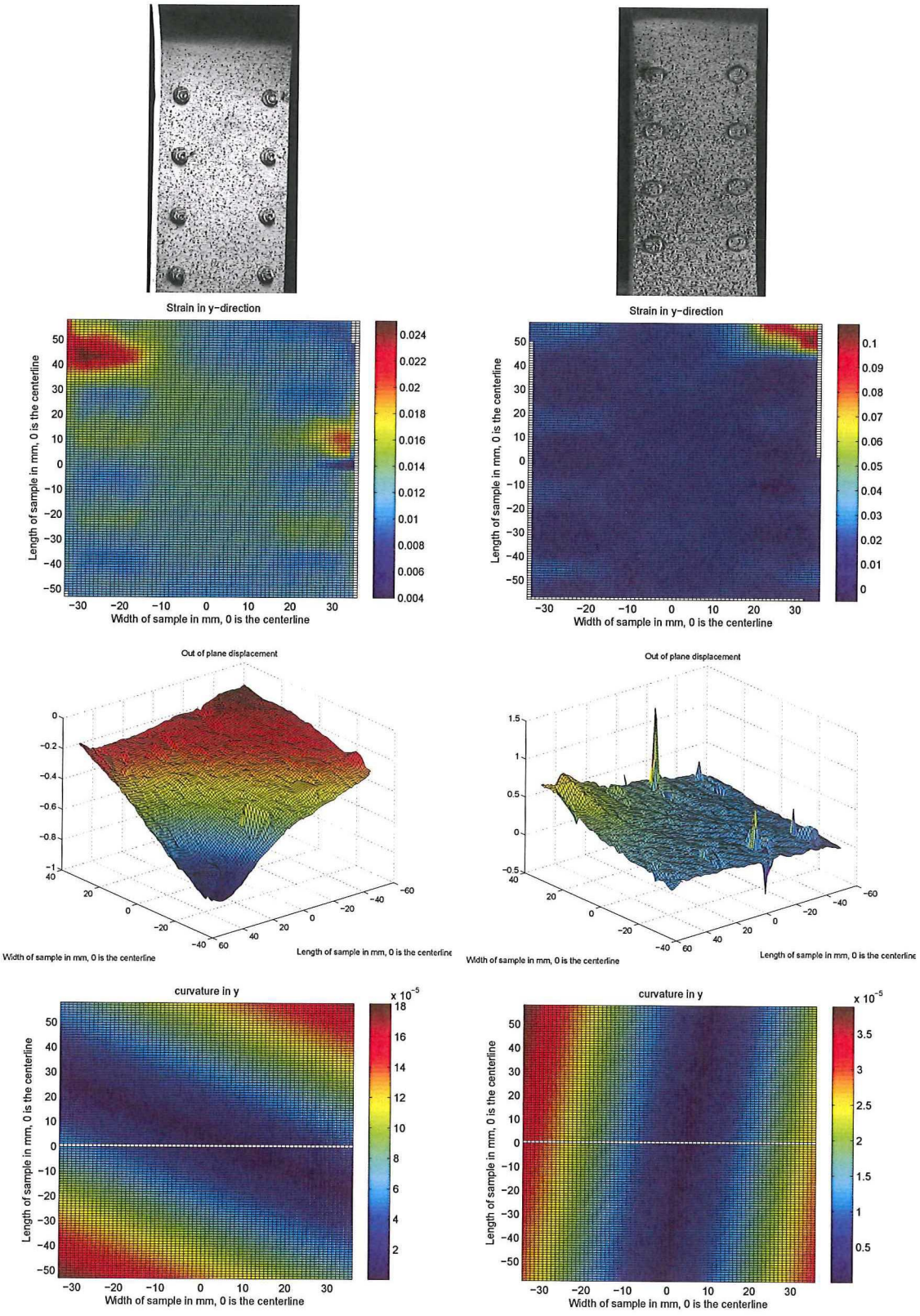

Figure A.8: FS01416A8

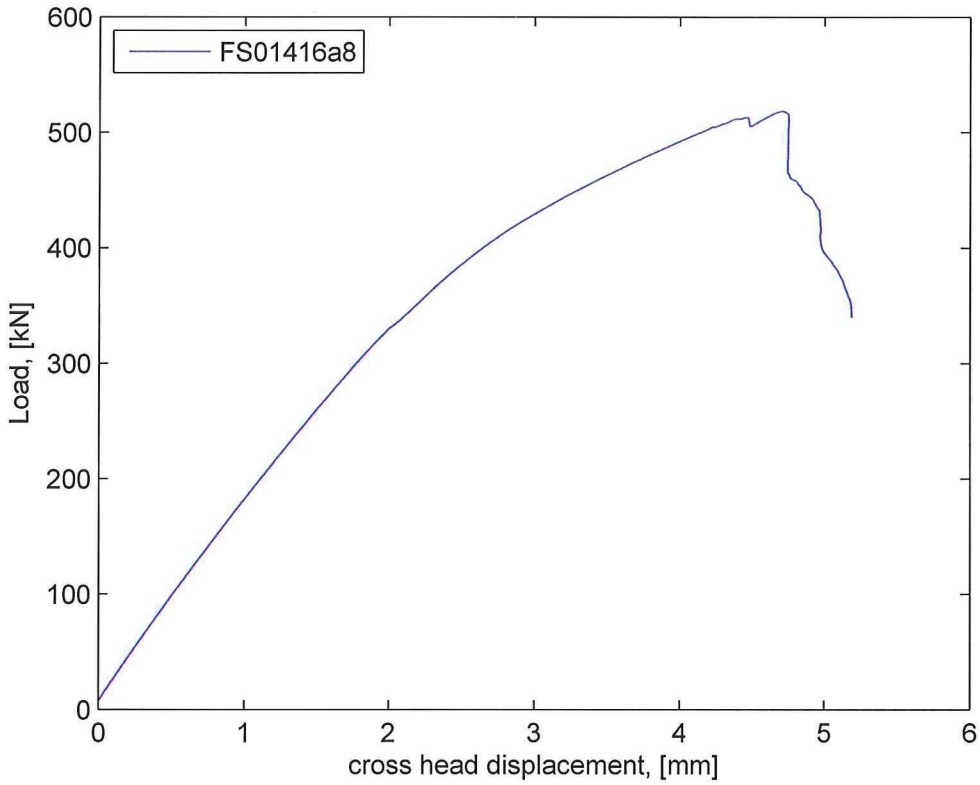

Figure A.9: FS01416a8

FS01416a9

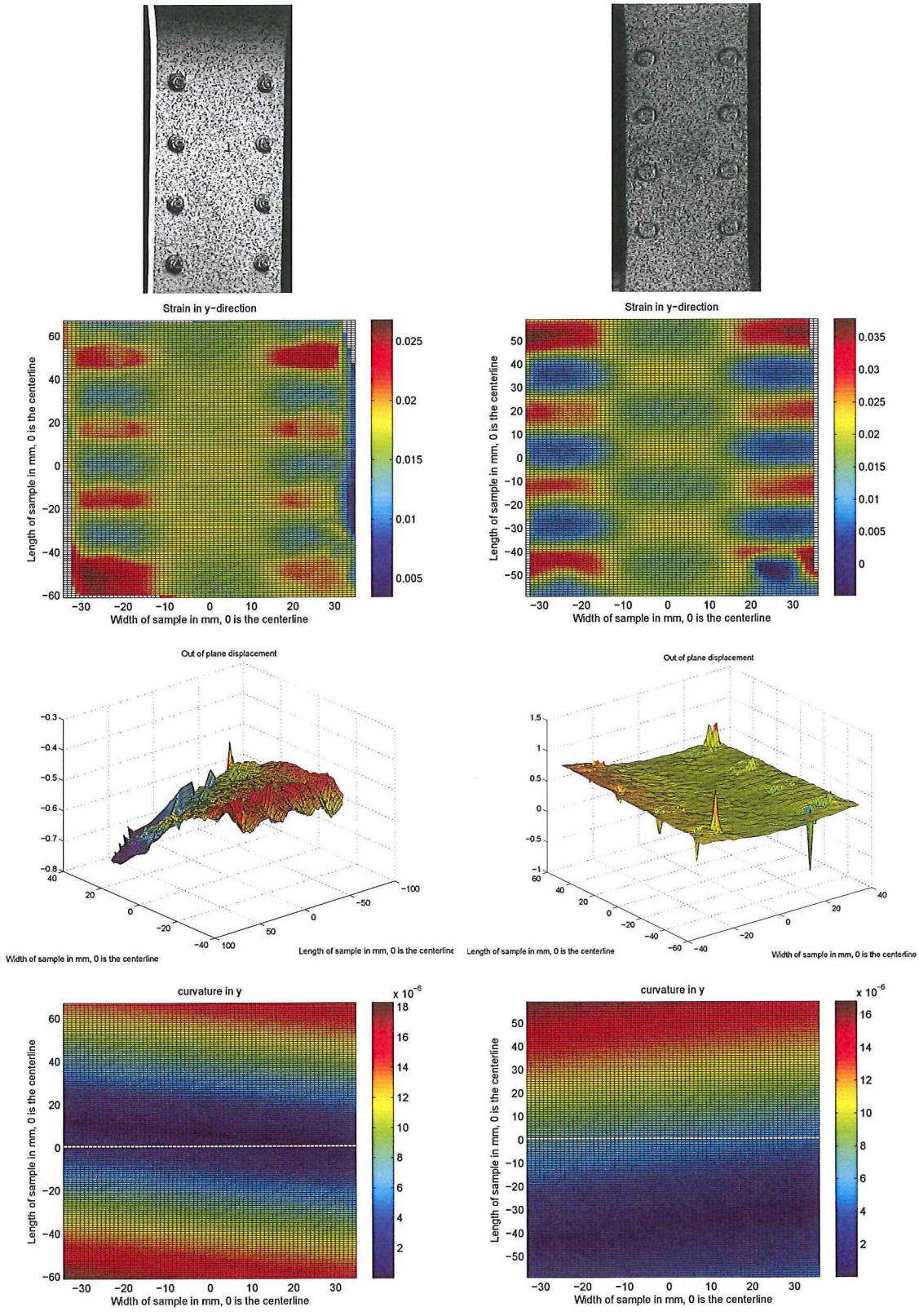

Figure A.10: FS01416A9

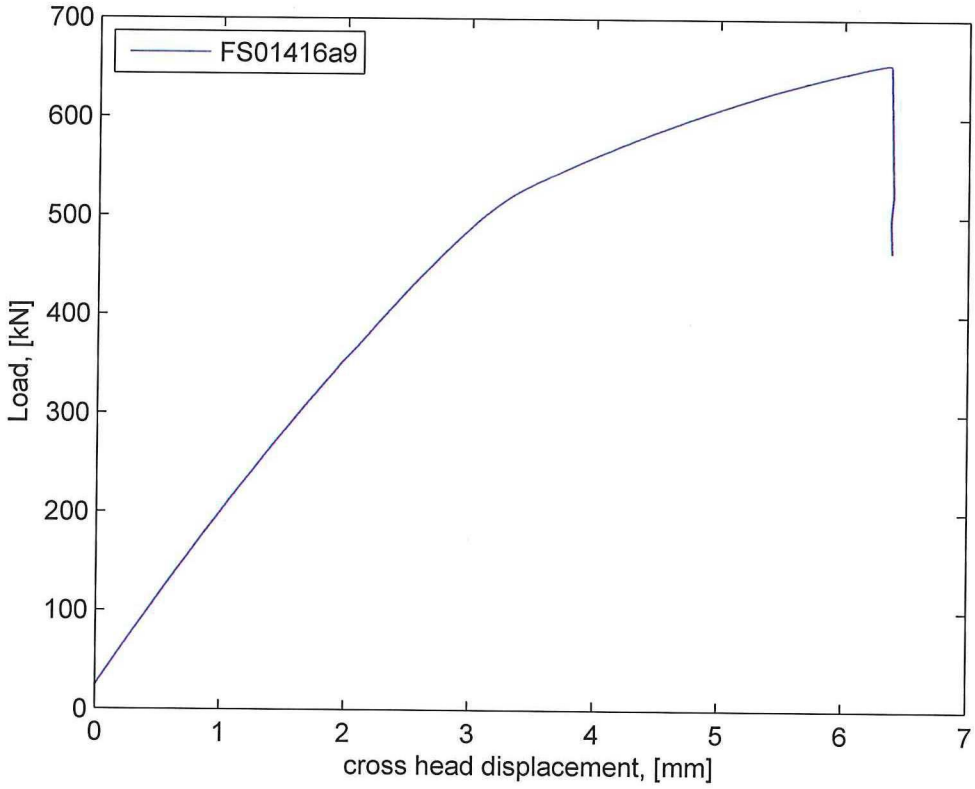

Figure A.11: FS01416a9

FS01416a10

Table A.5: Fatigue crack lengths in sample FS01416a10

	Left Rivet		Right Rivet	
Layer	Left crack [mm]	Right crack [mm]	Left crack [mm]	Right crack [mm]
1	0,0	0,0	1,9	0,0
2	1,6	1,6	2,0	0,3
3	2,2	2,0	0,3	0,4
4	2,3	2,1	0,0	2,6
5	2,2	2,3	0,0	2,4
6	1,6	2,8	2,2	1,7
7	1,0	2,6	1,8	1,3
8	1,7	0,0	0,0	0,0
9	0,0	0,0	1,4	1,8
10	0,9	2,8	2,4	2,0
11	1,8	2,0	2,6	1,6
12	1,4	2,4	2,6	1,7
13	1,7	2,3	1,7	0,0
14	2,1	0,0	1,9	1,7
15	0,0	0,0	1,6	0,0
16	0,0	0,0	2,1	0,0

Failure mechanisms for each coupon

- For the pristine sample FS01416a9, which can be regarded as baseline, there is a very low curvature in the sample. This can be explained as there is no delamination between the flange and the Glare 2A laminate. There is no delamination because there is no stress concentration / fibre briding because there are no cracks in the flange. Additionally, Sample FS01416a9 shows a very clean failure curve, with a clear elastic aluminium followed by an elastic glass fibre part. Sample FS01416a9 shows a very equally strained laminate. It makes sense that the top or bottom rivet row fails, as stress concentration is highest.

- For sample FS01416a8, with only a small fatigue crack in the flange, the curvature at failure is only slightly higher. During residual strength testing, the fatigue crack opens, and, at Vic3D snap 55, a vertical crack appears at the other side of the rivet hole with fatigue crack. This corresponds with the dip in the residual strength curve just before failure. After this, first the Glare2A cracks, visible at Vic3D-059-1 and MatchID-0057-0. It is also seen that the aluminium flange is plastically deformed, increasing the load on the fibres. Additionally a small delamination occurs between the flange and glare at this location. Then after, a crack from the edge of the sample to the rivet hole appears on the aluminium side. Then it takes 26 sec to drop from max load to end of test. This corresponds with the propagation of the crack in glare side.

- For sample FS01416a10: Crack opens, causes crack in the loading direction in the

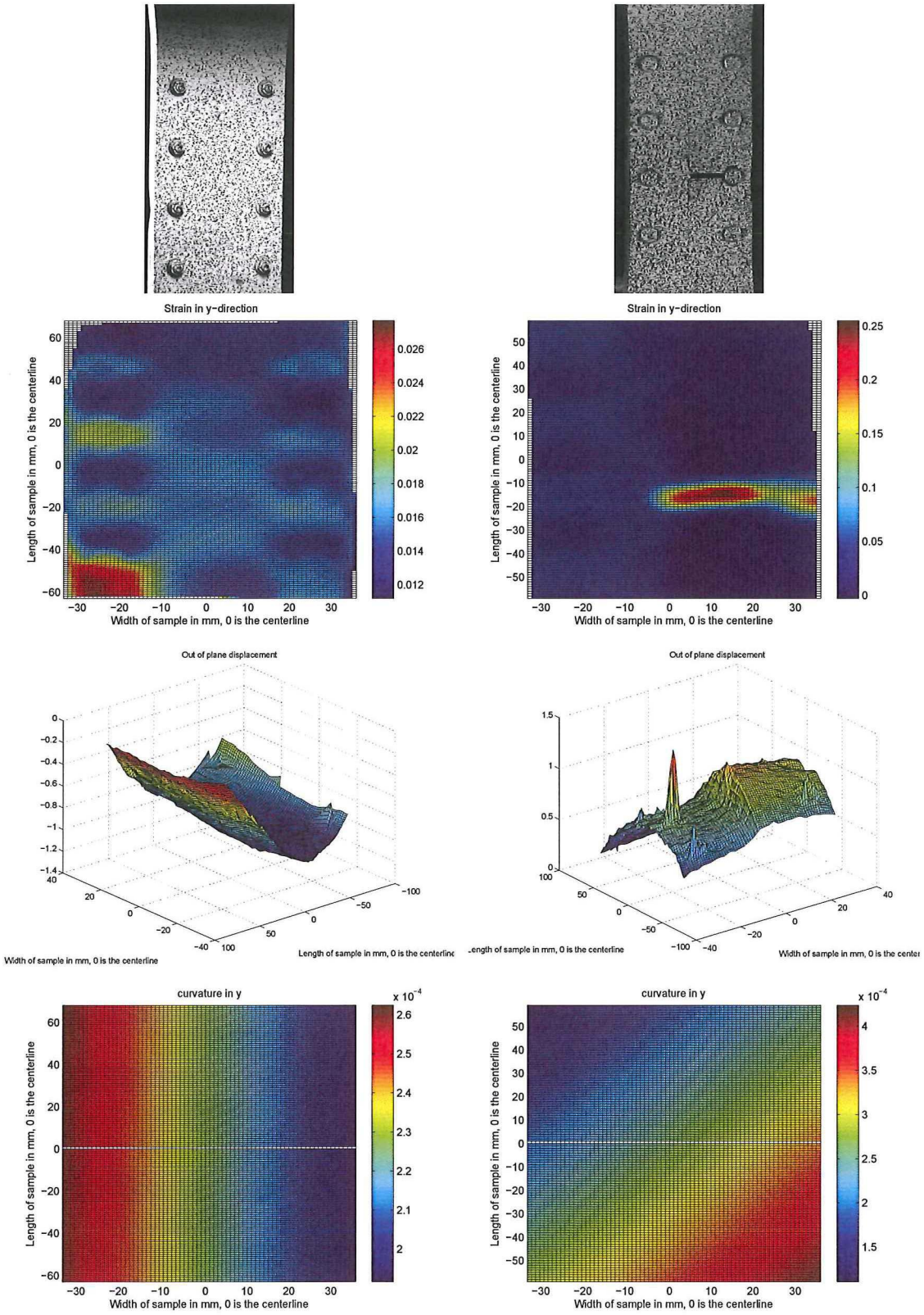

Figure A.12: FS01416A10

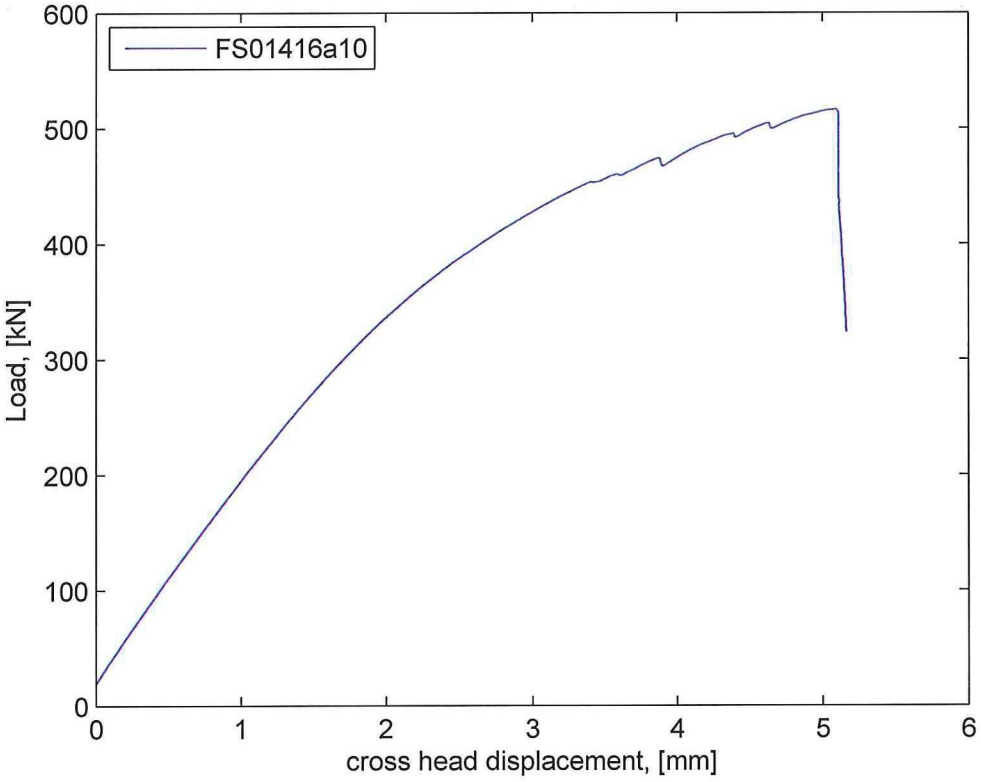

Figure A.13: FS01416a10

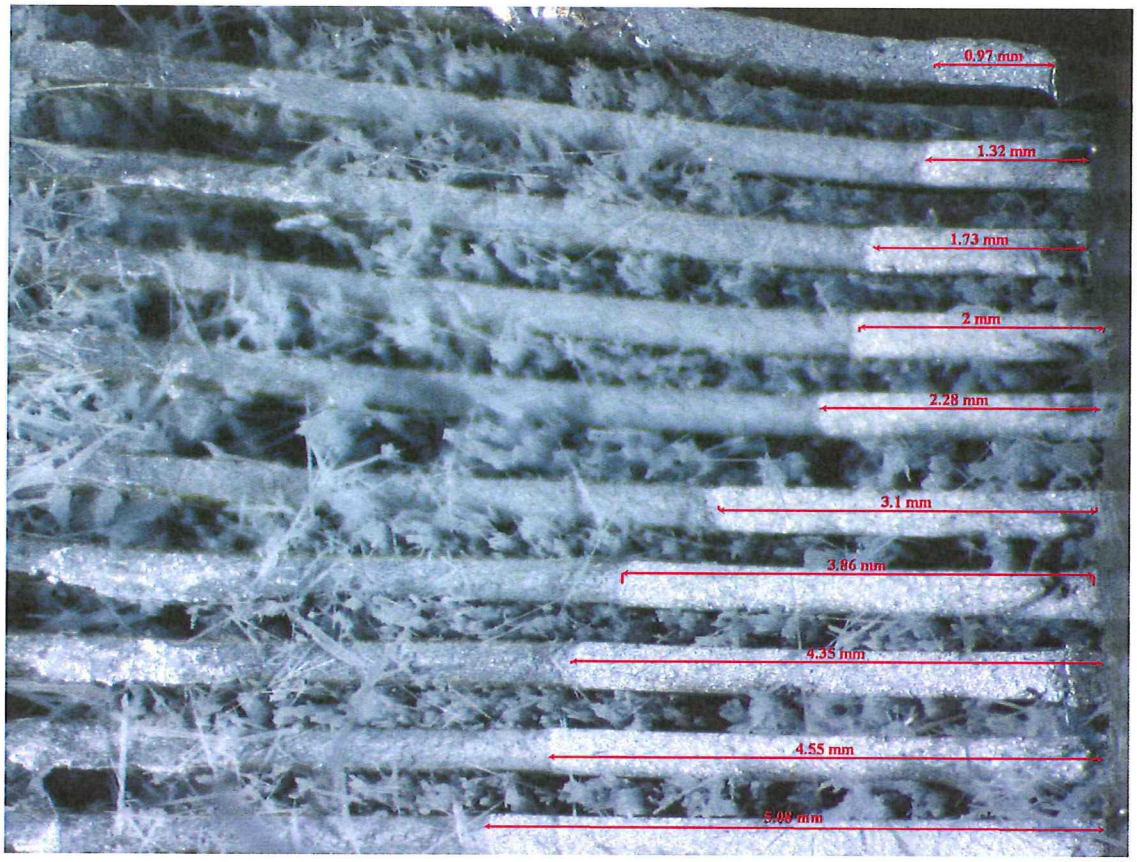

Figure A.14: Fatigue crack length measurement with microscope

flange. Now the area above and below the crack can delaminate (see difference between in displacement in flange when the vertical crack starts this delamination also starts growing. Then the coupon fails at the rivet row that has the highest stress concentration, which is always the top or bottom rivet row.

- For sample: FS01416a7: Again, crack opens, vertical crack starts growing, together with a delamination. **Effectively this causes the glare laminate behind the crack to carry the load for this part of the laminate! This has less stiffness because reduced thickness, so part of the load is distributed to the other side of the laminate. Ultimately the coupon fails on the location where the delamination starts**

- For sample FS01416a6: Again, large crack, which will be spanned by a delamination. The creation of this static delamination is also visible in the load displacement diagram as a drop just before the end. Sample starts failing at the side of the large crack in the flange, and first grows only the length of delamination. Then it grows further and the whole laminate fails.

- For sample FS01416a5: No large delaminations take place because other rivet rows already cracked, which enable the aluminium in between rivet rows to deform together with the glass fibre. Now sample just fails at stress location at bottom (could also have been top row) In this case, curvature is highest in bottom row, probably due to crack configuration in the sample.